الجمهورية الجزائرية الديمقراطية الشعبية
REPUBLIQUE ALGERIENNE DEMOCRATIQUE ET POPULAIRE
وزارة التعليم العالي والبحث العلمي
MINISTERE DE L'ENSEIGNEMENT SUPERIEUR ET DE LA RECHERCHE SCIENTIFIQUE
جامعة فرحات عباس سطيف 1
UNIVERSITE FERHAT ABBAS SETIF1
UFAS1 (ALGERIE)

THESE

Présenté à la Faculté de Technologie

Pour l'Obtention du Diplôme de

Doctorat

Domaine : Science et Technologie
Filière : Electronique
Option : Electronique et commande industrielles

Par

Mr. Kihal Abbes

Approche avancée pour l'optimisation d'une installation Photovoltaïque interconnectée au réseau

Soutenue le : 19 / 09 /2019 devant un jury composée de :

HASSAM Abdelwahab	Professeur	Univ. Sétif 1	Président
KRIM Fateh	Professeur	Univ. Sétif 1	Directeur de thèse
HARRAG Abdelghani	Professeur	Univ. Sétif 1	Examinateur
SEMECHEDDINE Samia	Professeur	Univ. Sétif 1	Examinateur
MENDIL Boubaker	Professeur	Univ. Bejaia	Examinateur

Advanced Approach for the Optimization of a Grid-Tied Photovoltaic System

by

KIHAL Abbes

A thesis
presented to the University of Sétif 1
in fulfillment of the
thesis requirement for the degree of
Doctor of Philosophy
in
Industrial Electronics and Control

To my mother

To my Father

To my wife

To my sweet daughter

To my sisters and my brothers

To all the kihal's family

Acknowledgement

*In the name of **ALLAH**, the Most Gracious and the Most Merciful. Thanks to **ALLAH** who is the source of all the knowledge in this world, for the strengths and guidance in completing this thesis.*

*I express my deep sense of gratitude and heart-felt thanks to my supervisor, Prof. **KRIM Fateh**, for his invaluable guidance, patience, kindness and consistent encouragement throughout the course of this work. I am very glad that I have pursued my doctoral studies under his excellent supervision.*

*I would like to express my appreciation to my thesis committee members: Prof. **HASSAM Abdelwahab**, Prof. **MENDIL Boubaker**, Prof. **HARAG Abdelghani** and Prof. **SEMECHEDDINE Samia** for their discussions, suggestions, and feedbacks to improve my thesis.*

*I cannot forget to mention all my friends, **LEPCI** group, **LAIB Abdelbaset**, **TALBI Billel**, **SAHLI Abdeslem**, **FEROURA Hamza**, **BELAOUT Abdesslam**, **MESAOUD Sebihi**, **ARABI Abderrazak** , and **BEY Habib** for their great friendship, help and support.*

KIHAL Abbes

Abstract

This Ph. D thesis is one of the core research activities of the exploitation of photovoltaic (PV) energy. The use of PV energy has drawn global attention for future electricity production to meet the increased energy demand. Amongst the application fields of this energy type, the grid-tied PV system is considered as the most requested on the PV market because it allows a better use of PV energy and does not need energy storage devices, which reduces cost with less maintenance. The grid-tied PV systems are broadly classified into two categories, single and two conversion stages. The efficiency resulting from these systems depends not only on the working conditions, but also on the complete conversion chain. This can be achieved by a judicious choice of configurations or topologies, good sizing of components and effective control techniques. The research work presented in this thesis is to contribute to the efficiency optimization of grid-tied PV systems. This contribution concerns the modeling, sizing and control of a two-stage grid connected PV system. Nevertheless, the main part of our research is to propose powerful control scheme capable to attain the aforementioned objective. Firstly, the development of a Maximum power point tracking (MPPT) methods based on a non-linear approach called sliding mode control (SMC) to achieve an optimal exploitation of PV generator under solar irradiation changes. Also, the development of new design based on SMC theory for DC-Link voltage controller to maintain the DC-link voltage constant at the desired value during any case of solar irradiation changes. Afterwards, the development of a voltage oriented control (VOC) based on SMC and space vector modulation for proper inverter operation as well sinusoidal currents injection into the mains grid with low total harmonic distortion (THD < 5%).In addition, these schemes have been performed through numerical simulation with MATLAB/Simulink® environment, and validated practically through real-time hardware in the loop system using a dSPACE DS 1104 system.

Keywords: Photovoltaic energy; Grid-tied photovoltaic system; MPPT; Sliding mode control; Total harmonic distortion.

Table of Contents

List of Figures

List of Tables

List of Acronyms

AC	Alternative current
ANN	Artificial neural network
C-MPPT	Current based MPPT
DC	Direct current
DPC	Direct power control
DER	Distributed energy resources
EPIA	European Photovoltaic Industry Association
FCS-MPC	Finite control set model predictive control
FLC	Fuzzy logic control (controller)
GA	Genetic algorithm
GSEC	Global Solar Energy Council
GW	Gigawatt
HIL	Hardware in the loop
IGBT	Insulated gate bipolar transistor
IC	Incremental conductance
IEC	International Electro-technical Commission
IEEE	Institute of Electrical and Electronics Engineers
ISMC	Integral sliding mode control
I-V	Current-voltage
KCL	Kirchhoff's Current Law
KVL	Kirchhoff's Voltage Law
MPC	Model predictive control
MPP	Maximum power point
MPPT	Maximum power point tracking
OCV	Open-circuit voltage
P&O	Perturb and observe
PCC	Point of common coupling
PI	Proportional-integral
PID	Proportional-integral-derivative
PSO	Particle swarm optimization
PV	Photovoltaic

P-V	Power-voltage
PWM	Pulse width modulation
SCC	Short-circuit current
STC	Standard test conditions
SMC	Sliding mode control
SSE	Steady state error
SVM	Space vector modulation
THD	Total Harmonic Distortion
VOC	Voltage oriented control
V-MPPT	Voltage based MPPT
VO-MPPT	Voltage oriented MPPT
VSI	Voltage source inverter

List of Symbols

C_{in}	Boost input capacitor (μF)
C_{dc}	Boost capacitor (μF)
f_c	Switching frequency of the boost converter (kHz).
G	Solar irradiation (w/m^2)
I_d	Diode current (A)
I_{inv}	Inverter input voltage (A)
I_L	Boost input current (A)
I_o	Reverse saturation current of the diode (A)
I_{ph}	Photovoltaic cell photocurrent (A)
I_{pv}	Photovoltaic array output current (A)
I_r	Derived current by the shunt resistance (A)
I_{SC}	Photovoltaic array short-circuit current
k	Boltzmann constant (1.38×10^{-23} J/K)
L	Boost input inductor (mH)
L_g	Inverter side inductor (H).
n	Diode ideality factor
N_p	Number of cells connected in parallel
N_{pp}	Number of modules connected in parallel
N_s	Number of cells connected in series
N_{ss}	Number of modules connected in series
q	Electronic charge (1.6×10^{-19} C)
R	Boost resistive load (Ω)
R_g	Internal resistance of the filter (Ω)
R_s	Photovoltaic cell series resistance (Ω)
R_{sh}	Photovoltaic cell shunt resistance (Ω)
S	Switching signal of the Boost converter
S_a, S_b, S_c	Switching signals of the inverter.
T	Absolute temperature (K)
T_s	Sample time of the P&O algorithm (μs)
$v_{a,g}$, $v_{b,g}$, $v_{c,g}$	Grid voltage (V)
v_{ao}, v_{bo}, v_{co}	Phase-to-neutral voltages of the inverter (V)

v_{out}	Boost output voltage (V)
v_{dc}	DC-link voltage (V)
V_{OC}	Photovoltaic array open-circuit voltage (V)
v_{pv}	Photovoltaic array output voltage (V)
V_t	Thermal voltage (V)
ω	Rotational frequency of the generated sine wave (rad/s)

Chapter 1

Introduction

1.1 INTRODUCTION TO PHOTOVOLTAICS

To satisfy the growing energy demand with a reduction in global warming caused by fossil fuels (natural gas, oil, coal, etc.), renewable energy sources, especially solar photovoltaic (PV) energy has attracted attention in today's world. According to the Global Solar Energy Council (GSEC) and European Photovoltaic Industry Association (EPIA) [1.1-2], the solar energy capacity has grown fast from 2007 to 2018 with about 104 gigawatt (GW) installed only in 2018. Figure 1.1 represents the global solar energy capacity and annual additions from 2007 to 2018 [1.2]. In fact, the global installed PV energy capacity reached 506 GW at the end of 2018 (representing an increase of 20.55% more than the previous year 2017), stating that PV energy plays an important role in the modern energy resource system [1.1]. The secret of this rapid growth in total installed capacity lies in the increased competitiveness of PV energy due to reduced prices of PV system components, especially the PV modules and the introduction of economic incentives or subsidies intended at reducing the use of fossil fuels according to the objectives of the Kyoto Protocol [1.3].

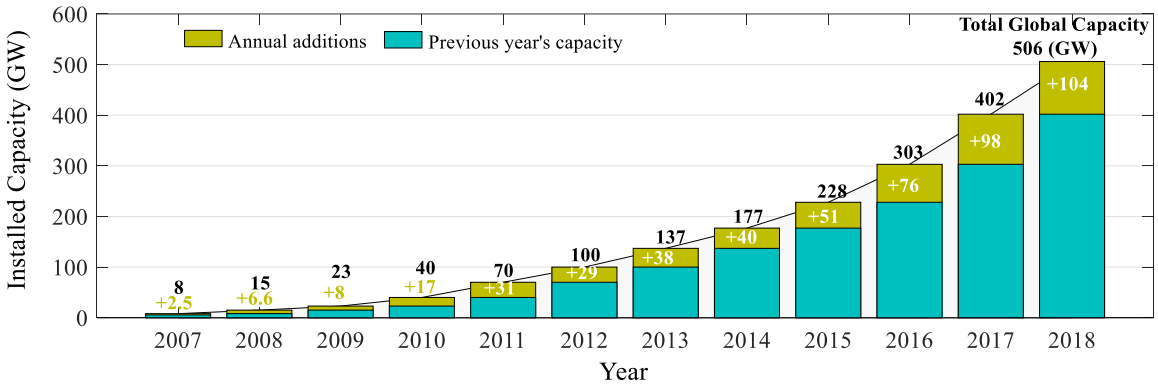

Figure 1.1: Solar PV global capacity and annual additions from 2007 to 2018.

Principally, PV systems can be classified into two application fields which are off-grid and grid-tied [1.4]. In off-grid applications, the PV generator is used to supply energy to remote DC or AC loads that are not attached to the electric grid which is unavailable or expensive. Similarly, storage batteries are required in this application to store excess energy. There are different manners of the use as, small-scale production systems, water pumping system [1.5].

In grid-tied applications, the energy produced from PV generator can be directly converted to AC and injected into the utility grid, where the power injection must be in accordance with internationally agreed conditions. Furthermore, this application includes two systems types which are distributed generation and centralized power systems. The first type is installed to supply power to a grid-tied customer or directly to the grid. Whilst, the other type is mainly installed to reduce greenhouse gases caused by polluted energy sources[1.6].

1.2 OVERVIEW OF GRID-TIED PHOTOVOLTAIC SYSTEMS

Owing to the cost reduction of solar photovoltaic and the development in power electronics helps to produce electricity at high efficacy and make it possible to supply power directly to the utility grid. Currently, Grid connection is the most requested on the PV market, because there is better usage of PV energy and more energy is acquired. Also, it is not relying on energy storage devices which allows a reduced cost with less maintenance[1.7-11].

Typically, there are different management topologies for these PV systems connected to the grid. Nevertheless, the main function of these approaches is to convert the DC power generated by PV panels into grid-synchronized AC power. This processes is specified only by inverters , which is considered as the key elements of PV systems connected to the grid. The

progress made in the development of PV inverters allowed to a significant improvement of these management systems. The inverters are not limited only to the principal operation (DC-AC conversion), but they also exploit the current provided by the photovoltaic generator for forcing it to operate at its maximum power point. In addition, they provide reliable grid monitoring to finally protect against failures and interruptions, in case of power problems, whether the grid or the installation[1.9-11]. Currently, there are three PV power plant topologies offer good technical solutions: the centralized inverters, string inverters and multi-string inverters as shown in Figure 1.2.

In centralized inverters, a number of PV modules was assembled in series and in parallel connection, so called PV array, to provide high power levels. In this topology, a central DC-AC inverter is placed between the PV array and utility grid, as shown in Figure 1.2(a). The main benefit of the this topology is its low cost compared to other topologies, as well as the easiness of maintenance of the inverter. Nevertheless, several limitations are noted in this topology, such as significant power losses due to a centralized maximum power point tracking and mismatch losses between the photovoltaic modules [1.9-11].

In the string inverters, a number of PV modules connected in series is called string. As their name indicates, each string is attached to individual DC-AC inverter, as shown in Figure 1.2(b); consequently, the reliability of the system is improved. Additionally, since each string can operate separately at its own maximum power point, the losses due to partial shading are reduced. But, depending on the number of inverters, the main disadvantage is the expensive cost [1.9-11].

In multi-string inverters, each string is connected to its individual DC-DC converter for the maximum power point tracking and voltage amplification. All the DC-DC converters are then linked to a common DC-AC inverter via a DC bus, as shown in Figure 1.2(c). This topology encompasses the benefits of string and centralized topologies. So, the output power is increased since every string can be controlled individually, then the total cost is reduced as it uses only one inverter. Conversely, there is an increase in losses due to the DC-DC converters that are added [1.9-11].

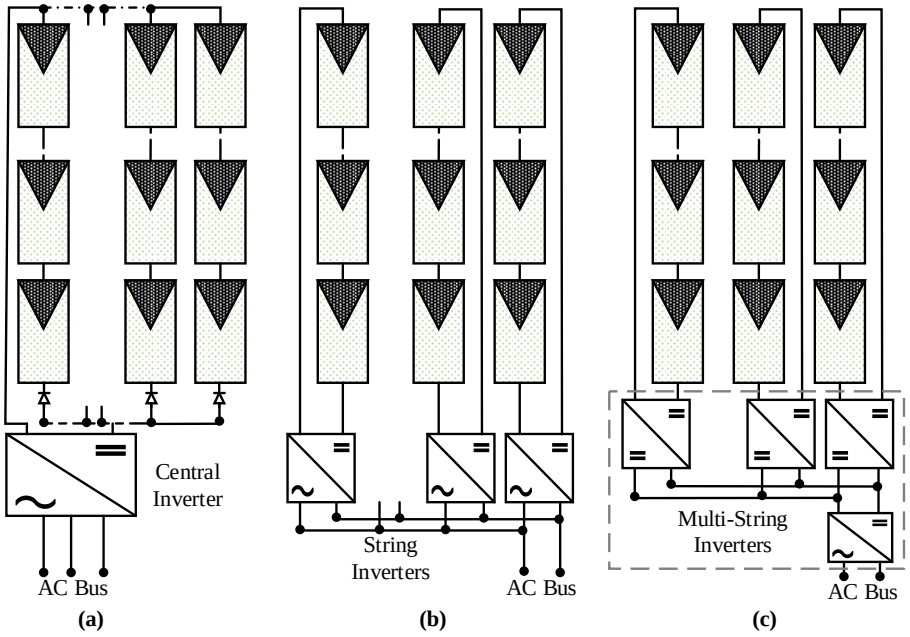

Figure 1.2: PV grid-tied systems topologies a).Central Inverter; b). String Inverters; c).Multi-String Inverters.

In term of power processing stages, a grid-tied PV system can be classified into two configurations type, single and dual stages configuration[1.11-26].

In single-stage configurations, the conversion process includes only a DC-AC inverter to perform all the control tasks as maximum power point tracking (MPPT), control of grid current and voltage amplification. Thus, this configuration poses difficulties of control and implementation offering less efficiency. Different types of DC-AC inverters have been employed to improve and regulate the performance, such as two-level [1.11-14], multilevel [1.15-18], Z source voltage inverters [1.19] and split-source inverter [1.20]. Figure 1.3 illustrates the block diagram of a single-stage grid-tied PV system.

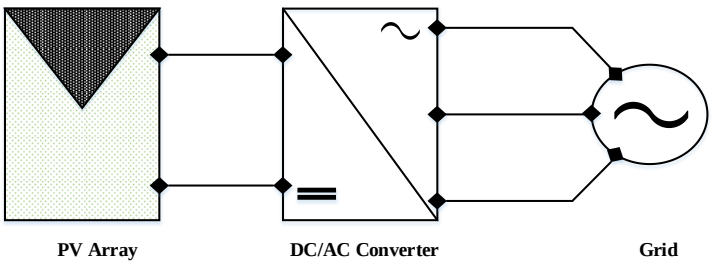

Figure 1.3: Block diagram of a single-stage grid-tied PV system.

In two-stage configuration, the conversion process contains two stages. The first stage is the DC-DC converter used to amplify the PV array voltage and track the maximum power. To perform these operations, different types of DC-DC converters are employed such as boost

[1.21-24], buck-boost[1.25] and zeta [1.26]. The second stage is the DC-AC inverter used to regulate the DC-Link voltage and to control the injected grid current. Two-stage systems provide high flexibility in control as compared to single-stage systems, since the control tasks are divided among the two converters. A block diagram of a two-stage grid-tied PV system is shown in Figure 1.4.

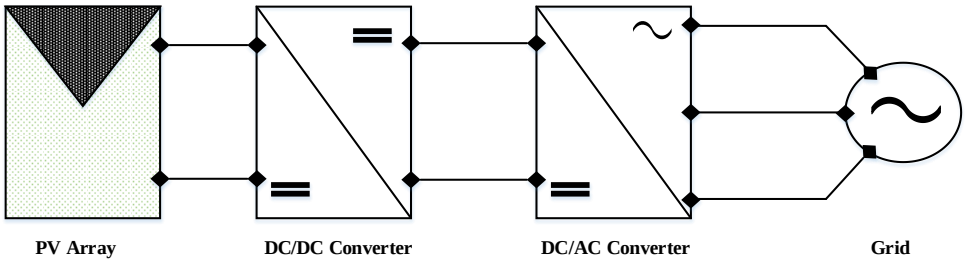

Figure 1.4: Block diagram of a two-stage grid-tied PV system.

1.3 STANDARDS FOR GRID CONNECTION OF PHOTOVOLTAIC SYSTEMS

At the first, an interconnection system is the equipment that makes up the physical link amongst distributed energy resources (DER) and the electric grid. In the grid-tied photovoltaic application, the inverter is the key element which converts the DC power into AC power. But, it also generates an important harmonic disturbance caused by its switching devices. For this purpose, the interconnection of DER with the grid is restricted by several international standards like International Electro technical Commission (IEC), Institute of Electrical and Electronics Engineers (IEEE) [1.7-11]. For uninterrupted operation within the limits specified in standards, some important terms such as total harmonic distortion, DC injection, galvanic isolation, detection and counter-voltage must be included in the frequency bands [1.27-28].

In this section, we will present briefly the most relevant standards IEC 61727 and IEEE 1547–2003. Similarly, Table 1.1 presents the parameters of these standards depending on the previous terms.

IEC 61727 standard focuses on grid-tied photovoltaic (PV) systems that use inverters based on a semiconductor device for DC to AC conversion. It provides specific recommendations for systems of 10 kVA or less that can be used in individual-home, whether single-phase or three-phase. This standard concerns the connection to the grid with low-voltage distribution, as well explained in literature [1.29] shows the necessity and important information for proper installation of PV system.

IEEE 1547-2003 Standard provides guidelines for the interconnection of distributed energy resources (DER) with a grid system. It provides requirements for the performance, operation, testing, security, and maintenance of the interconnection[1.30].

TABLE 1.1: Standards for grid-tied PV system.

Parameters	IEC 61727	IEEE 1547
THD	< 5 %	< 5 %
Power Factor	0.90	0.90
DC current injection	Less than 1% of rated output current	Less than 0.5 % of rated output current
Voltage range for normal operation	85 % to 110 %	88 % to 110 %
Frequency range for normal operation	49 Hz to 51 Hz	59.3 Hz to 60.5 Hz

1.4 MOTIVATION

The efficiency of a grid-tied photovoltaic system depends on the choice of configurations or topologies, the types of power converters and their control. In this way, it is important to know the effect of different operating conditions on the complete power conversion chain, then deal with them, or rather to achieve the best performance from each system element under any operating conditions. Also, it is necessary to design an effective controller able to harvest as much as possible the produced energy from the photovoltaic generator under changing atmospheric conditions, then to inject it into the electrical grid with a high quality. In other hand, it is due to the high flexibility in the control provided by two-stage grid-tied PV systems. Hence, in each control part, several controller schemes have been proposed in the literature; nevertheless, most of those controllers suffer from disadvantages.

The motivation for this thesis is to develop new control strategies that are simple and robust to working condition changes. The proposed strategies are based on sliding mode control theory and involve three control parts. The MPPT methods should be capable of extracting maximum power from the PV array taking into account all the challenges that are existing in the literature (e.g. sudden changing atmospheric conditions, tracking accuracy, etc.). Then, the DC-AC inverter in the system should have a good DC-Link controller, which can offer fast transient response and high control accuracy. Finally, the current injected into the electrical grid must have a low total harmonic distortion (THD <5%) in accordance with international limits.

1.5 STRUCTURE OF THE THESIS

Beside the current chapter, the remaining of the thesis is structured asfollows:

Chapter-2: This chapter provides the modeling and sizing of all constituent elements in a two-stage grid-tied photovoltaic system. Because these procedures are used in the later chapters for clarifying the control design and simulation work.

Chapter-3: This chapter presents a comprehensive review of the maximum power point tracking (MPPT) control, the DC-Link voltage regulation, and the injected grid current control for two-stage grid-tied PV system.

Chapter-4: This chapter presents a maximum power point tracking technique based on sliding mode control. The proposed adaptive integral derivative sliding mode controller is combined with voltage based on perturb and observe algorithm. Numerical simulations and real-time hardware in the loop implementations are provided to validate the performance enhancement of the proposed schemes.

Chapter-5: This chapter presents a robust control of two-stage grid-tied photovoltaic system. The overall proposed control scheme based on the integral sliding mode control theory. Numerical simulations and real-time hardware in the loop implementation are provided to validate the performance enhancement of the proposed control scheme.

Chapter-6: This chapter presents the summary and conclusion of the thesis. Moreover, this chapter describes the contributions of the thesis presented and possible extensions to the research presented in this thesis.

REFERENCES

[1.1] Renewable Energy Policy Network for the 21st Centuray (REN21), 2018. Global Solar Energy Council (GSEC). [Online]. Available: http://www.ren21.net/.

[1.2] European Photovoltaic Industry Association (EPIA), 2012, Global Market Outlook for Photovoltaics until 2018. [Online]. Available: http://www.epia.org/.

[1.3] Romero-Cadaval, E., Spagnuolo, G., García Franquelo, L., Ramos-Paja, C.A., Suntio, T. and Xiao, W.M., 2013. Grid Connected Photovoltaic Generation Plants. Components and Operation. IEEE Industrial Electronics Magazine, 7 (3), 6-20.

[1.4] Madeti, S.R., Singh, S.N., 2017. Monitoring system for photovoltaic plants: A review. Renew. Sustain. Energy Rev. 67, 1180–1207.

[1.5] Talbi, B., 2018. Contribution à l'Amélioration de la commande d'un système de pompage photovoltaïque. PhD. thesis, University of Ferhat Abbas Sétif 1.

[1.6] Kouro, S., Leon, J.I., Vinnikov, D. and Franquelo, L.G., 2015. Grid-connected photovoltaic systems: An overview of recent research and emerging PV converter technology. IEEE Industrial Electronics Magazine, 9(1), 47-61.

[1.7] Teodorescu, R., Liserre, M. and Rodriguez, P., 2011. Grid converters for photovoltaic and wind power systems (Vol. 29). John Wiley & Sons.

[1.8] Zhang, L., Sun, K., Xing, Y., Feng, L. and Ge, H., 2011. A modular grid-connected photovoltaic generation system based on DC bus. IEEE transactions on power electronics, 26(2), 523-531.

[1.9] Omran, W., 2010. Performance analysis of grid-connected photovoltaic systems. PhD. thesis, University of Waterloo.

[1.10] Abu-Rub, H., Malinowski, M. and Al-Haddad, K., 2014. Power electronics for renewable energy systems, transportation and industrial applications. John Wiley & Sons.

[1.11] Malek, H., 2014. Control of grid-connected photovoltaic systems using fractional order operators. PhD. thesis, University of Utah State.

[1.12] Libo, W., Zhengming, Z. and Jianzheng, L., 2007. A single-stage three-phase grid-connected photovoltaic system with modified MPPT method and reactive power compensation. IEEE Transactions on Energy Conversion, 22(4), 881-886.

[1.13] Libo, W., Zhengming, Z. and Jianzheng, L., 2007. A single-stage three-phase grid-connected photovoltaic system with modified MPPT method and reactive power compensation. IEEE Transactions on Energy Conversion, 22(4), 881-886.

[1.14] Shayestehfard, A., Mekhilef, S. and Mokhlis, H., 2017. IZDPWM-based feedforward controller for grid-connected inverters under unbalanced and distorted conditions. IEEE Transactions on Industrial Electronics, 64(1), 14-21.

[1.15] Selvaraj, J. and Rahim, N.A., 2009. Multilevel inverter for grid-connected PV system employing digital PI controller. IEEE transactions on industrial electronics, 56(1), 149-158.

[1.16] Jain, S. and Sonti, V., 2017. A highly efficient and reliable inverter configuration based cascaded multilevel inverter for PV systems. IEEE Transactions on Industrial Electronics, 64(4), 2865-2875.

[1.17] Kim, J.S., Kwon, J.M. and Kwon, B.H., 2018. High-efficiency two-stage three-level grid-connected photovoltaic inverter. IEEE Transactions on Industrial Electronics, 65(3), 2368-2377.

[1.18] Rojas, F., Kennel, R., Cardenas, R., Repenning, R., Clare, J.C. and Diaz, M., 2017. A new space-vector-modulation algorithm for a three-level four-leg NPC inverter. IEEE Transactions on Energy Conversion, 32(1), 23-35.

[1.19] Hanif, M., Basu, M. and Gaughan, K., 2011. Understanding the operation of a Z-source inverter for photovoltaic application with a design example. IET Power Electronics, 4(3), 278-287.

[1.20] Abdelhakim, A., Mattavelli, P., Boscaino, V. and Lullo, G., 2017. Decoupled control scheme of grid-connected split-source inverters. IEEE Transactions on Industrial Electronics, 64(8), 6202-6211.

[1.21] Singh, A.K., Hussain, I. and Singh, B., 2018. Double-stage three-phase grid-integrated solar PV system with fast zero attracting normalized least mean fourth based adaptive control. IEEE Transactions on Industrial Electronics, 65(5), 3921-3931.

[1.22] Chen, Y. and Smedley, K., 2008. Three-phase boost-type grid-connected inverter. IEEE Transactions on Power Electronics, 23(5), 2301-2309.

[1.23] Sebaaly, F., Vahedi, H., Kanaan, H.Y., Moubayed, N. and Al-Haddad, K., 2016. Design and implementation of space vector modulation-based sliding mode control for grid-connected 3L-NPC inverter. IEEE Transactions on Industrial Electronics, 63(12), 7854-7863.

[1.24] Hu, Y., Du, Y., Xiao, W., Finney, S. and Cao, W., 2015. DC-link voltage control strategy for reducing capacitance and total harmonic distortion in single-phase grid-connected photovoltaic inverters. IET Power Electronics, 8(8), 1386-1393.

[1.25] Chomsuwan, K., Prisuwanna, P. and Monyakul, V., 2002, May. Photovoltaic grid-connected inverter using two-switch buck-boost converter. In Conference Record of the Twenty-Ninth IEEE Photovoltaic Specialists Conference, 2002. (pp. 1527-1530). IEEE.

[1.26] Lopez, H.F.M., Viero, R.C., Zollmann, C., Tonkoski, R., Reckzielgel, L., Gomes, H. and Dos Reis, F.S., 2009, October. Analog signal processing for photovoltaic panels grid-tied by Zeta converter. In 2009 IEEE Electrical Power & Energy Conference (EPEC) (pp. 1-6). IEEE.

[1.28] Francisco, C.D.L.R., 2015. Harmonics, Power Systems, and Smart Grids. CRC press.

[1.27] Karimi, M., Mokhlis, H., Naidu, K., Uddin, S. and Bakar, A.H.A., 2016. Photovoltaic penetration issues and impacts in distribution network–A review. Renewable and Sustainable Energy Reviews, 53, 594-605.

[1.29] Rangarajan, S.S., Collins, E.R., Fox, J.C. and Kothari, D.P., 2017, February. A survey on global PV interconnection standards. In 2017 IEEE Power and Energy Conference at Illinois (PECI) (pp. 1-8). IEEE.

[1.30] Obi, M. and Bass, R., 2016. Trends and challenges of grid-connected photovoltaic systems–A review. Renewable and Sustainable Energy Reviews, 58, 1082-1094.

Chapter 2

Description, Modeling and Sizing the overall elements of a Grid-Tied Photovoltaic System

2.1 INTRODUCTION

As mentioned previously, two-stage grid-tied PV system is a capable solution that ensuring the appropriate conversion of PV energy over a wide range. Figure 2.1 describes a common schematic principle for a two- stage grid-tied photovoltaic (PV) system. The different elements of this configuration are classified as following; the PV array formed by a group of PV module connected in series and parallel, which is used to produce the electrical energy through the photovoltaic effect. The input filter is used to decrease the oscillatory nature of power achieved from PV array. DC-DC boost converter, which is used to amplify the voltage of the PV array and track the maximum power. The DC-Link capacitor (or power decoupling) is placed between the output of DC-DC boost converter and DC-AC inverter input. The inverter is used to transform the DC voltage to AC voltage. The inductor filter is then used to provide a suitable coupling with the grid and reduce the current fluctuations in the lines.

After having mentioned all the components of the two-stage grid-tied PV system, as well as the role of its components on the PV system, we proceed to modeling our system. The modeling step is important and requires a set of equations that describe all elements of the studied system. In this chapter, we will represent the mathematical model of PV array, boost converter, inverter, L-filter and electrical grid. Also, we will size the value of the electrical components such as, the input capacitor, the boost inductor and the DC-Link capacitor.

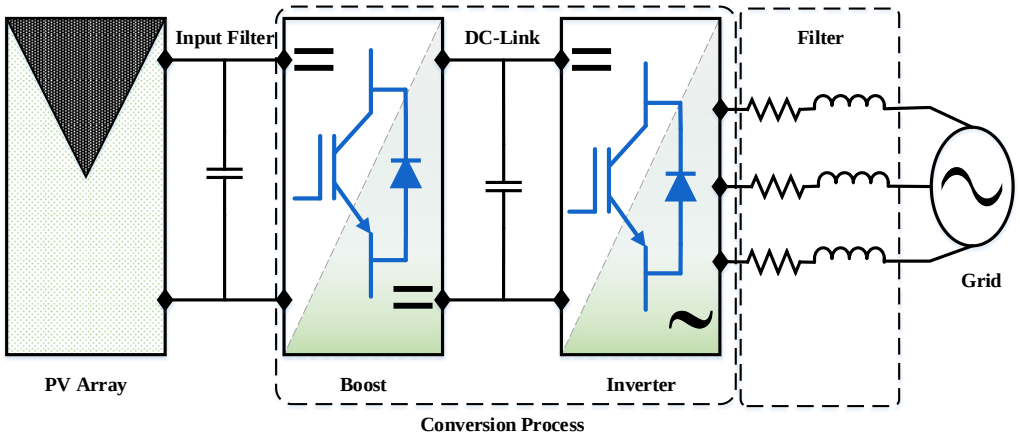

Figure 2.1: Block diagram of two-stage grid-tied PV system.

2.2 MODELING OF PHOTOVOLTAIC ARRAY

The basic element of a PV array system is the PV cell. Where, cells may be assembled to form PV modules which in turns assembled to form PV arrays as illustrated in Figure 2.2. The series and parallel PV modules provide the required voltage and current.

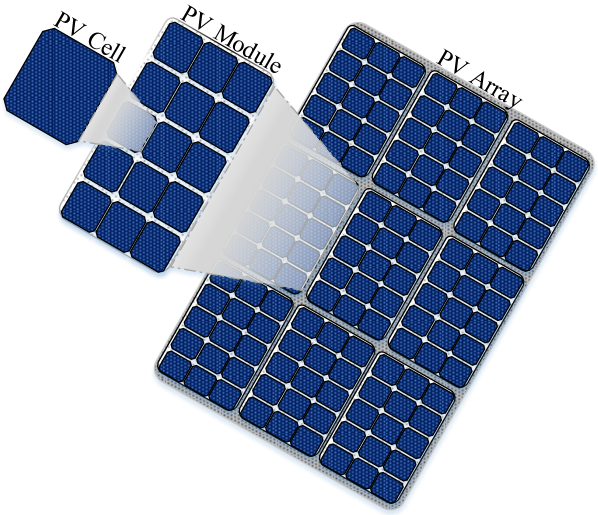

Figure 2.2: PV array system.

2.2.1Electrical Model of a PV Cell

The PV cell is semiconductor devices that convert sunlight to electricity through photovoltaic effect. The modeling of PV cell necessarily involves a careful choice of equivalent electrical circuits. Several mathematical models have been developed to represent a strongly nonlinear behavior, resulting from that of the semiconductor junctions which are at the base of their realizations. These models differ from each other by the mathematical

procedures and the number of parameters involved in the calculation of the voltage and current of the photovoltaic module [2.1-5]. A single diode electric model is the most quoted in the literature, the photovoltaic module is characterized by its equivalent electrical circuit as illustrated in Figure 2.3 which consists of a current source that models the conversion of light flux into electrical energy, a shunt resistor (R_{sh}) is a consequence of the surface state along the periphery of the cell, a series resistance (R_s).

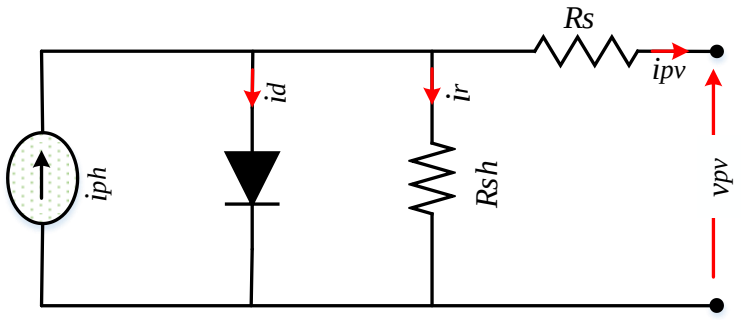

Figure 2.3: The equivalent circuit of a PV cell.

TABLE 2.1: PV cell parameters

Variables	Parameter
i_{ph}	Cell photocurrent (A).
i_d	Diode current (Shockley equation) (A).
i_r	Derived current by the shunt resistance (A).
v_{pv}	Cell output voltage (V)
i_{pv}	Cell output current (A)
R_s	Cell series parasitic resistance (Ω).
R_{sh}	Cell shunts parasitic resistance (Ω).
q	Electronic charge (1.6×10^{-19} C)
T	Absolute temperature (K).
k	Boltzmann constant (1.38×10^{-23} J/K).
n	Diode ideality factor
i_o	Reverse saturation current of the diode (A).

In view of that, the current to the load can be given as [2.1]:

$$i_{pv} = i_{ph} - i_d - i_r = i_{ph} - i_o \left[e^{\frac{q(v_{pv}+R_s\, i_{pv})}{n\, k\, T}} - 1 \right] - \frac{v_{pv} + R_s i_{pv}}{R_{sh}} \qquad (2.1)$$

Where i_{pv} is the output current of the PV cell, which is a function of its output voltage v_{pv}, and a number of variables as defined in Table 2.1.

2.2.2 PV Module I-V and P-V Characteristics

Typically, each individual PV cells gives a small power which makes it insufficient for the majority of PV applications. To provide the required power, several PV cells connected either in series or parallel are grouped to form PV module. The performance of PV modules is generally evaluated based on their maximum DC output power under standard test conditions (STC). The standard test conditions are defined by an operating temperature of the PV cell of 25 °C and an incident solar irradiance level of 1000 W / m^2. For PV modules, assuming all cells are identical and under uniform irradiance and temperature. The current expression of PV module $i_{pv,m}$ can be written as [2.1]:

$$i_{pv,m} = N_p\, i_{ph} - N_p\, i_o \left[e^{\frac{N_s\, v_{pv}+(N_s/N_p)R_s\, i_{pv}}{N_s\, n\, v_t}} - 1 \right] - \frac{N_s\, v_{pv} + (\frac{N_s}{N_p})R_s i_{pv}}{\left(\frac{N_s}{N_p}\right) R_{sh}} \qquad (2.2)$$

Where:

N_s : is the number of cells connected in series

N_p : is the number of cells connected in parallel

Different types of PV modules exist for different applications. In this thesis, the BP-MSX 120 of 120 Wp, is considered. The datasheet values for this module are represented in Table 2.2. Moreover, Figure 2.4 shows the current-voltage (I-V) and Power-voltage (P-V) characteristics of the considered PV module at STC mode. From (I-V) and (P-V) characteristic, it can be distinguished three operating points of the PV module; short-circuit current (I_{SC}) which is corresponding to zero voltage, another extreme point corresponding to zero current which called the open-circuit voltage (V_{OC}). Whilst, the third operating point is the optimal operating point MPP. These operating points are particular interest to define the performance of each PV module.

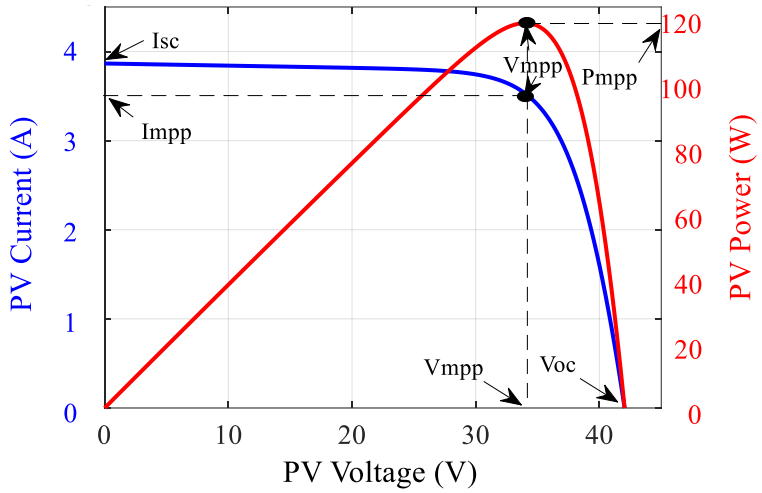

Figure 2.4: I-V and P-V characteristics of solar BP-SMX 120 module under STC.

TABLE 2.2: BP-MSX 120 module datasheet parameters [2.6]:

PV array	**Values (STC)**
Open-circuit voltage (V_{oc})	42.1 V
Optimum operating voltage (V_{mpp})	33.7 V
Short-circuit current (I_{sc})	3.87 A
Optimum operating current (I_{mpp})	3.56 A
Maximum power (P_{mpp})	120 Wp
Temperature coefficient of V_{oc}	-0.160 V/°C
Temperature coefficient of I_{sc}	0.065 %/°C

2.2.3 PV Array

Multiple modules can be wired together in series and parallel to deliver the required voltage and current. The group of connected modules is called a PV array. From equations (2.3) and (2.4), the output current and voltage of a PV array can be calculated as [2.7]:

$$i_{pv,t} = N_{pp}\, i_{pv,m} \tag{2.3}$$

$$v_{pv,t} = N_{ss}\, v_{pv,m} \tag{2.4}$$

where:

$i_{pv,t}$: is the array output current (A).

N_{pp} : is the number of modules connected in parallel

i_{pv} : is the module output current (A).

$v_{pv,t}$: is the array output voltage (V).

N_{ss} : is the number of modules connected in series

v_{pv} : is the module output voltage (V).

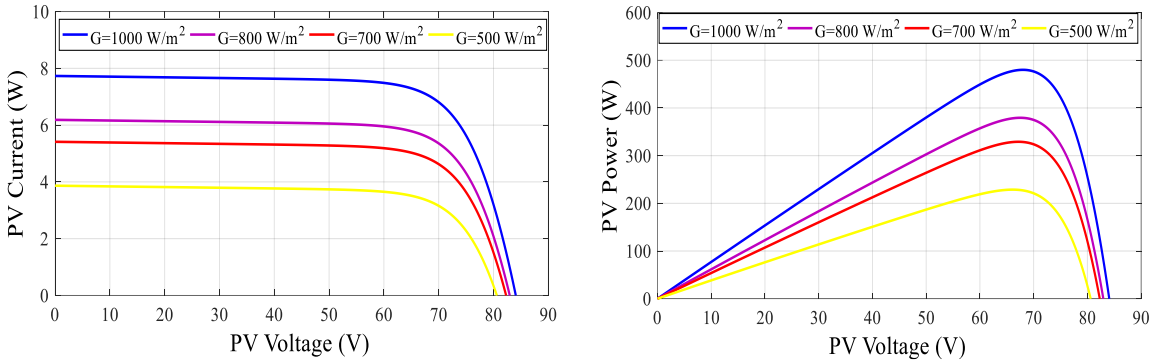

(**a**) (**b**)

Figure 2.5: (a) I-V and (b) P-V characteristics of PV array under different levels of solar irradiation at 25°C.

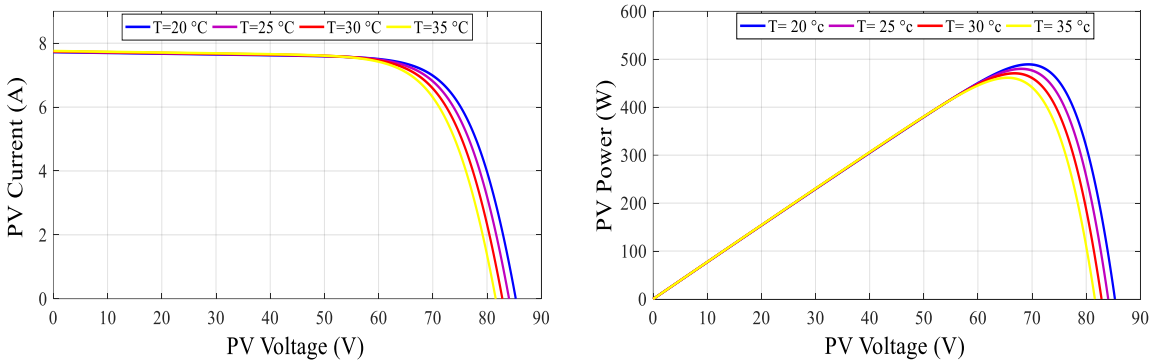

(**a**) (**b**)

Figure 2.6: (a) I-V and (b) P-V characteristics of PV array under different temperatures at 1000 W/m².

According to our consideration, the PV array is formed by four PV modules BP-MSX 120 connected 2 × 2 in series and in parallel. To display the effect of irradiation and temperature variations on the PV array, the (I–V) and (P–V) characteristics are usually introduced in order to present the electrical behavior of PV array. In Figure 2.5, a strong dependence links the PV array current to the irradiation which affects strongly the MPP of the PV array. Nevertheless, the voltage increases a little bit when the solar irradiation G is increased. In contrast, as shown in Figure 2.6, the temperature change has little effect on the MPP of the PV array. Also, it is worth noting that the temperature variations during the day are generally not important.

2.3 SIZING OF THE INPUT CAPACITANCE

The input capacitor is connected in parallel amongst the PV array and the boost converter, which is used to decrease the oscillatory nature of power achieved from PV array. As discussed in the previous section, in case of variation in temperature and irradiation, the capacitance will see the voltage ripple from the PV array MPP as Δv_{pv}, as irradiation change from 500 w/m^2 to 1000 w/m^2 , the (V_{oc}) of PV array also sees these variations and change by, $\Delta v_{pv} = 2\,V$. So, the input capacitance can be obtained using the analysis which assumes the continuous conduction mode (CCM) of the boost converter [2.8].

$$\Delta v_{pv} = \frac{D.v_{pv}}{4.f_c^2.L.C_{in}} \tag{1.5}$$

Thus, the input capacitance can be estimated as;

$$C_{in} = \frac{D.v_{pv}}{4.f_c^2.L.\Delta v_{pv}} \tag{2.6}$$

With D is the duty cycle of the boost converter and given by;

$$D = 1 - \frac{v_{pv}}{v_{dc}} \tag{2.7}$$

Where:

v_{pv}: is the boost input voltage (V).

v_{dc}: is the boost output voltage (V).

i_{pv}: is the photo-generated current (A).

L : is the boost input inductor (mH).

C_{in}: is the input capacitor (μF).

f_c : is the switching frequency of the boost converter (kHz).

2.4 POWER CONVERTERS STAGE

As known, the power converters are used to regulate the transit of electrical energy from the source to the receiver with possibly modifying the form in which this energy is presented. In PV system application, the power converter has more attention due to its control flexibility. Where, in two-stage grid-tied PV system, the conversion process consists of two stages converter (DC-DC and DC-AC converters). The first one is used to amplify the voltage of the PV array and to track the maximum power, because the energy produced by PV systems is

adversely affected by unstable weather conditions. The second stage is the DC-AC inverter used to inject the PV power into the electrical grid [2.9], as shown in Figure 2.1.

2.4.1 DC-DC Boost Converter Modeling

The DC-DC boost converter is usually used in PV systems for tracking the MPP produced by the PV array due to some of its important features, such as simplicity, robustness, and continuous input current. Figure 2.7 shows the equivalent boost circuits for both on and off switching states, with the state variables chosen as: i_L and v_{pv}.

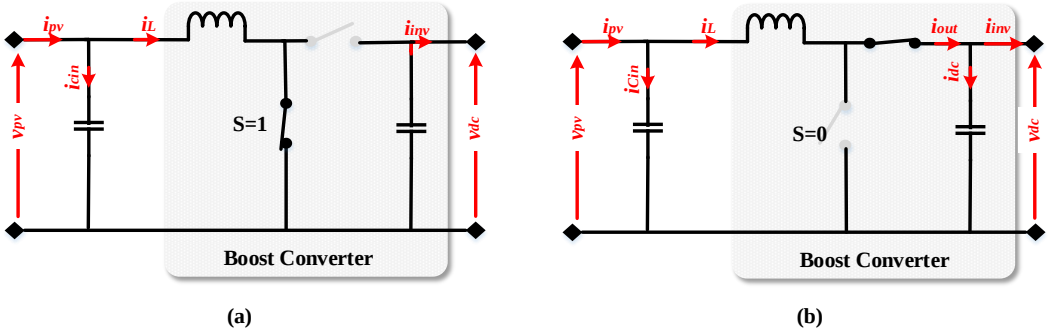

Figure 2.7: Equivalent boost circuit: (**a**) on state; (**b**) off state.

State on: when the IGBT conducting, the diode is in open circuit (Figure 2.7(a)), the state variables equations can be modeled as:

$$\begin{cases} \dfrac{dv_{pv}}{dt} = \dfrac{i_{pv} - i_L}{C_{in}} \\ \dfrac{di_L}{dt} = \dfrac{v_{pv}}{L} \end{cases} \tag{2.8}$$

State off: the IGBT in this case is considered as open (Figure 2.7(b)), the preceding equation system can be rewritten as:

$$\begin{cases} \dfrac{dv_{pv}}{dt} = \dfrac{i_{pv} - i_L}{C_{in}} \\ \dfrac{di_L}{dt} = \dfrac{v_{pv} - v_{dc}}{L} \end{cases} \tag{2.9}$$

The dynamic model of the boost converter in term of duty cycle "D" can be expressed, using averaging method presented in [2.10], as

$$\begin{cases} \dfrac{dv_{pv}}{dt} = \dfrac{i_{pv} - i_L}{C_{in}} \\ \dfrac{di_L}{dt} = \dfrac{v_{pv} - v_{dc} + Dv_{dc}}{L} \end{cases} \tag{2.10}$$

Where:

i_L: is the boost input current (A).

v_{pv}: is the boost input voltage (V).

v_{dc}: is the boost output voltage (V).

i_{pv}: is the photo-generated current (A).

L : is the boost input inductor (mH).

C_{in}: is the input capacitor (μF).

D : is the duty cycle considered as input variable.

2.4.1.1 Sizing of Boost Inductor

The inductor value is usually provided in the datasheet according to the required application. However, it is possible to estimate this value directly and without datasheet by using the following equation [2.11-12].

$$L = \frac{v_{pv}}{\Delta i_L \,.\, f_c}\left(\frac{v_{dc} - v_{pv}}{v_{dc}}\right) \tag{2.11}$$

Thus, the value of inductor ripple current Δi_L can be estimated as;

$$\Delta i_L = \varepsilon_i . i_{pv,max}\left(\frac{v_{dc}}{v_{pv}}\right) \tag{2.12}$$

Where;

ε_i : is a percentage of 20% to 40% of the maximum output current generated by the PV array $i_{pv,max}$,

f_c : is the switching frequency (KHz),

v_{dc} : is the desired DC-Link output voltage (V),

L : is the boost inductor (mH),

v_{pv}: is the input voltage of the boost (V).

2.4.1.2 Sizing of DC-Link Capacitor

Firstly, the DC-Link voltage must be regulated to a desired value higher than the grid peak voltage to ensure transfer of produced PV power into the grid, the V_{dc} reference is estimated as follows:

$$V_{dc}^{*} = \mu \sqrt{3}\, V_{m} \qquad \text{,where } \mu > 1 \tag{2.13}$$

Then, the DC-Link capacitor can be sized according to the following equation [2.11-12].

$$C_{dc} = \frac{p_{pv}}{2 \,.\, \omega \,.\, V_{dc}^{*} \,.\, \Delta V} \tag{2.14}$$

Where,

ΔV : is the amplitude of voltage ripple, then equal to 10% of grid peak voltage (V_m),

p_{pv} : is the nominal power of PV modules,

ω : is the rotational frequency of the generated sine wave,

V_{dc}^{*} : is the mean voltage across the capacitor.

2.3.2 DC-AC Inverter Model

The PV inverter is the key part of grid-tied PV power systems. The main role is to convert the harvested PV power from DC form into grid-synchronized AC form and controls the power flow between the DC-DC boost converter and the grid by controlling the current injected into the grid. Depending on the PV power plant configuration, there are some PV inverter topologies and categories; a two-level voltage source inverter (VSI) is one of them. Where, six switches are used in the main circuit, each composed traditionally of a power insulated gate bipolar transistor (IGBT) and a free-wheeling diode to provide bidirectional current flow and a unidirectional voltage blocking capability, as presented in Figure 2.8. To avoid the short-circuit of the DC-Link; both of the switches in the same leg must be turned in a complementary mode [2.10-13].

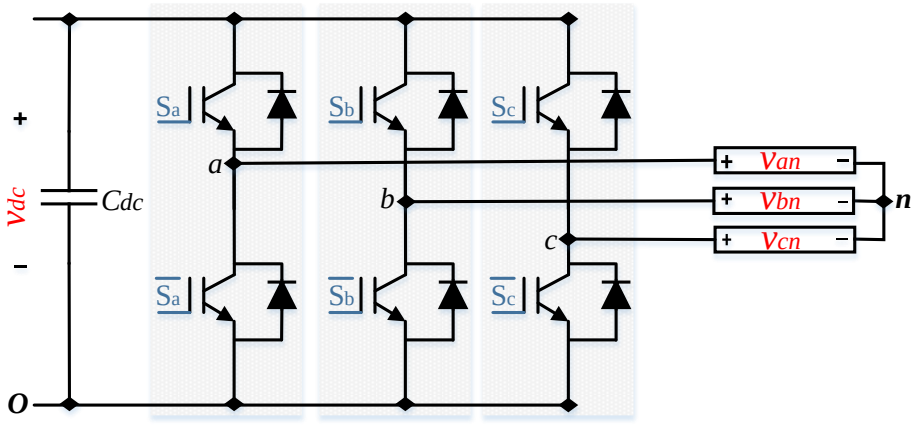

Figure 2.8: Three-phase two-level inverter topology.

The inverter has eight switch states given in Table 2.3, two of these switch states provide zero AC line voltage at the output. In this case, the AC line currents freewheel through either the upper or lower components. The other states provide no zero AC output line voltages. In order to generate a given voltage waveform, the inverter switches from one state to another. Thus the resulting AC output line voltages consist of discrete values of voltages, which are" $-v_{dc}$", "0", and"v_{dc}" [2.13].

TABLE 2.3: The switching states in a three-phase inverter.

S_a	S_b	S_c	v_{ab}	v_{bc}	v_{ca}
0	0	0	0	0	0
0	0	1	0	$-v_{dc}$	v_{dc}
0	1	0	$-v_{dc}$	v_{dc}	0
0	1	1	$-v_{dc}$	0	v_{dc}
1	0	0	v_{dc}	0	$-v_{dc}$
1	0	1	v_{dc}	$-v_{dc}$	0
1	1	0	0	v_{dc}	$-v_{dc}$
1	1	1	0	0	0

By assuming that the switches and diodes are ideal, the composite voltages (v_{ab}, v_{bc}, v_{ca}) are obtained from these relationships:

$$\begin{cases} v_{ab} = v_{aO} - v_{bO} \\ v_{bc} = v_{bO} - v_{cO} \\ v_{ca} = v_{cO} - v_{aO} \end{cases} \quad (2.15)$$

Where;

v_{ao}, v_{bo}, v_{co} are the phase-to-neutral voltages of the inverter. The point "O" is taken as a reference for these last voltages.

The three voltages at the continuous input are given by the following relations:

$$\begin{cases} v_{aO} = v_{an} - v_{no} \\ v_{bO} = v_{bn} - v_{no} \\ v_{cO} = v_{cn} - v_{no} \end{cases} \quad (2.16)$$

Where v_{an}, v_{bn}, v_{cn} are the output voltages of the inverter (phase voltages) and v_{nO} is the neutral voltage of the load related to "O" point.

As we are dealing with balanced voltages, which means

$$v_{an} + v_{bn} + v_{cn} = 0 \quad (2.17)$$

By replacing equation (2.17) into equation (2.16), we get

$$v_{nO} = \frac{1}{3}(v_{aO} + v_{bO} + v_{cO}) \quad (2.18)$$

Then replacing equation (2.18) in equation (2.16) we get:

$$\begin{cases} v_{an} = \frac{1}{3}(2v_{aO} - v_{bO} - v_{cO}) \\ v_{bn} = \frac{1}{3}(2v_{bO} - v_{aO} - v_{cO}) \\ v_{cn} = \frac{1}{3}(2v_{cO} - v_{aO} - v_{bO}) \end{cases} \quad (2.19)$$

The inverter output voltages can be expressed in terms of DC-Link voltage and switching states as follows [2.10]:

$$\begin{cases} v_{aO} = v_{dc}.S_a \\ v_{bO} = v_{dc}.S_b \\ v_{cO} = v_{dc}.S_c \end{cases} \quad (2.20)$$

By replacing the previous equation into equation (2.20), equation (2.19) becomes,

$$\begin{pmatrix} v_{an} \\ v_{bn} \\ v_{cn} \end{pmatrix} = \frac{v_{dc}}{3} \begin{bmatrix} 2 & -1 & -1 \\ -1 & 2 & -1 \\ -1 & -1 & 2 \end{bmatrix} . \begin{bmatrix} S_a \\ S_b \\ S_c \end{bmatrix} \quad (2.21)$$

where:

S_a, S_b, S_c : are the switching signals of the inverter,

v_{dc} : is the inverter input voltage (V).

2.5 GRID SIDE FILTER MODELLING

The inverter cannot be directly coupled to the grid, because the inverter is based on switching devices and gating signals in the form of pulses must be provided for the switches, which led to an important harmonic disturbance on the output current which degrades power quality. For this reason, in this design, the connection of the inverter to the grid is done through a first-order LR-filter in order to reduce the harmonics present in the current as shown in Figure 2.9, respect the alternation of sources and to prevent the components, so that it is within limits set by the standards that are in place for grid connection of PV system [2.14].

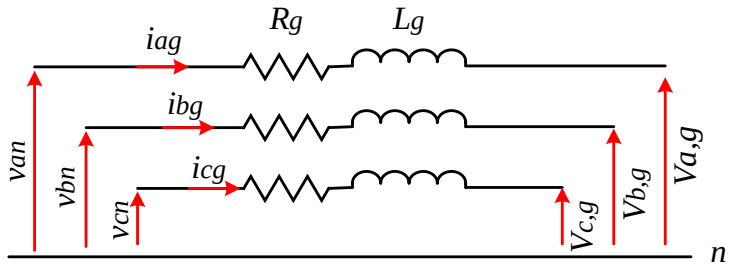

Figure 2.9: RL filter representation.

By applying Kirchhoff's voltage law (KVL), each phase at the connection point of the filter gives the equations which link the voltages modulated by the converter and the currents passing through the filter:

$$\begin{cases} v_{an} = R_g.i_{ag} + L_g\dfrac{di_{ag}}{dt} + V_{a,g} \\ v_{bn} = R_g.i_{bg} + L_g\dfrac{di_{bg}}{dt} + V_{b,g} \\ v_{cn} = R_g.i_{cg} + L_g\dfrac{di_{cg}}{dt} + V_{c,g} \end{cases} \tag{2.22}$$

From where;

$$\begin{cases} \dfrac{di_{ag}}{dt} = \dfrac{1}{L_g}\left(v_{an} - V_{a,g} - R_g.i_{ag}\right) \\ \dfrac{di_{bg}}{dt} = \dfrac{1}{L_g}\left(v_{bn} - V_{b,g} - R_g.i_{bg}\right) \\ \dfrac{di_{cg}}{dt} = \dfrac{1}{L_g}\left(v_{cn} - V_{c,g} - R_g.i_{cg}\right) \end{cases} \tag{2.23}$$

To calculate the inductor "L_g" values, considering all the calculations are made for a single phase, the inverter side inductor is estimated as [2.14],

$$L_g = \frac{\sqrt{3}.m.v_{dc}}{12.h.f_s.\Delta i_{L_g}} \quad (2.24)$$

Then, "Δi_{L_g}" denotes a ripple current of 5% of the rated current.

Where;

L_g : is the inverter side inductor (*mH*),

R_g : is the internal resistance of the filter (Ω),

f_s : is the switching frequency of the inverter (*Hz*),

v_{dc}: is the desired DC-Link voltage (*V*),

h: is the overloading factor, which value equal to1.2,

m: is the modulation indices chosen between [0.5-1].

2.5 GRID MODELLING

In any electrical system, loads are the elements that consume electrical energy. Then, the consumption of this electrical power depends on the characteristics of the load. A correct modeling of these characteristics is essential to represent finely the behavior of the load connected to the inverter. In our work, the electrical grid is considered as a load and a mathematical model of three-phase voltage source can be expressed by the following equations.

$$\begin{cases} V_{a,g}(t) = V_m.\sqrt{2}.\sin(wt) \\ V_{b,g}(t) = V_m.\sqrt{2}.\sin\left(wt - \frac{2\pi}{3}\right) \\ V_{c,g}(t) = V_m.\sqrt{2}.\sin\left(wt - \frac{4\pi}{3}\right) \end{cases} \quad (2.25)$$

Where,

$V_{a,g}(t)$, $V_{b,g}(t)$ and $V_{c,g}(t)$: are the grid voltages (*V*),

w : is the angular frequency (*rad/s*),

V_m : is the max value of grid peak voltage (*V*).

2.6 CONCLUSION

The main purpose of this chapter is to modeling and sizing the different components of the PV plant, including in the proposed grid-tied PV system. This step is necessary for the control system and simulation work in the next chapters. Firstly, the mathematical model of; the photovoltaic cell, module and array, and their characteristic curves have been defined.

Then, the electrical circuit and the mathematical model of the power converter used in the proposed system have been presented. Moreover, the L-filter and the electrical grid are modeled to facilitate the injection control operation. Finally, an approach to estimate the component size such as, input capacitor, boost inductor, DC-Link capacitor and output filter (L-filter) has been presented, which in turns allows to simplify the sizing calculation of the proposed system in the next chapter.

REFERENCES

[2.1] Villalva, M.G., Gazoli, J.R., Filho, E.R., 2009. Comprehensive approach to modeling and simulation of photovoltaic arrays. IEEE Trans. Power Electron. 24, 1198– 1208.

[2.2] Farivar, G., Asaei, B., 2011. A new approach for solar module temperature estimation using the simple diode model. IEEE Trans. Energy Convers. 26 (4), 1118–1126.

[2.3] Rekioua, D., Matagne, E., 2012. Optimization of Photovoltaic Power Systems. Springer Verlag.

[2.4] Bishop, J.W., 1988. Computer simulation of the effects of electrical mismatches in photovoltaic cell interconnection circuits. Solar Cells 25, 73–89.

[2.5] Kassis, A., Saad, M., 2010. Analysis of multi-crystalline silicon solar cells at low illumination levels using a modified two-diode model. Solar Energy Materials and Solar Cells 94 (12), 2108–2112.

[2.6] BP Solar Arrays Datasheet, 2001. [Online]. Available: http://www.eastcountysolar. com/pdf/BPSX120.pdf.

[2.7] Alajmi, B., 2013. Design and control of photovoltaic systems in distributed generation. PhD. thesis, University of Strathclyde.

[2.8] Gao, F., Li, D., Loh, P.C., Tang, Y. and Wang, P., 2009, September. Indirect dc-link voltage control of two-stage single-phase PV inverter. In 2009 IEEE energy conversion congress and exposition. 1166-1172.

[2.9] Abu-Rub, H., Malinowski, M., Al-Haddad, K., 2014. Power electronics for renewable Energy systems, transportation and industrial applications. John Wiley & Sons.

[2.10] Luo, F. L., Ye, H., 2004. Advanced DC-DC converters. CRC Press Boca Raton.

[2-11] Singh, A.K., Hussain, I. and Singh, B., 2018. Double-stage three-phase grid-integrated solar PV system with fast zero attracting normalized least mean fourth based adaptive control. IEEE Transactions on Industrial Electronics. 65(5), 3921-3931.

[2-12] Massawe, H.B., 2013. Grid Connected Photovoltaic Systems with SmartGrid functionality (Master's thesis, Institutt for elkraftteknikk).

[2-13] Orłowska-Kowalska, T., Blaabjerg, F. and Rodríguez, J. eds., 2014. Advanced and intelligent control in power electronics and drives (Vol. 531). Springer.

[2.14] Singh, B., Chandra, A. and Al-Haddad, K., 2014. Power quality: problems and mitigation techniques. John Wiley & Sons.

Chapter 3

An Overview on Control of Two Stage Grid-Tied PV Systems

3.1 INTRODUCTION

The efficiency of complete power conversion chain depends not only on the types of power converters and their configurations or topologies, but also on the control scheme applied. In the present chapter, the two stage grid-tied photovoltaic (PV) configurations have been studied. The typical control requirements for this configuration included maximum power point tracking (MPPT), DC-Link voltage control, grid synchronization, and control of power injected into the grid. The main purpose of these control tasks is to confirm that the grid-tied PV system is working at the MPP during different operating conditions as well as to ensure injection of the produced power into the electrical grid with minimum loss and low total harmonic distortion at all operating points.

This chapter gives an overview of control structures for two stage grid-tied PV systems. In the first section, the concepts of numerous conventional and advanced MPPT methods are described. In the second section, the different control designs of DC-Link voltage are presented. The third section presents a brief description of used phase looked loop (PLL) to synchronize the PV system with utility grid. Finally, the last section gives an overview of the state of the art in grid-tied inverter control and highlights acknowledged weakness in these methods.

3.2 MAXIMUM POWER POINT TRACKING

Since the discovery of photovoltaic cells, many researches have been developed to strengthen the PV array to provide the maximum power. Several MPPT techniques and designs are available in the literature. Each technique has its specific features, limitations and applications. This section presents briefly some MPPT strategies which have been proposed with different levels of complexity, cost, convergence speed, and overall output efficiency [3.1-7].

3.2.1 Basic MPPT Algorithms

3.2.1.1 Open-circuit voltage (OCV) & short-circuit current (SCC) methods

At the MPP, the PV voltage is approximately linear to its open-circuit voltage (*Voc)*, which makes it possible to implement this method. The relationship is given in equation (3.1) where the proportionality constant (*koc*) depends mainly on the PV fill factor, cell technology and climatic conditions.

$$V_{mpp} = k_{oc}\, V_{oc} \tag{3.1}$$

This property can be implemented with the flowchart shown in Figure 3.1(a). The system is periodically interrupted to measure the open-circuit voltage. Subsequently, the MPP is updated based on the relation given in equation (3.1) and the operating voltage is adjusted to the optimum voltage point. Although, this method is apparently simple, it is difficult to choose an optimal value for the constant (*koc*). However, the literature [3.4-5] reports (*koc*) values ranging from 0.73 to 0.80. The reference voltage represented by the open-circuit voltage (*Voc*) is chosen as a fixed fraction, and it remains constant for a widely varying climatic conditions. The accuracy of the operating voltage to match the maximum voltage (*Vmpp*) depends on the choice of this fraction compared with the real relationship of (*Vmpp*) and (*Voc*). Hence, the extracted power is not maximized.

Similar to the open-circuit tracking method, this tracking method is based on the observed fact of the linear dependency between the PV current at MPP and the short-circuit current, thus satisfying the relationship of equation (3.2). As does the previous method, the proportionality constant depends mainly on the PV cell technology, meteorological conditions and the fill factor. However, the constant (*ksc*) can be considered to be around 0.85 for poly-crystalline PV modules [3.4-5].

$$I_{mpp} = k_{sc}\, V_{sc} \tag{3.2}$$

However, in many cases (*ksc*) is determined by performing a PV scanning every several minutes. After (*ksc*) is obtained, the system remains with the approximation of equation (3.2), until the next calculation of (*ksc)*. The flowchart of short-circuit current method is shown in Figure 3.1(b). Therefore, this method offers the same advantages and disadvantages as the above-mentioned control method [3.5].

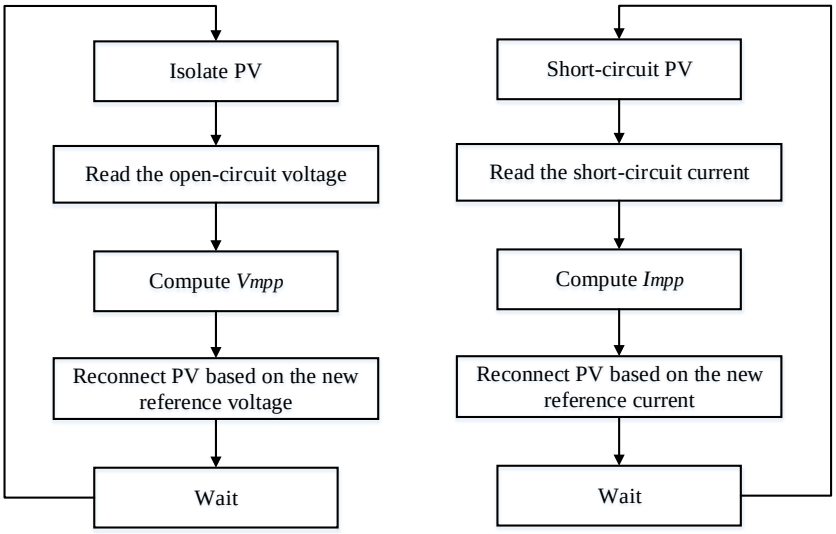

Figure 3.1: (a) Open-circuit voltage algorithm flowchart, (b) short-circuit current algorithm flowchart.

3.2.1.2 Perturb and observe (P&O) technique

The P&O technique is the most frequently employed in practice. This technique is based on the permanent perturbation of the operating point voltage and observation of the effect of this perturbation on the output power in order to determine the direction of the next perturbation leading to the MPP. If the PV array power increases with the operating voltage ($dPpv/dVpv > 0$), the control system adjusts the PV array operating point in the same direction. Otherwise, the operating point is moved in the inverse direction [3.8-10]. This process is repeated until reaching the MPP. The maximum point is reached when ($dPpv/dVpv = 0$). The P&O algorithm can be used as an external control loop to generate a reference signal (voltage or current) or as a duty cycle signal of the DC-DC interfacing converter. The basic flowchart of the P&O algorithm is shown in Figure 3.2. The main advantage of this technique is that the knowledge of the PV characteristics is not essential and applies to all types of PV modules. However, this technique suffers from some disadvantages such as; the

tracking speed and the perturbation step as indicated in [3.9]. For fixed perturbation step values, the steady-state fluctuations are related to the step value. Bigger step values cause greater oscillations. Unfortunately, lesser step values result in a slower response. Therefore, the problem of resolution between faster response and smaller steady-state oscillations is inherent. For an improved performance, P&O with variable steps have been reported in many researches [3.10]. Although these techniques exhibit improved behavior compared to the fixed step P&O, they suffer from a high calculation limit due to aggressive derivatives [3.11].

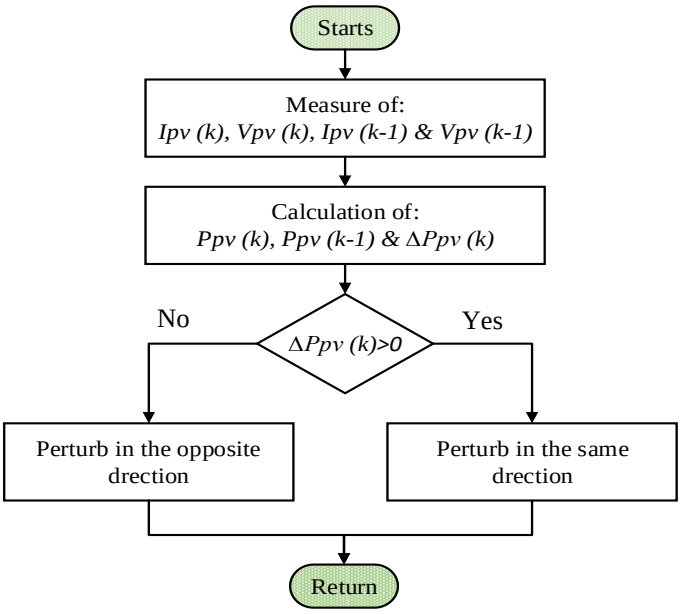

Figure 3.2: Conventional P&O algorithm flowchart.

3.2.1.3 Incremental conductance (IC) technique

The main key of the incremental conductance (IC) algorithm is that, at the MPP, the derivative of the PV power with respect to the PV voltage becomes zero because the MPP is the maximum point of the power curve [3.11, 17-18], as depicted in Figure 3.3. From this figure, we note that the power increases with the voltage in the left side of the MPP, i.e. $dP_{pv}/dV_{pv} > 0$, and in the right side of the MPP, the power decreases with voltage, i.e. $dP_{pv}/dV_{pv} < 0$. This can be rewritten in the following equations:

$$\begin{cases} \frac{dP_{pv}}{dV_{pv}} = 0\,, & \text{at MPP} \\ \frac{dP_{pv}}{dV_{pv}} > 0\,, & \text{left to MPP} \\ \frac{dP_{pv}}{dV_{pv}} < 0, & \text{right to MPP} \end{cases} \tag{3.3}$$

In addition, these equations can be written in terms of the PV array current and voltage using:

$$\frac{dP_{pv}}{dV_{pv}} = \frac{d(I_{pv}V_{pv})}{dV_{pv}} = I_{pv} + V_{pv}\frac{dI_{pv}}{dV_{pv}} \tag{3.4}$$

Hence, equation (3.4) can be rearranged in the following form:

$$\frac{1}{V_{pv}}\left(\frac{dP_{pv}}{dV_{pv}}\right) = \frac{I_{pv}}{V_{pv}} + \frac{dI_{pv}}{dV_{pv}} \tag{3.5}$$

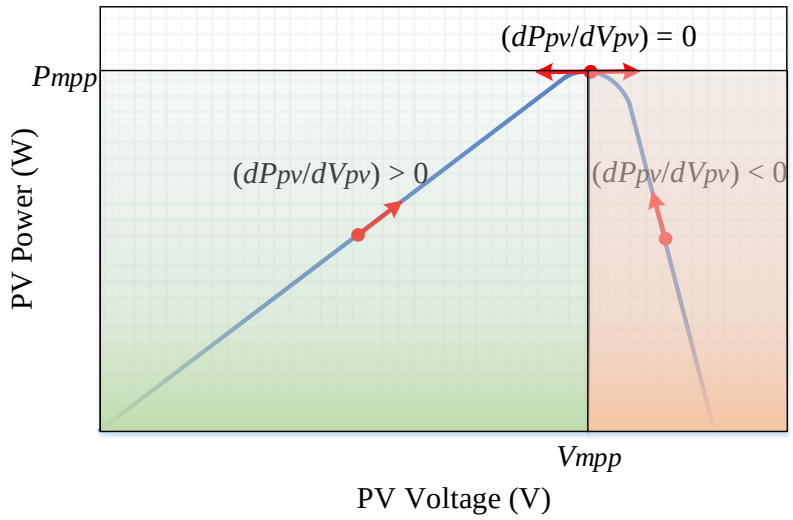

Figure 3.3: Basic idea of the IC algorithm on a Power-Voltage curve of a PV array.

Therefore, the PV array voltage can be adjusted relatively to the MPP voltage by measuring the incremental and instantaneous conductance of the PV array (dI_{pv}/dV_{pv} and I_{pv}/V_{pv}) making use of the previous equations. The detailed operation of the IC algorithm is illustrated in the flowchart of Figure 3.4.

The main advantage of this algorithm is that it offers a good yield method under fast changing in atmospheric conditions. Also, it achieves lower oscillations around the MPP than the P&O method, even though, when the P&O method is optimized, the MPPT efficiency of the IC and the P&O MPPT algorithms are essentially the same [3.17]. However, this method requires a complex control circuit.

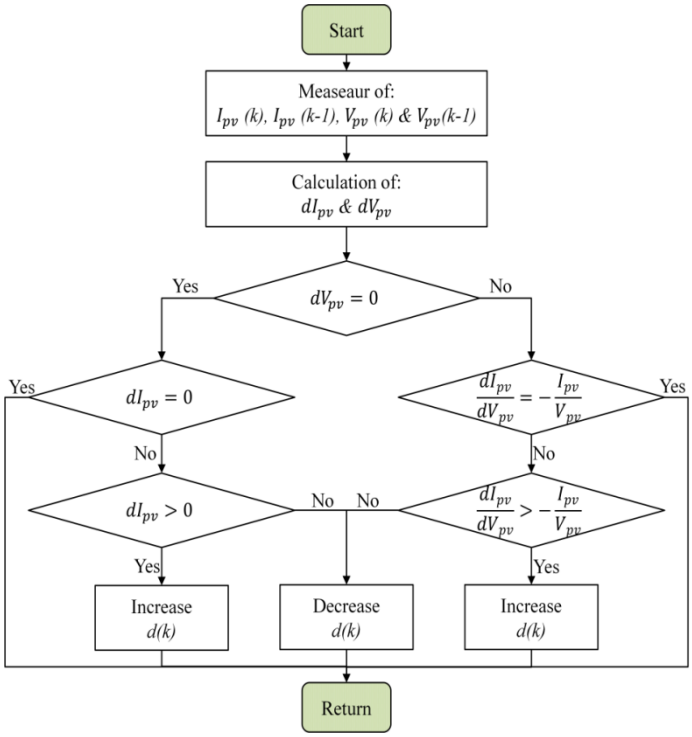

Figure 3.4: Flowchart of the IC algorithm.

3.2.2 FLC-Based MPPT

Fuzzy logic control (FLC) in MPPT applications has become increasingly popular due to its simplicity and ease of implementation. The advantage of FLC is that it does not require a precise mathematical model, and it is able to handle system non-linearity. In general, FLC has three main functional blocks: fuzzification, rule inference diagram and defuzzification as shown in Figure 3.5. During fuzzification, numerical input variables are converted into linguistic variables via membership functions. The rule inference stage is intended to control the output variables conferring to an inference engine that applies rules to membership functions using a rule base table. Lastly, the main task of defuzzification is to convert the output linguistic values via membership functions into relevant numerical values [3.19-24]. Typically, the error E and the change in error ΔE are considered as inputs for an FLC-based MPPT system. These values are computed as:

$$E = \frac{p_{pv}(k) - p_{pv}(k-1)}{v_{pv}(k) - v_{pv}(k-1)} \tag{3.6}$$

$$\Delta E = E(k) - E(k-1) \tag{3.7}$$

The FLC-based MPPT methods possess some advantages compared to the conventional techniques such as superior performance, fast response and good stability. However, the

implementation of these MPPTs is difficult in practice because of the high computational burden of the fuzzy controller [3.25].

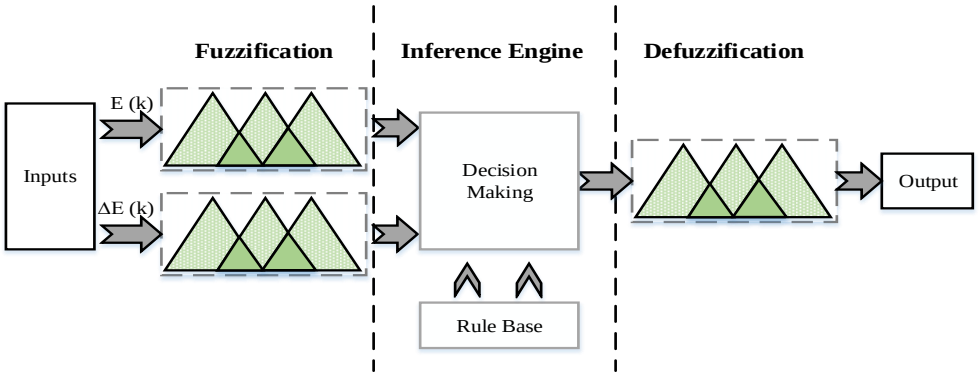

Figure 3.5: Bloc diagram of fuzzy logic controller.

3.2.3 Other MPPT Methods

In the literature review, other expert approaches have been introduced in MPPT controls such as artificial neural networks (ANN) [3.26-29], genetic algorithm (GA) [3.30-31] and particle swarm optimization (PSO) [3.32-35]. In comparison with classical methods, these approaches permit to increase the tracking performance, especially during partially shading conditions. However, the practical implementation of these techniques is limited due to the high computation load. Furthermore, other hybrid MPPT methods that combining the conventional techniques with advanced controls have been proposed in literature [3.36-43]. Amongst these methods, voltage-oriented MPPT (VO-MPPT) and current-oriented MPPT (CO-MPPT) are largely investigated in the recent time [3.37-42]. These methods involve an outer current or voltage loop in cascade with current or voltage controller respectively. The outer loop generates the reference signal and is commonly based on conventional algorithms such as P&O and IC, while the cascade controller enforces the measured (current or voltage) to track the reference signal generated by the outer MPPT unit. Numerous control strategies have been employed to design an effective cascade controller such sliding mode control (SMC) and model predictive control (MPC). Compared to the conventional methods, VO-MPPTs and CO-MPPTs offer better dynamic performances with easy hardware implementation.

3.3 GRID-TIED INVERTER CONTROL

The main control task of the grid-tied inverter is to control the DC-Link capacitor voltage and injected grid currents as well as providing grid synchronization.

3.3.1 DC-Link Voltage Control

To ensure transfer of the extracted power from the PV array into the electrical grid, it is essential to regulate the DC-Link voltage at its desired reference value and estimate the amplitude of the injected grid currents. So, the desired reference value must be selected higher than the grid peak voltage for a proper power injection. Conventionally, this control task is performed by a simple PI controller [3.45-46]. Nevertheless, there are other controllers based on artificial intelligence (AI) approach and sliding mode control (SMC) theory has also proposed in literature [3.47-50]. Brief notes on the above-mentioned controllers are presented in the subsections below.

3.3.1.1 Simple PI controller

Due to its simplicity, the PI controller is considered as one of the most used in the scientific research and industrial applications for the regulation of the DC-Link voltage [3.45-46]. However, it has some drawbacks summarized in the long time response, large overshoot at sudden irradiation changes with important voltage fluctuations in steady-state operation. The block diagram of DC-Link voltage control based on a simple PI is illustrated in Figure 3.6.

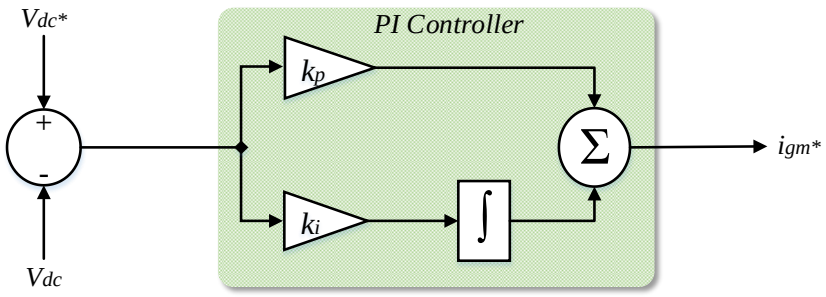

Figure 3.6: Bloc diagram of the DC-Link voltage control based on a simple PI.

3.3.1.2 Artificial intelligence controllers

The artificial intelligence (AI) such as fuzzy logic, neuro-fuzzy networks (ANFIS) and particle swarm optimization (PSO) have been employed in many research works to design an effective DC-Link controller that overcome the drawbacks of the PI controller [3.47-50]. For example, the PI controller is replaced by the fuzzy logic controller. The error "*e*" and its derivative "*de*" are used as inputs of the fuzzy controller as illustrated in Figure 3.7. Compared to the conventional controller, almost the AI controllers contributed to achieve

high performance. However, the implementation of these controllers is limited due to its high computational burden.

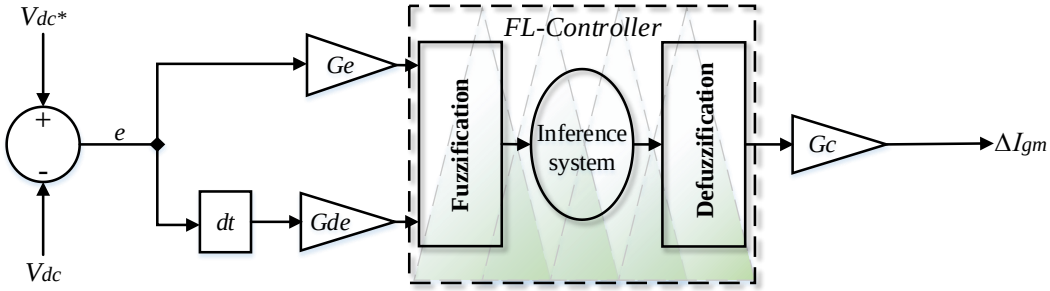

Figure 3.7: Bloc diagram of the DC-Link voltage control based on a fuzzy logic.

3.3.1.3 Other DC-Link voltage controllers

Recently, other DC-Link voltage controllers have been developed to enhance the dynamic performance of the conventional controller with an easiness of practical implementation. The authors in [3.51-52] have added a feed-forward term to the PI controller; this method particularly improves the dynamic performance during changing climatic conditions, while it still suffers from significant steady state ripple. Moreover, sliding mode control (SMC) theory has also been introduced in the control of DC-Link voltage due to its robustness [3.53-54]. The sliding controllers offer high performance operations despite the climatic conditions changes, in addition to the ease of hardware implementation.

3.3.2 Grid Synchronization

Regularly, the injected current must be synchronized with the grid voltage to attain power flow among the distributed energy resource and electrical grid. Several techniques designs have been employed for grid synchronization such as filtering of grid voltages, zero crossing method and phase locked loop (PLL). The main objective of these techniques is to find the phase information of grid voltages. Moreover, it may be needed in the transformation from natural reference frame to stationary or synchronous reference frame for injected grid currents control [3.55]. Among the aforementioned techniques, PLL is the most widely used technique. A brief description of PLL is presented below.

3.3.2.1 Phase-Locked Loop (PLL)

PLL offers a high rejection of harmonics and disturbances. Figure 3.8 displays the block diagram of PLL. Generally, the basic structure of PLL involves three essential blocks; a phase

detector (PD) generates an output signal relative to the phase difference between the input signal and the signal generated by the internal oscillator of the PLL. Furthermore, a loop filter (LF) may be used to reduce the high-frequency AC components at the output of PD block. Usually, this block is founded by a first-order low-pass filter or a PI controller. Besides, a Voltage Controlled Oscillator (VCO) generates at its output an AC signal whose frequency is shifted with respect to a given central frequency ωc, as a function of the input voltage delivered by the LF [3.56]. By means of a control loop, PLL estimates the difference between the phase angle of the input signal and that of the output signal, so it regulates this value to zero. Consequently, in addition to the advantages mentioned above, conventional PLL has some drawbacks especially during grid unbalance condition; a further improvement has been conducted to this technique. More details of the concept and development of this technique are presented in [3.57].

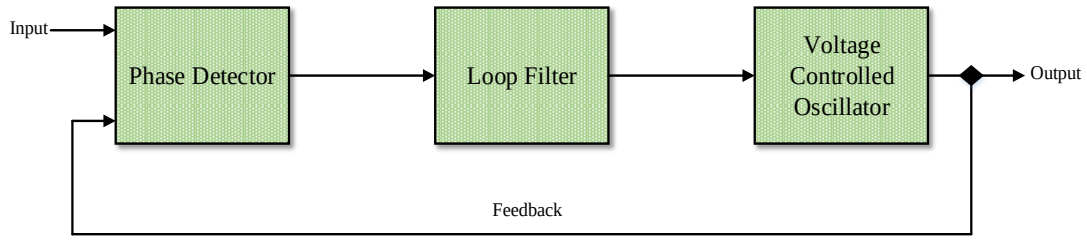

Figure 3.8: Phase-locked-loop scheme.

3.3.3 Grid Currents Control

The injection of the produced PV power into the grid must be performed with low total harmonic distortion (THD %) for grid currents. In this context, numerous research works are interested in hysteresis control, direct power control (DPC), finite-set model predictive control and voltage-oriented control (VOC). The following subsections give a brief overview of the state of the art in control for grid-tied voltage source converter (VSI) in PV applications.

3.3.3.1 Hysteresis Control

The hysteresis controller is classified as a nonlinear method. Figure 3.9 shows the complete structure of the hysteresis current control. The basic operation of this method is simple and based broadly on the hysteresis (bang-bang) controllers. Where, the errors between the measured currents and their references pass through the hysteresis bands which in turn help to generate the control signals. Moreover, the reduction in the hysteresis band width permits to minimize the tracking errors. It may be noted that the modulator is not required in

this method, and then the switching frequency of the converter is variable depending on the operating conditions, filter parameters and hysteresis band width [3.58]. Many researches have been proposed in an effort to use the benefit of this controller. As well as, to exclude the main disadvantage called the uncontrollable switching frequency [3.58].

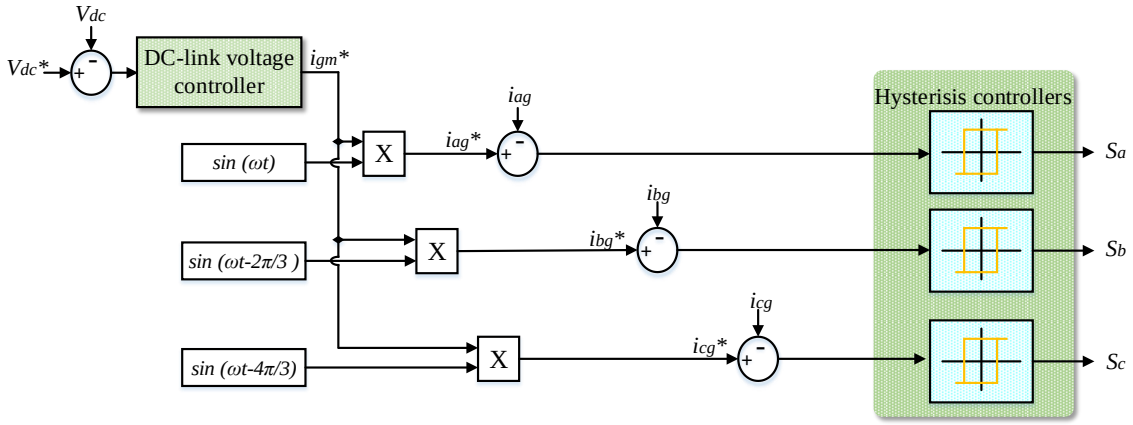

Figure 3.9: Bloc diagram of the hysteresis control.

3.3.3.2 Direct Power Control (DPC)

The basic concept of the direct power control (DPC) is planned by author in [3.59], this scheme derives from the concept of the direct control of the torque (DTC) that applied to the electric machines. In DPC strategy, the modulation stage and internal current loops are not required since the switching states of the inverter are suitably selected by a switching table based on the errors between the estimated reference and their measured values of active and reactive powers as well as the angular position of the grid voltage vector [3.57, 59]. So, the acquaintance of the estimated voltage sector *Sx* is essential to determine optimal switching states. Figure 3.10 represents the plane α-β divided into twelve sectors. Moreover, the hysteresis comparators are used to determine the logical state (higher or lower) of the power errors (*Sp*, *Sq*) for the switching table represented in Table 3.1. The block diagram of the DPC strategy is showed in Figure 3.11.

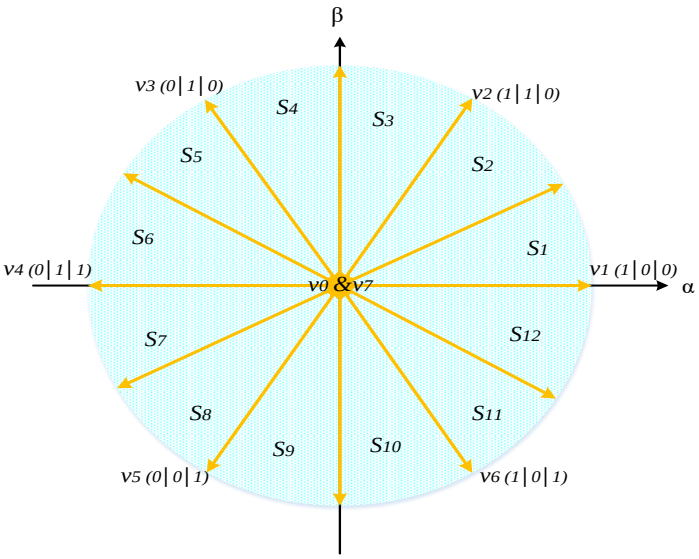

Figure 3.10: Voltage vectors generated in α-β coordinate.

TABLE 3.1: Switching table for the DPC strategy.

Sp	Sq	S_1	S_2	S_3	S_4	S_5	S_6	S_7	S_8	S_9	S_{10}	S_{11}	S_{12}
1	0	v_5	v_5	v_6	v_6	v_1	v_1	v_2	v_2	v_3	v_4	v_4	v_4
1	1	v_3	v_3	v_4	v_4	v_5	v_5	v_6	v_6	v_1	v_1	v_2	v_2
0	0	v_6	v_1	v_1	v_2	v_2	v_3	v_3	v_4	v_4	v_5	v_5	v_6
0	1	v_1	v_2	v_2	v_3	v_3	v_4	v_4	v_5	v_5	v_6	v_6	v_1

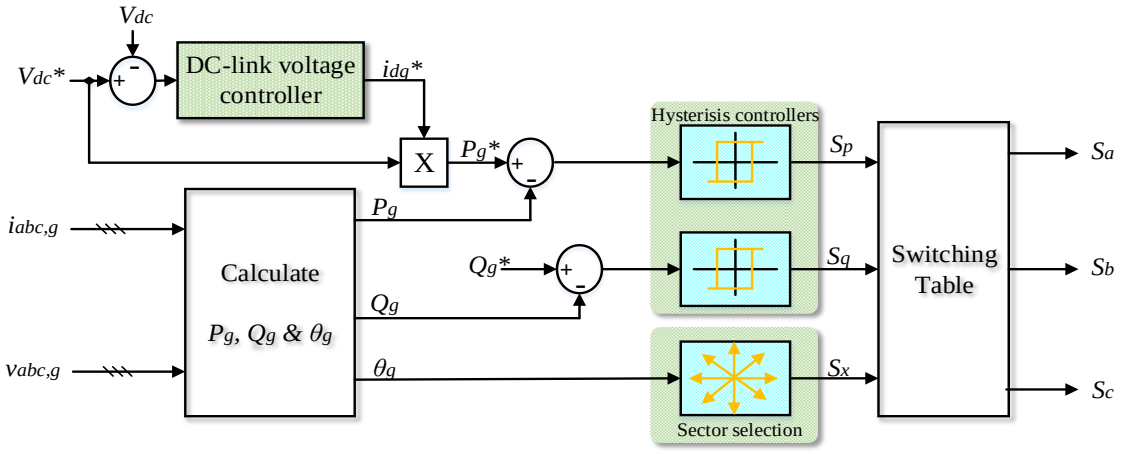

Figure 3.11: Block diagram of the DPC strategy.

Despite its efficiency and simplicity, the DPC strategy requires a high sampling frequency to achieve optimal performance.

3.3.3.3 Finite-Control Set Model Predictive Control (FCS-MPC)

Finite control set model predictive control has also been investigated to control VSI tied to the grid due to its concept easy to understand. Also, FCS-MPC eliminates the need for PI controllers and modulation stages in comparison with linear control techniques [3.60-61]. As illustrated in the scheme presented in Figure 3.12, the state variables are predicted for all possible switching states and compared by using a cost function. The switch state achieving a minimum cost function value is applied to the VSI during the next sampling period. From the results presented in literature, FCS-MPC provides high performance operation. However, it suffers from the variable switching frequency and high computational burden.

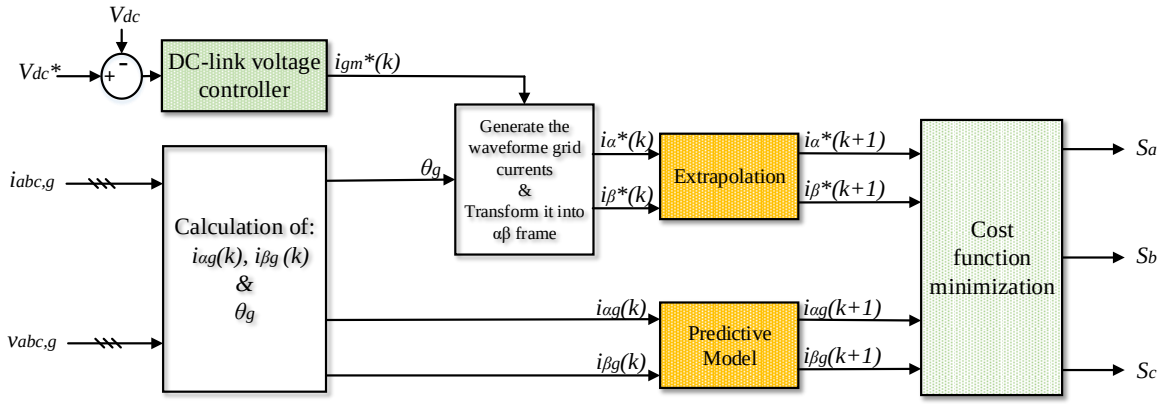

Figure 3.12: Block diagram of FCS-MPC strategy.

3.3.3.4 Voltage Oriented Control (VOC)

At the outset, note that VOC technique is the most used to control the grid-tied inverters in PV applications [3.57]. As the name implies, VOC employs a rotational *dq* reference frame transformation oriented with the grid voltage vector to transform all AC quantities to DC values to simplify the control structure and to permit the use of PI controller [3.37, 62]. The measured three phase currents (*iabc,g*), and voltages (*vabc,g*) are transformed into *dq* values for feedback purposes. Moreover, the grid voltage vector angle θ_g must be calculated for a correct *dq* transformation as well as for the grid synchronization. Figure 3.13 represents the block diagram of the VOC technique. Globally, this technique based on two current control loops that estimate the *dq* reference voltages through the instantaneous errors between the measured grid currents in *dq* form (*id*, *iq*) and their reference (*id**, *iq**) respectively. The outer loop (DC-Link voltage controller) estimates the " *id**" which is proportional to the active power and

hence represents the peak value of the injected currents while the " iq*" is proportional to the reactive power and estimated by the grid operator demand. Then, the estimated reference voltages (vd*, vq*) were transformed in abc natural frame for pulse width modulation (PWM) stage or in $\alpha\beta$ frame for space vector modulation (SVM) stage.

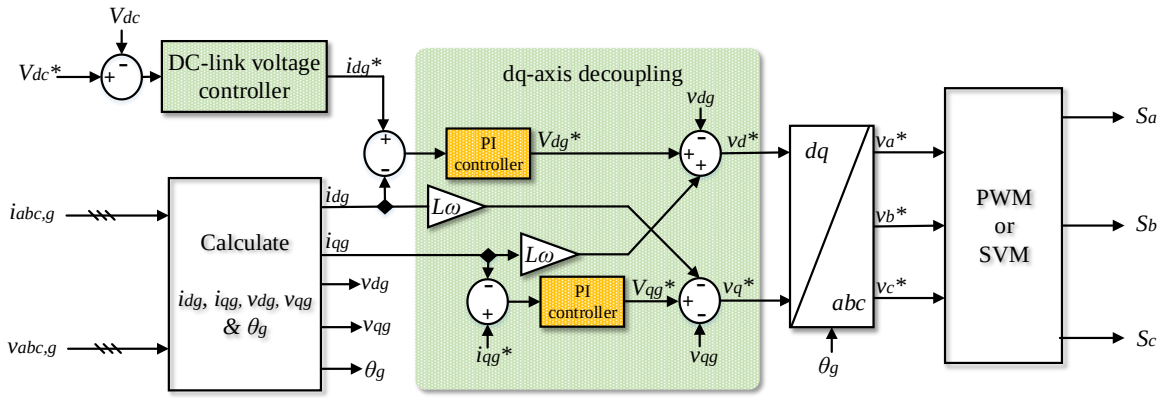

Figure 3.13: Block diagram of the VOC technique.

In addition to its simplicity in design, the main advantage of this strategy is the fixed switching frequency. However, it has slow response time and significant lower order harmonics du to PI controllers [3.57].

3.3.3.5 Other Grid-Tied Inverter Controllers

To overcome the disadvantages of the above techniques, other grid-tied inverter techniques have been proposed in the literature which modify or combine conventional techniques with intelligent control techniques, such as fuzzy logic [3.63], artificial neural network [3.64] and neuro-fuzzy [3.65]. These techniques offer low total harmonic distortion (THD) and increase robustness against changing climatic conditions. Contrariwise, the computational burden of these controllers is high which makes them difficult to implement in real time. On the other side, sliding mode control (SMC) has attracted more interest in recent years, particularly in power converter control due to its effectiveness, robustness and implementation easiness [3.66-67]. In the grid-tied inverter control, sliding mode control is usually introduced with the VOC strategy. Where, the PI controllers are replaced by the sliding controllers to make the tracking errors close to zero by enforcing the measured grid currents (id, iq) to slide on a predefined trajectory. Compared to the classical controllers, this control method gives robust and stable response even during the system parameter changes [3.67].

3.4 CONCLUSION

In this chapter, the state of the art of maximum power point tracking (MPPT) algorithms for photovoltaic (PV) systems are reviewed, and followed by an overview of the grid-tied inverter control techniques. The implementation and operating principle of the main MPPT control techniques are presented. The issues and challenges related to different algorithms, such as the tracking accuracy, power oscillations, and computational burden are discussed. In addition, the most extensively used high-performance control strategies for grid-tied inverter as hysteresis control, direct power control (DPC), finite control set model predictive control (FCS-MPC), voltage oriented control (VOC) and other techniques are described.

REFERENCES

[3.1] Esram, T., Chapman, P.L., 2007. Comparison of photovoltaic array maximum power point tracking techniques. IEEE Trans. Energy Conver. 22 (2), 439–449.

[3.2] Eltawil, M.A., Zhao, Z., 2013. MPPT techniques for photovoltaic applications. Renew. Sustain. Energy Rev. 25, 793–813.

[3.3] de Brito, M.A.G., Galotto, L., Sampaio, L.P., e Melo, G.A., Canesin, C.A., 2013. Evaluation of the main MPPT techniques for photovoltaic applications. IEEE Trans. Ind. Electron. 60 (3), 1156–1167.

[3.4] Mohanty, P., Bhuvaneswari, G., Balasubramanian, R., Dhaliwal, N.K., 2014. MATLAB based modeling to study the performance of different MPPT techniques used for solar PV system under various operating conditions. Renew. Sustain. Energy Rev. 38, 581–593

[3.5] Karami, N., Moubayed, N., Outbib, R., 2017. General review and classification of different MPPT Techniques. Renew. Sustain. Energy Rev. 68, 1–18.

[3.6] Hart, G.W., Branz, H.M., Cox, C.H., 1984. Experimental tests of open loop maximum-power-point tracking techniques. Solar Cells 13, 185– 195.

[3.7] Salameh, Z., Dagher, F., Lynch, W., 1991. Step-down maximum power point tracker for photovoltaic systems.Sol. Energy 46, 279–82.

[3.8] Eftichios, K., Kostas, K., Voulgaris, N., 2001. Development of a microcontroller-based, photovoltaic maximum power point tracking control system. IEEE Trans. Power Electron. 16 (1), 46–54.

[3.9] Femia, N., Petrone, G., Spagnuolo, G., Vitelli, M., 2012. Power Electronics and Control Techniques for Maximum Energy Harvesting in Photovoltaic Systems. CRC Press.

[3.10] Femia, N., Petrone, G., Spagnuolo, G., Vitelli, M., 2005. Optimization of perturb and observe maximum power point tracking method. IEEE Trans. Power Electron. 20 (4), 963–973.

[3-11] Hussein, K.H., Muta, I., Hoshino, T., Osaka, M., 1995. Maximum photovoltaic power tracking: an algorithm for rapidly changing atmospheric conditions. IEE Proc. Gener.

Transnm. Distrib. 142 (1), 59–64.

[3.12] Kim, Y., Jo, H., Kim, D., 1996. A new peak power tracker for cost effective photovoltaic power systems. IEEE Proceedings 3 (1), 1673– 1678.

[3.13] Chomsuwan, K., Prisuwanna, P., Monyakul, V., 2002. Photovoltaic grid-connected inverter using two-switch buck-boost converter. In: Proceedings of the photovoltaic specialists conference, 1527–1530.

[3.14] Fermia, N., Lisi, G., Petrone, G., Spagnuolo, G., Vitelli, M., 2008. Distributed maximum power point tracking of photovoltaic arrays: novel approach and system analysis. IEEE Trans. Ind. Electron. 55(7), 2610–2621.

[3.15] Figueres, E., Garcera, G., Sandia, J., Gonzalez-Espín, F., Calvo, J., 2009. Sensitivity study of the dynamics of three-phase photovoltaic inverters with an LCL grid filter. IEEE Trans. Ind. Electron. 56(3), 706–17.

[3.16] Patel, H., Agarwal, V., 2010. Investigations into the performance of photovoltaics based active filter configurations and their control schemes under uniform and non-uniform radiation conditions. IET Renew. Power Gener. 4(1), 12-22.

[3.17] Safari, A., Mekhilef, S., 2011. Simulation and hardware implementation of incremental conductance MPPT with direct control method using cuk converter. IEEE Trans. Ind. Electron. 58 (4), 1154–1161.

[3.18] Tey, K.S., Mekhilef, S., 2014. Modified incremental conductance MPPT algorithm to mitigate inaccurate responses under fast-changing solar irradiation level. Sol. Energy 101, 333–342.

[3.19] Gounden, N.A., Ann Peter, S., Nallandula, H., Krithiga, S., 2009. Fuzzy logic controller with MPPT using line-commutated inverter for threephase grid-connected photovoltaic systems. Renew. Energy 34, 909– 915.

[3.20] Alajmi, B.N., Ahmed, K.H., Finney, S.J., Williams, B.W., 2011. Fuzzy-logic-control approach of a modified hill-climbing method for maximum power point in microgrid standalone photovoltaic system. IEEE Trans. Power Electron. 26 (4), 1022–1030.

[3.21] Al Nabulsi, A., Dhaouadi, R., 2012. Efficiency optimization of a DSP-based standalone PV system using fuzzy logic and dual-MPPT control. IEEE Trans. Ind. Informa. 8 (3),

573–584.

[3.22] Bendib, B., Belmili, H., Krim, F., 2015. A survey of the most used MPPT methods: Conventional and advanced algorithms applied for photovoltaic systems. Renew. Sustain. Energy Rev. 45, 637–648.

[3.23] Altin, Necmi, Ozdemir, Saban, 2013. Three-phase three-level grid interactive inverter with fuzzy logic based maximum power point tracking controller. Energy Convers. Manage. 69, 17–26.

[3.24] Hasan, M., Mekhilef, S., Metselaar, I.H., 2013. Photovoltaic system modeling with fuzzy logic based maximum power point tracking algorithm. Int. J. of Photoenergy, 1-10.

[3.25] Whei-Min, L., Chih-Ming, H., Chiung-Hsing, C., 2011. Neural-network based MPPT control of a stand-alone hybrid power generation system. IEEE Trans. Power Electron. 26(12), 3571–3581.

[3.26] Liu, Y.-H., Liu, C.-L., Huang, J.-W., Chen, J.-H., 2013. Neural-network based maximum power point tracking methods for photovoltaic systems operating under fast changing environments. Sol. Energy 89, 42–53.

[3.27] Rizzo, S.A., Scelba, G., 2013. ANN based MPPT method for rapidly varible shading conditions. Appl. Energy 145, 124–132.

[3.28] Punitha, K., Devaraj, D., Sakthivel, S., 2013. Artificial neural network based modified incremental conductance algorithm for maximum power point tracking in photovoltaic system under partial shading conditions. Energy 62, 330–340.

[3.29] Chikh, A., Chandra, A., 2014. Adaptive neuro-fuzzy based solar cell model. IET Renew. Power Gener. 8(6), 679–686.

[3.30] Chikh, A., Chandra, A., 2015. An optimal maximum power point tracking algorithm for PV systems with climatic parameters estimation. IEEE Trans. Sust. Energy 6(2), 644–652.

[3.31] Larbes, C., Ait Cheikh, S.M., Obeidi, T., Zerguerras, A., 2009. Genetic algorithms optimized fuzzy logic control for the maximum power point tracking in photovoltaic system. Renw. Energy 34, 2093–2100.

[3.32] Shaiek, Y., Smida, M.B., Sakly, A., Mimouni, M.F., 2013. Comparison between conventional methods and GA approach for maximum power point tracking of shaded solar PV generators. Sol. Energy 90, 107–122.

[3.33] Ishaque, K., Salam, Z., Amjad, M., Mekhilef, S., 2012. An improved particle swarm optimization (PSO)–based MPPT for PV with reduced steady-state oscillation. IEEE Trans. Power Electron. 27 (8), 3627–3638.

[3.34] Yi-Hwa, L., Shyh-Ching, H., Jia-Wei, H., Wen-Cheng, L., 2012. A particle swarm optimization-based maximum power point tracking algorithm for PV systems operating under partially shaded conditions. IEEE Trans. Energy Convers. 27(4), 1027–1035.

[3.35] Lian, K.L., Jhang, J.H., Tian, I.S., 2014. A maximum power point tracking method based on perturb-and-observe combined with particle swarm optimization. IEEE J. Photovoltaics 4 (2), 626–633.

[3.36] Pradhan, R. and Subudhi, B., 2016. Double integral sliding mode MPPT control of a photovoltaic system. IEEE Transactions on Control Systems Technology, 24(1), 285-292.

[3.37] Kihel, A., Krim, F. and Laib, A., 2017, May. MPPT voltage oriented loop based on integral sliding mode control applied to the boost converter. In 2017 6th International Conference on Systems and Control (ICSC) (pp. 205-209). IEEE.

[3.38] Farhat, M., Barambones, O. and Sbita, L., 2017. A new maximum power point method based on a sliding mode approach for solar energy harvesting. Applied energy, 185, 1185-1198.

[3.39] Kihal, A., Krim, F., Laib, A., Talbi, B. and Afghoul, H., 2019. An improved MPPT scheme employing adaptive integral derivative sliding mode control for photovoltaic systems under fast irradiation changes. ISA transactions, 87, 297-306.

[3.40] Armghan, H., Ahmad, I., Armghan, A., Khan, S. and Arsalan, M., 2018. Backstepping based non-linear control for maximum power point tracking in photovoltaic system. Solar Energy, 159, 134-141.

[3.41] Kollimalla, S.K. and Mishra, M.K., 2014. A novel adaptive P&O MPPT algorithm considering sudden changes in the irradiance. IEEE Transactions on Energy conversion,

29(3), 602-610.

[3.42] Kakosimos, P.E. and Kladas, A.G., 2011. Implementation of photovoltaic array MPPT through fixed step predictive control technique. Renewable energy, 36(9), 2508-2514.

[3.43] Talbi, B., Krim, F., Rekioua, T., Laib, A. and Feroura, H., 2017. Design and hardware validation of modified P&O algorithm by fuzzy logic approach based on model predictive control for MPPT of PV systems. Journal of Renewable and Sustainable Energy, 9(4), 043503.

[3.44] Bianconi, E., Calvente, J., Giral, R., Mamarelis, E., Petrone, G., Ramos-Paja, C.A., Spagnuolo, G. and Vitelli, M., 2013. A fast current-based MPPT technique employing sliding mode control. IEEE Transactions on Industrial Electronics, 60(3), 1168-1178.

[3.45] Krama, A., Laid, Z. and Boualaga, R., 2017. Anti-windup proportional integral strategy for shunt active power filter interfaced by photovoltaic system using technique of direct power control. Rev. Roum. Sci. Tech. Électrotech. Énerg, 62, 252-257.

[3.46] Laib, A., Krim, F., Talbi, B., Kihal, A. and Feroura, H., 2018. Improved Control for Three Phase dual-Stage Grid-Connected PV Systems Based on Predictive Control Strategy. Journal of Control Engineering and Applied Informatics, 20(3), 12-23.

[3.47] Krama, A., Zellouma, L., Rabhi, B. and Laib, A., 2017, October. Fuzzy Logic Controller for Improving DC Side of PV Connected Shunt Active Filter Based on MPPT Sliding Mode Control. In International Conference in Artificial Intelligence in Renewable Energetic Systems (pp. 224-235). Springer, Cham.

[3.48] Talbi, B., Krim, F., Rekioua, T., Mekhilef, S., Laib, A. and Belaout, A., 2018. A high-performance control scheme for photovoltaic pumping system under sudden irradiance and load changes. Solar Energy, 159, 353-368.

[3.49] Singh, M. and Chandra, A., 2013. Real-time implementation of ANFIS control for renewable interfacing inverter in 3P4W distribution network. IEEE Transactions on industrial electronics, 60(1), 121-128.

[3.50] Krama, A., Zellouma, L., Benaissa, A., Rabhi, B., Bouzidi, M. and Benkhoris, M.F., 2018. Design and Experimental Investigation of Predictive Direct Power Control of Three-Phase Shunt Active Filter with Space Vector Modulation using Anti-windup PI

Controller Optimized by PSO. Arabian Journal for Science and Engineering, 1-15.

[3.51] Jain, C. and Singh, B., 2016. A three-phase grid tied SPV system with adaptive DC link voltage for CPI voltage variations. IEEE Transactions on Sustainable Energy, 7(1), 337-344.

[3.52] Laib, A., Krim, F. and B. Talbi, 2016. An improved control for two-stage grid-connected photovoltaic systems, in In: Proc. ICESTI'16, Annaba, Algérie.

[3.53] Zellouma, L., Rabhi, B., Krama, A., Benaissa, A. and Benkhoris, M.F., 2018. Simulation and real time implementation of three phase four wire shunt active power filter based on sliding mode controller. Rev. Roum. Des. Sci. Tech. Ser. Electrotech. Energ, 63, 77-82.

[3.54] Kihal, A., Krim, F., Talbi, B., Laib, A. and Sahli, A., 2018. A Robust Control of Two-Stage Grid-Tied PV Systems Employing Integral Sliding Mode Theory. Energies, 11(10), 2791.

[3.55] Abu-Rub, H., Malinowski, M., Al-Haddad, K., 2014. Power electronics for renewable Energy systems, transportation and industrial applications. John Wiley & Sons.

[3.56] Malek, H., 2014. Control of grid-connected photovoltaic systems using fractional order operators. Ph. D. desertation, Utah State Univ., Logan Utah.

[3.57] Teodorescu, R., Liserre, M. and Rodriguez, P., 2011. Grid converters for photovoltaic and wind power systems (Vol. 29). John Wiley & Sons.

[3.58] Yaramasu, V., 2014. Predictive control of multilevel converters for megawatt wind energy conversion systems (Doctoral dissertation, Ph. D. dissertation, Ryerson Univ., Toronto, ON, Canada).

[3.59] Noguchi, T., Tomiki, H., Kondo, S. and Takahashi, I., 1996, October. Direct power control of PWM converter without power source voltage sensors. In IAS'96. Conference Record of the 1996 IEEE Industry Applications Conference Thirty-First IAS Annual Meeting (Vol. 2, pp. 941-946). IEEE.

[3.60] Rodriguez, J. and Cortes, P., 2012. Predictive control of power converters and electrical drives (Vol. 40). John Wiley & Sons.

[3.61] Rodriguez, J., Kazmierkowski, M.P., Espinoza, J.R., Zanchetta, P., Abu-Rub, H., Young, H.A. and Rojas, C.A., 2013. State of the art of finite control set model predictive control in power electronics. IEEE Transactions on Industrial Informatics, 9(2), 1003-1016.

[2.62] Yaramasu, V., Wu, B. and Chen, J., 2014. Model-predictive control of grid-tied four-level diode-clamped inverters for high-power wind energy conversion systems. IEEE transactions on power electronics, 29(6), 2861-2873.

[2.63] Cirstea, M., Dinu, A., McCormick, M. and Khor, J.G., 2002. Neural and fuzzy logic control of drives and power systems. Elsevier.

[2.64] Bose, B.K., 1986. Power electronics and AC drives. Englewood Cliffs, NJ, Prentice-Hall, 1986, 416 p.

[2.65] Vas, P., 1999. Artificial-intelligence-based electrical machines and drives: application of fuzzy, neural, fuzzy-neural, and genetic-algorithm-based techniques (Vol. 45). Oxford university press.

[2.66] Massing, J.R., Stefanello, M., Grundling, H.A. and Pinheiro, H., 2012. Adaptive current control for grid-connected converters with LCL filter. IEEE Transactions on Industrial Electronics, 59(12), 4681-4693.

[2.67] Herran, M.A., Fischer, J.R., González, S.A., Judewicz, M.G. and Carrica, D.O., 2013. Adaptive dead-time compensation for grid-connected PWM inverters of single-stage PV systems. IEEE transactions on power electronics, 28(6), 2816-2825.

Chapter 4

Development of an Adaptive MPPT Scheme based on Sliding Mode Control

4.1 INTRODUCTION

Maximum power point tracking (MPPT) is necessary to achieve an optimal exploitation of photovoltaic (PV) system, which depends strongly on climatic conditions (irradiation and temperature). Currently, the largest part of MPPT schemes are Voltage-Oriented MPPT (VO-MPPT), due to the almost-zero change in PV voltage at the MPP under irradiation changes, which considered to be a fast MPP tracking strategy. This method involves MPPT voltage-based algorithm (V-MPPT) in cascade with voltage control loop. However, the efficiency of this method depends on the voltage regulator design.

For this purpose, the current chapter proposes a novel voltage-oriented MPPT (VO-MPPT) method, where the conventional perturb and observe (P&O) algorithm is combined with the proposed external voltage control based on an adaptive integral derivative sliding mode (AIDSM). It is designed with new sliding surface, in addition, the derivative and integral terms are chosen to eliminate the overshoot during fast changes in solar irradiation and to minimize the steady-state fluctuation. Furthermore, an adaptation mechanism is combined to adjust the controller gains under each irradiation level. The proposed MPPT is tested and compared by simulations with the most widely used MPPT methods using MATLAB/Simulink^{TM} and real time hardware in the loop (HIL) implementation. The results obtained with the proposed MPPT show excellent dynamic performance under fast irradiation changes.

4.2 STATE OF THE ART OF THE MPPT METHODS

In order to push the PV system to deliver its maximum power under each operating conditions, many control strategies have been proposed in the literature [4.1-28]. Perturb and observe (P&O) [4.2-4] and Incremental Conductance (INC) [4.5-7] are two well-known conventional MPPT control methods. They are intuitive to understand and easy to be implemented. However, they are not being able to work properly when fast changes in environmental conditions occur; afterwards, they present large oscillations at the maximum power point (MPP) in steady-state. In this context, artificial intelligence is adopted to overcome these drawbacks in the form of different methods such as, neural networks [4.8-9], fuzzy logic (FLC) [4.10-12], genetic algorithms (GA) [4.13], pattern swarm optimization (PSO) [4.14], and Green Wolf optimization (GWO) [4.15]. Unlike the classical methods, the advanced algorithms provide better performance. However, they are complex in design and rigorous to be implemented practically. Therefore, several papers were interested on voltage-oriented MPPT (VO-MPPT) and current-oriented MPPT (CO-MPPT) [4.16-22]. These methods involve either MPPT current-based algorithm (CMPPT) in cascade with current controller or MPPT voltage-based algorithm (V-MPPT) in cascade with voltage controller. Due to the nonlinear relationship between the PV voltage and irradiation level, VO-MPPT is considered as a fast alternative [4.16-17]. However, the efficiency of this method depends on the voltage regulator concept.

Generally, the voltage regulator is performed by a simple PI controller [4.19]. The application of this controller provides a long time response, large overshoot and significant steady-state error. For these reasons, sliding mode control (SMC) has been interested by numerous researches in order to improve the voltage regulation which enhances the MPP tracking. A type of SMC with a simple sliding surface is proposed in [4.20]. This method suffers from chattering phenomena and variable switching frequency. Other works have added an integral term to the sliding surface (ISMC) in order to reduce the steady-state error (SSE) compared to SMC [4.21]. This controller is performed through PWM-based control action which offers a fixed frequency operating. However, overshoot problem has been observed using this ISMC controller. A more SSE reduction has been achieved by adding another integral term to the sliding surface as presented in [4.22]. This method is called double integral sliding mode control (DISMC). The DISMC operates with a fixed frequency

and consequently more reduction in SSE is attained. Conversely, the overshoot problem is growing.

On the other hand, numerous adaptive MPPT methods have been developed to improve the aforementioned methods under changing atmospheric conditions [4.23-30], they consist of two steps: the first step uses the obtained parameter into aforementioned MPPT methods. The second step is used for adaptation mechanism; most of the proposed adaptive mechanisms are designed based on intelligent artificial approaches. An adaptive- step of P&O algorithm has been planned to accelerate the tracking performance according to the irradiance level changing by the authors in [4.25]. The proposed MPPT method uses the fuzzy logic controller (FLC) to tune the step-size for P&O algorithm. The authors in [4.26] proposed a modified P&O voltage-based algorithm combined with proportional-integral-derivative (PID), the gains of PID controller are tuned by genetic algorithms (GA). An adaptive $H\infty$ based on FLC was proposed to ensure the fast and robust tracking for MPPT method founded on sliding mode controller (SMC) current by the authors in [4.27], where the SMC controller gains can be automatically tuned according to external condition changes. The authors in [4.28] use artificial neural networks (ANN) structure to adapt the controller gains for an MPPT method based on SMC. Whatever the system applications, artificial intelligence based adaptive MPPT methods are effective and provide high control performance in comparison with conventional methods. However, they are hard to be implemented practically.

4.3 SYSTEM CONFIGURATION

The simplified control scheme of the PV system configuration discussed in this chapter is presented in Figure 4.1. It is mainly composed of the PV Array connected to the capacitive filter to stabilize PV voltage output. The capacitive filter is in turn connected to the boost converter whose IGBT transistor gate is controlled by a PWM signal generated from the MPPT unit, and finally a resistive load. The control scheme is based on the voltage regulation loop and consists of two blocks. The major role of the first block, V-MPPT, is to generate a reference voltage corresponding to the MPP under variable irradiations. The second block, AIDSM, aims to enforce the GPV voltage to track accurately the reference generated by the MPPT unit and to provide a duty cycle (D) for (PWM) switching operation.

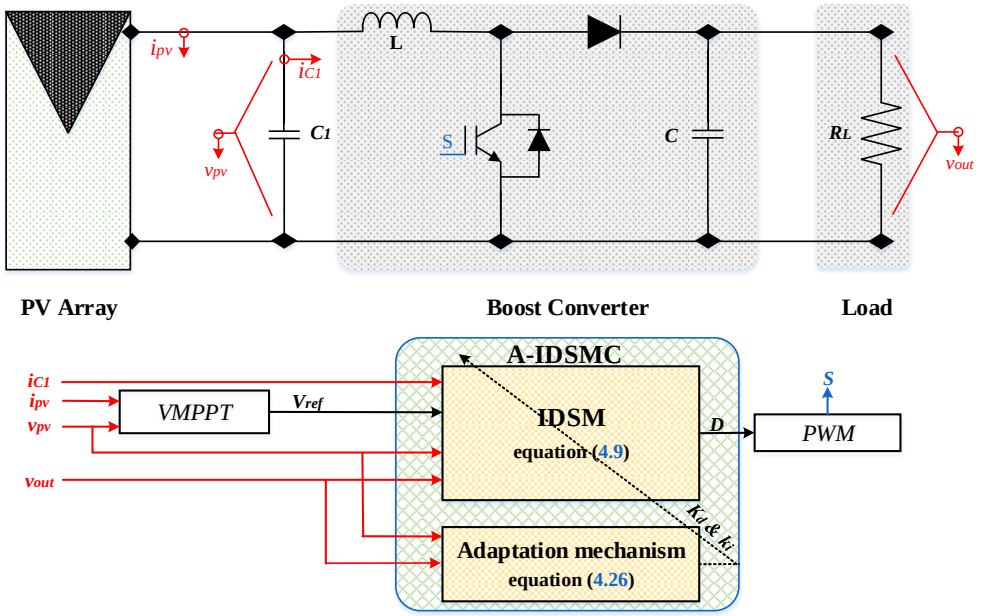

Figure 4.1: Proposed control scheme for the PV system.

4.4 PROPOSED MPPT CONTROL

As shown in Figure 4.1, the proposed control scheme is divided into two loops. The first one, a P&O voltage-based MPPT (V-MPPT) controller generates the reference voltage "V_{ref}". The second one, an adaptive integral derivative sliding mode controller (AIDSM) is proposed to enforce the "v_{pv}"to track V_{ref} and to provide the duty ratio D in order to achieve an optimal exploitation of the GPV under step changing irradiation.

4.4.1 P&O Voltage-Based MPPT (V-MPPT)

The P&O voltage-based MPPT algorithm is widely employed due to the featuring effectiveness and simplicity. This technique works by perturbing the operation PV voltage, the perturbation effect is observed at the output power for deciding the direction of the next perturbation; if the present power value is greater than the previous, the perturbation remains in the same direction (the sign of the next perturbation is kept up), otherwise the direction is reversed as shown in Figure 4.2.

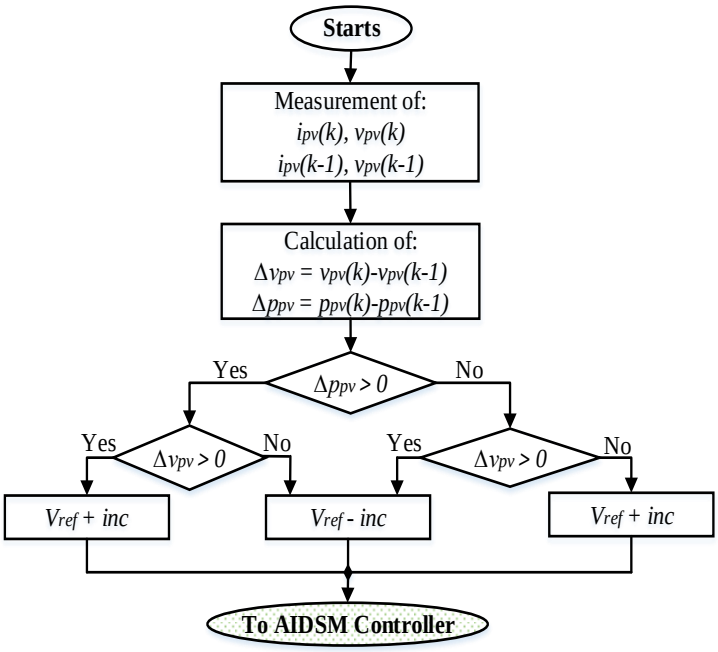

Figure 4.2: Flowchart of P&O voltage-based algorithm (V-MPPT).

4.4.2 Adaptive Integral Derivative Sliding Mode (A-IDSM) Controller

Usually, the VO-MPPT method is performed by a PID controller. The error between the actual PV voltage and its reference passing through the PID controller allows defining the duty cycle of PWM control. As mentioned previously, the application of this controller shows some disadvantages. So, an Adaptive Integral Derivative Sliding Mode (A-IDSM) Controller is proposed to overcome these disadvantages and to take benefit from the strengths of sliding mode (SM) control. According to Figure 4.1 this controller consist of two blocks. The IDSM block aims to generating the duty ratio D. As for the adaptation block, its role is to estimating the controller gains (k_d, k_i).

4.4.2.1 IDSM control design

Principally, each design based on sliding mode control involves three steps: the choice of sliding surfaces, the determination of control law and the reachability conditions [4.29].

As mentioned previously the proposed cascade voltage regulator IDSM provides the duty ration D of the signal driving the boost converter towards V_{ref} voltage. Hence, in order to improve the PV voltage behavior, IDSM is designed with a novel equilibrium sliding surface given by equation (4.1),

$$s(t) = k_d \dot{e}(t) + e(t) + k_i \int e(t)\, dt \qquad (4.1)$$

Where $e(t)$ is the voltage error between "V_{ref}"and "v_{pv}",$\dot{e}(t)$ and $\int e\,(t)$ are respectively the error derivative and integral terms. k_d, k_i are the corresponding sliding surface coefficients, to be adapted in the next section.

Typically, SMC includes two parts; equivalent and discontinuous parts, as given in equation (4.2).

$$D(t) = D_{eq}(t) + D_{dis}(t) \tag{4.2}$$

To get the equivalent control signal, equation (4.1) must be derived and made equal to zero as follows:

$$\begin{aligned} \dot{s} &= k_d\ddot{e}(t) + \dot{e}(t) + k_i e(t) = 0 \\ &= -k_d\ddot{v}_{pv} - \dot{v}_{pv} + k_i e(t) = 0 \end{aligned} \tag{4.3}$$

The dynamic model of the boost converter with resistive load can be rewritten as,

$$\begin{cases} \dot{v}_{pv} = \dfrac{1}{C_1}\left[\dfrac{v_{pv}}{r_{pv}} - i_L\right] \\ \dot{i}_L = \dfrac{1}{L}\left[v_{pv} - v_{out} + v_{out}.D\right] \end{cases} \tag{4.4}$$

where:

i_L: is the boost input current (A),

v_{pv}: is the boost input voltage (V),

v_{out}: is the boost output voltage (V),

i_{pv}: is the photo-generated current (A),

r_{pv} : is dynamic resistance of GPV, which is defined as $r_{pv} = -(\partial v_{pv}/\partial i_{pv})$,

L : is the boost input inductor (mH),

C_1: is the input capacitor (μF),

D : is the duty cycle considered as input variable.

By substituting equation (4.4) in equation (4.3), it is possible to get equation (4.5),

$$-\frac{k_d}{C_1}\left[\frac{\dot{v}_{pv}}{r_{pv}} - \dot{i}_L\right] - \frac{1}{C_1}\left[\frac{v_{pv}}{r_{pv}} - i_L\right] + k_i e(t) = 0 \tag{4.5}$$

Substitution of the terms $\dot{v}_{pv}$and $\dot{i}_L$ given by equation (4.4) in equation (4.5) yields

$$-\frac{k_d}{C_1}\left(\frac{1}{C_1 r_{pv}}\overbrace{\left[\frac{v_{pv}}{r_{pv}}-i_L\right]}^{i_{c1}}-\frac{1}{L}\left[v_{pv}-v_{out}+v_{out}.D\right]\right)-\frac{1}{C_1}\overbrace{\left[\frac{v_{pv}}{r_{pv}}-i_L\right]}^{i_{c1}}+k_i e(t)=0 \quad (4.6)$$

Hence from equation (4.6), the expression of D_{eq} is deduced as

$$D_{eq}=\frac{1}{v_{out}}\left(v_{out}-v_{pv}+L.i_{c1}\left[\frac{1}{C_1.r_{pv}}+\frac{1}{k_d}\right]-\frac{k_i}{k_d}.L.C_1.e(t)\right) \quad (4.7)$$

Discontinuous switching control D_{dis} is essential to take into consideration the external disturbance. In this work the sigmoidal approximation is chosen to reduce the chattering magnitude in which case it is given by equation (4.8),

$$D_{dis}=-K.\frac{s}{\|s\|+\varepsilon} \quad (4.8)$$

where K is a constant chosen large enough to ensure the stability condition and ε is a small positive number. The value of ε is designed by means of simulation and experiments, to remove the steady state error and to reduce the chattering phenomena.

Then the global control law is given as:

$$D=\frac{1}{v_{out}}\left(v_{out}-v_{pv}+L.i_{c1}\left[\frac{1}{C_1.r_{pv}}+\frac{1}{k_d}\right]-\frac{k_i}{k_d}.L.C_1.e(t)\right)-K.\frac{s}{\|s\|+\varepsilon} \quad (4.9)$$

To verify the stability condition of the controller designed in equation (4.9), Lyapunov function is used. It is considered as follows

$$V=\frac{1}{2}s^2 \quad (4.10)$$

To guarantee the convergence of V, it should be verified that the derivative of V is definite negative as follows

$$\dot{V}=s\dot{s}<0 \quad (4.11)$$

From equation (4.4), we get

$$\begin{cases} \dot{v}_{pv} = \dfrac{1}{C_1}\left[\dfrac{v_{pv}}{r_{pv}} - i_L\right] \\ \ddot{v}_{pv} = \dfrac{1}{C_1}\left[\dfrac{\dot{v}_{pv}}{r_{pv}} - \dfrac{1}{L}\left[v_{pv} - v_{out} + v_{out}.D\right]\right] \end{cases} \tag{4.12}$$

The time derivative of equation (4.1) is

$$\begin{aligned} \dot{s}(t) &= k_d\ddot{e}(t) + \dot{e}(t) + k_i e(t) \\ &= -k_d\ddot{v}_{pv} - \dot{v}_{pv} + k_i e(t) \end{aligned} \tag{4.13}$$

By substituting equation (4.12) into equation (4.13), we get

$$\dot{s} = -\frac{k_d}{C_1}\left[\frac{\dot{v}_{pv}}{r_{pv}} - \frac{1}{L}\left[v_{pv} - v_{out} + v_{out}.D\right]\right] - \frac{1}{C_1}\left[\frac{v_{pv}}{r_{pv}} - i_L\right] + k_i e(t) \tag{4.14}$$

Substitution of the control law assumed by equation (4.9) into equation (4.14) and after some simplification, yields

$$\begin{aligned} \dot{s} = -\frac{k_d}{C_1^2.r_{pv}}\left[\frac{v_{pv}}{r_{pv}} - i_L\right] + \frac{k_d}{C_1^2.r_{pv}}i_{c1} + \frac{1}{C_1}i_{c1} - k_i.e(t) - \frac{K.k_d.v_{out}}{L.C_1}\left(\frac{s(t)}{\|s(t)\| + \varepsilon}\right) \\ -\frac{1}{C_1}\left[\frac{v_{pv}}{r_{pv}} - i_L\right] + k_i e(t) \end{aligned} \tag{4.15}$$

Where $i_{c1} = C_1.\dot{v}_{pv} = \frac{v_{pv}}{r_{pv}} - i_L$

The equation (4.15) can be written as

$$\dot{s} = -K\overbrace{\left[\frac{k_d.V_{out}}{C_1.L}\right]}^{r}\frac{s}{\|s\| + \varepsilon} \tag{4.16}$$

The sign of the above equation depends on the sign of the constant K because the term r is always positive. So we can consider $\dot{s}$ as

$$\dot{s} = -K.\left(\frac{s}{\|s\| + \varepsilon}\right) \tag{4.17}$$

By substituting equation (4.17) into equation (4.11), we get

$$\dot{V} = s\dot{s} = \left\{-K.\left(\frac{s^2}{\|s\| + \varepsilon}\right)\right\} < 0 \tag{4.18}$$

Also as $\left(\frac{s^2}{\|s\|+\varepsilon}\right) > 0 \Rightarrow -K < 0$

It is clear that the convergence of equation (4.18) is verified only if K is chosen positive.

4.4.2.2 Adaptation mechanism

According to the global control law presented in equation (4.9), we appreciate judging, if the gains k_d and k_i take constant values, then the proposed IDSM controller will present some weakness in the design procedure. To overcome these drawbacks with high efficiency and also to adjust the IDSM controller gains according to irradiation level changes, an adaptation mechanism is proposed in this section. Firstly, the proposed sliding surface *s*, equation (4.1), is represented by the block diagram of Figure 4.3 and can be expressed by equation (4.19).

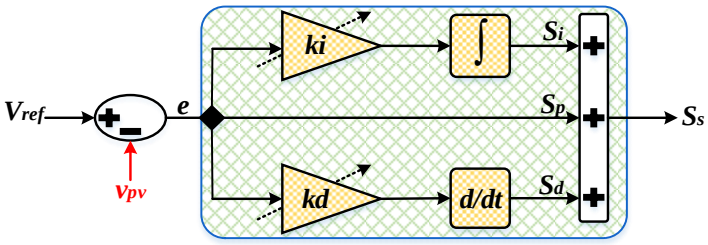

Figure 4.3: Block diagram of proposed sliding surface

where the error"e" is considered as input of the transfer function T(s) to obtain the sliding surface.

$$s_s(t) = s_i + s_p + s_d = k_i \int e\,(t)\,dt + e(t) + k_d \frac{d}{dt} e(t) \tag{4.19}$$

From equation (4.19), we get T(s) as:

$$T(s) = \frac{S(s)}{E(s)} = \frac{(k_d.s^2 + s + k_i)}{s} \tag{4.20}$$

By assuming ideal operating conditions of the system, the sliding surface must be equal to zero. From equation (4.20) it yields:

$$\left(s^2 + \frac{1}{k_d}.s + \frac{k_i}{k_d}\right).E(s) = 0 \tag{4.21}$$

Generally, a second-order system with the state variable x is described as follows:

$$\frac{d^2x}{dt^2} + 2\xi\omega_n \frac{dx}{dt} + {\omega_n}^2 x = 0 \tag{4.22}$$

Then, Laplace transform of equation (4.23) gives

$$(s^2 + 2\xi\omega_n.s + {\omega_n}^2).X(s) = 0 \tag{4.23}$$

where X is the Laplace transform of x.

The forms of equations (4.22) and (4.23) are identical. Therefore, the controller gains k_d and k_i can be determined directly by equation (4.24).

$$\Rightarrow \begin{cases} k_d = \dfrac{1}{2\xi\omega_n} \\ k_i = \dfrac{\omega_n}{2\xi} \end{cases} \tag{4.24}$$

The PV system is a second order system with its undamped natural frequency ω_n equal to

$$\omega_n = \frac{v_{pv}}{v_{out}}\sqrt{\frac{1}{L.C_1}} \tag{4.25}$$

By substituting equation (4.25) into equation (4.24), we get equation (4.26)

$$\Rightarrow \begin{cases} k_d = \dfrac{\sqrt{L.C_1}}{2\xi}.\left(\dfrac{v_{out}}{v_{pv}}\right) \\ k_i = \dfrac{1}{2\xi.\sqrt{L.C_1}}\left(\dfrac{v_{pv}}{v_{out}}\right) \end{cases} \tag{4.26}$$

Where; ξ is the damping-ratio.

4.5 SIMULATION RESULTS

In order to confirm and compare the performance of the proposed MPPT, numerical simulations are carried out using Matlab/Simulink^{TM}environment. The PV array, and boost converter parameters used for simulation are listed in Table 4.1. To provide a fair comparison, the proposed control technique is compared with conventional P&O and P&O/PI under the same conditions (sampling time and PWM frequency).The studied system is tested under fast change in solar irradiation as shown in Figure 4.6 and a fixed temperature of 25 C°.

TABLE 4.1 Parameters of the boost converter.

Boost converter	**Nominal values**
Input capacitance (C_{in})	550 μF
Inductance (L)	1 mH
Capacitance (C)	550 μF
Load resistive (R)	50 Ω

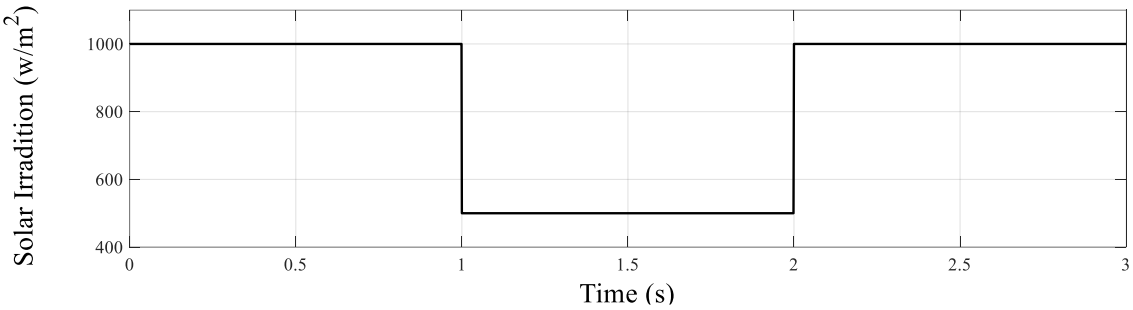

Figure 4.4 Solar irradiation profile

Figure 4.5 and 4.6 show PV voltage response corresponding to conventional P&O and P&O/PI respectively. Initially, the irradiation level is set to 1000 W/m².We observe the fluctuation of PV voltage around the reference voltage V_{ref} between (70.1-65V) and (69.4-66.5V) for conventional P&O and P&O/PI methods respectively. Whereas for the proposed P&O/A-IDSM as shown in Figure 4.7, the PV voltage tracks more accurately the reference V_{ref} where voltage fluctuation between (67.95-67.9V) has been recorded. Next, at instant t=1s, a step falling of solar radiation from 1000 w/m^2 to 500 w/m^2 is done. It is worth mentioning that compared to the others methods, the proposed control demonstrates performance superiority in terms of overshoot and response time. Indeed the proposed control takes only 1 ms to reach the reference with low overshoot and less voltage fluctuation in steady state between (65.84-65.88V), whereas P&O and P&O/PI controllers requires 120 ms and 100 ms respectively with larger overshoot and steady state voltage fluctuation. Finally, at instant t = 1.5s a step rising of solar radiation is done from 500 w/m^2 to 1000 w/m^2. In this case also we note the advantage of the proposed technique over the other methods, in terms of stability, response speed and accuracy. For more details, the key figures obtained for the different controllers are shown in Table 4.2.

The dynamic response of PV power for the conventional P&O, P&O/PI and proposed MPPT techniques are shown in Figure 4.8. It is worth mentioning that due to the relationship between the PV power and voltage, the performance of MPP tracking is affected by the PV voltage behavior, when the voltage ripple and tracking time are low, the power loss is low too and vice versa, this is why we also observe the superiority of the proposed method. For more details, Figure 4.9 illustrates a zoom of Figure 4.8; we observe clearly the performance improvement with the proposed scheme compared to other methods. Further, a comparative study through the key figures is presented in Table 4.3,

TABLE 4.2 Key results for MPPT techniques

Control Scheme	Step falling in irradiation 1000 W/m²→500 W/m²			Step rising in irradiation 500 W/m²→1000 W/m²		
	Voltage fluctuation (V)	Response time (ms)	Overshoot (V)	Voltage fluctuation (V)	Response time (ms)	Overshoot (V)
Conventional P&O	4.9	120	22.4	3	140	11.05
P&O /PI	2.9	100	6.7	2	100	4.65
Proposed P&O /A-IDSM	0.05	1	1.17	0.04	1	0.41

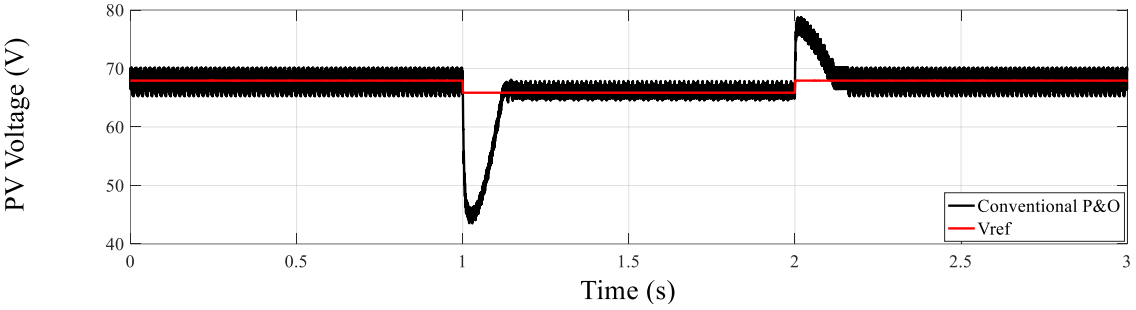

Figure 4.5 Simulated PV voltage with conventional P&O algorithm

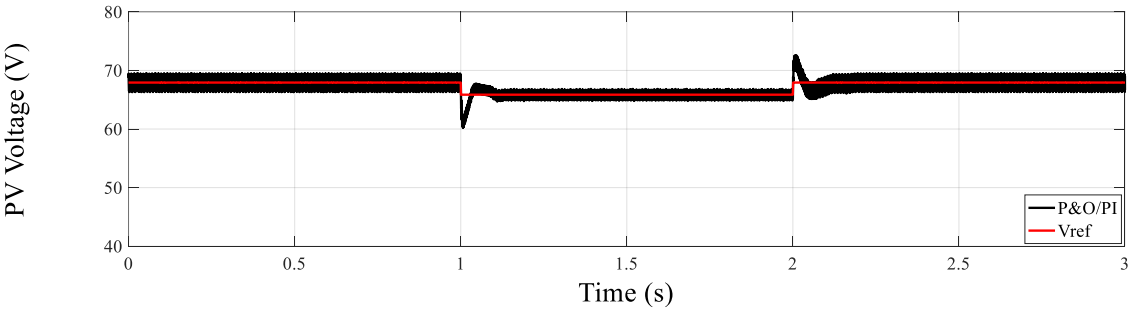

Figure 4.6 Simulated PV voltage with P&O/PI method

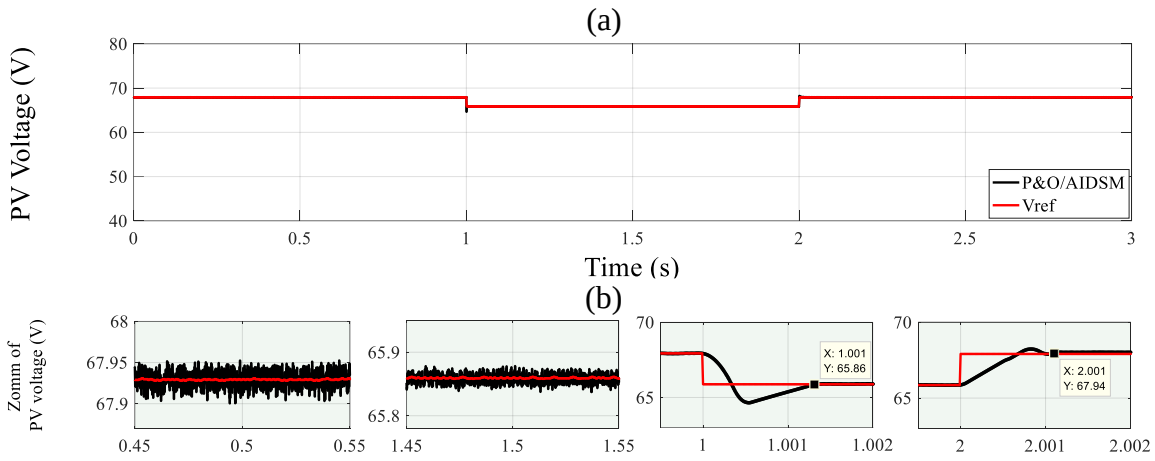

Figure 4.7 Simulated PV voltage with the proposed P&O/A-IDSM

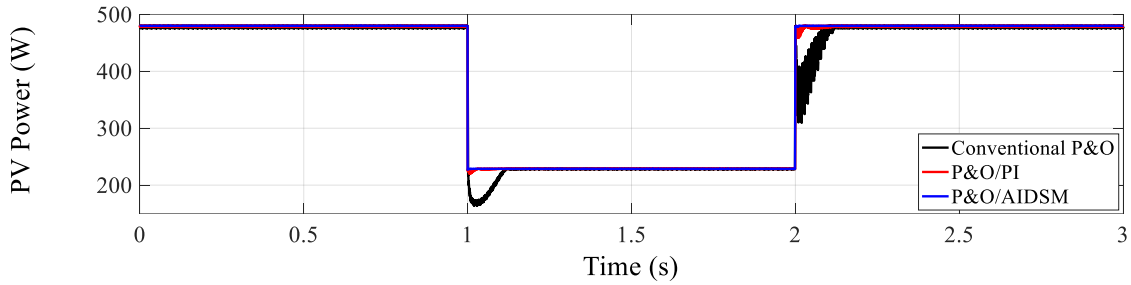

Figure 4.8 PV power waveforms for: conventional P&O (black),P&O/PI (red) and proposed P&O/AIDSM (blue)

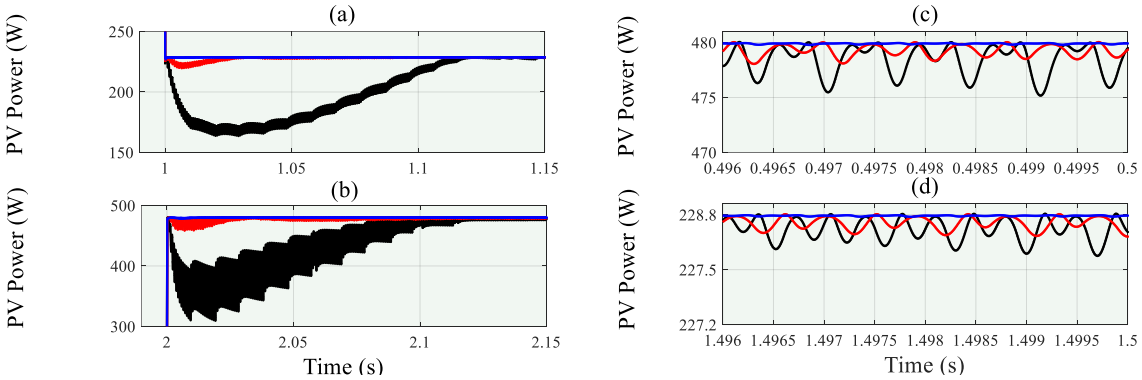

Figure 4.9 Zoom of Figure 4.8

Finally Figure 4.10 shows the behavior of the PV voltage using the proposed control under step change in solar irradiation: (a) from1000 W/m^2 to 500 W/m^2, (b) from 500 W/m^2 to 1000W/m^2 with different damping ratio ξ values. It can be observed clearly that the PV voltage behavior is significantly affected by this parameter.

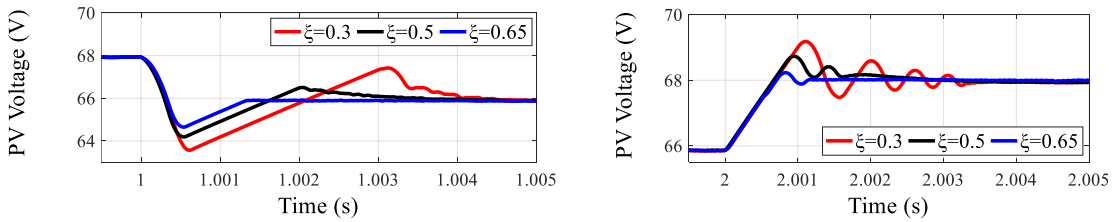

(a) **(b)**

Figure 4.10 PV voltage behaviors with different damping ratio (ξ). (a) in step decrease in irradiation from 1000 W/m^{2}to 500 W/m^2, (b) in step increase in irradiation from 500 W/m^2 to 1000 W/m^2

TABLE 4.3 Key figures of the proposed scheme and other MPPT methods.

Parameters	P&O [4.3]	PI [4.19]	FL [4.10]	DISMC [4.22]	Proposed MPPT
Steady state oscillation	Large	Medium	Low	Zero	Zero
Tracking speed	Slow	Medium	Fast	Fast	Very fast
Voltage overshot	High	Moderate	Small	Moderate	Insignificant

4.6 EXPERIMENTAL VERIFICATION

The performance of the proposed MPPT scheme is validated experimentally through a set up based on dSPACE (RTI1104) board. The hardware in the loop (HIL) setup, according to Figure 4.11, consists of an independent control processing unit (CPU), a real time simulator, a communication channel and a personal computer (PC) for monitoring the results. The real time simulator sends the state variables to CPU through the channel communication at each sample time. Therefore, the CPU computes the optimal control action and sends it to the real time simulator [4.30]. The parameters of the system and control scheme, used in HIL implementation tests, are the same as those used in the simulation. The experimental waveforms are recorded using Instek oscilloscope.

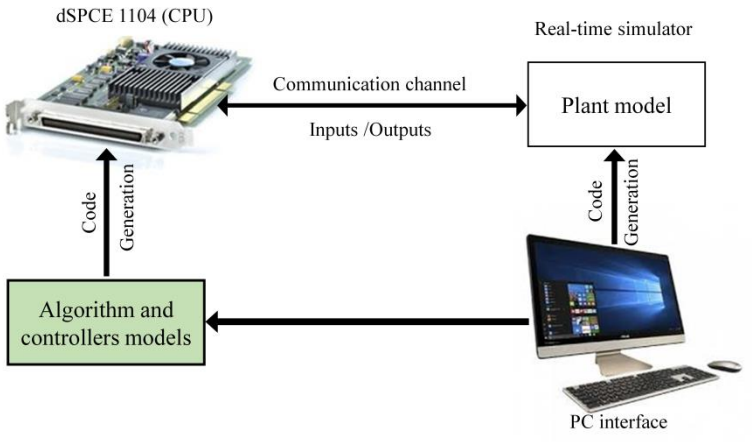

Figure 4.11: Schematic of the experimental set up

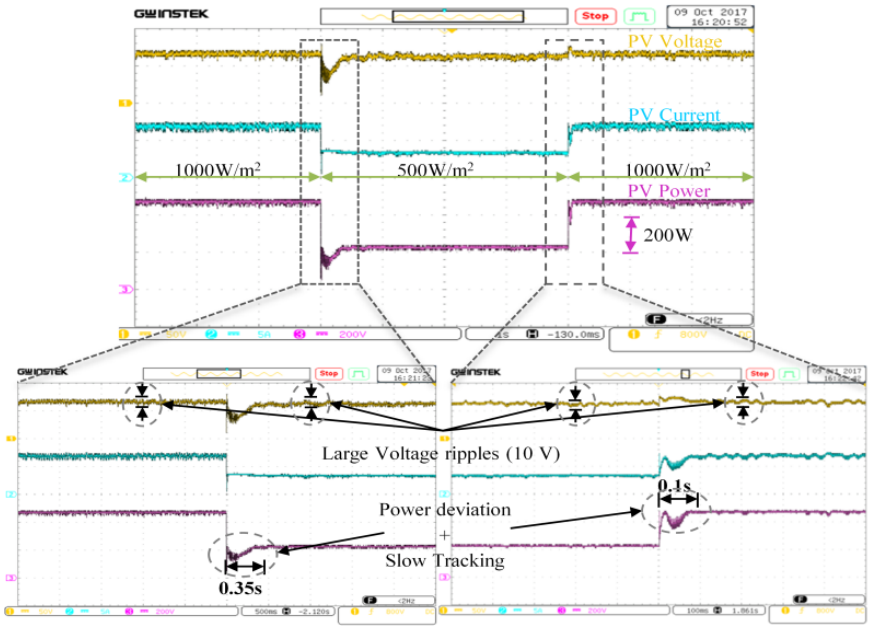

Figure 4.12: Experimental responses of the PV voltage, current and power for conventional P&O

Figures 4.12 to 4.14 show the experimental results regarding PV voltage, current and power for the conventional P&O algorithm, P&O/PI method and proposed MPPT respectively. The results obtained show clearly that the proposed scheme is fast with insignificant overshoot and low voltage ripples in steady state compared to the P&O/PI and conventional P&O. From Figure 4.12, it is observed that the PV voltage has large voltage ripples in steady state of about 10 V, which leads to significant oscillation in the PV power. In case of sudden changes in solar irradiation, from 1000 W/m² to 500 W/m² and from 500 W/m²

to 1000 W/m², the algorithm requires 350ms and 100 ms respectively to achieve the MPP with significant overshoot.

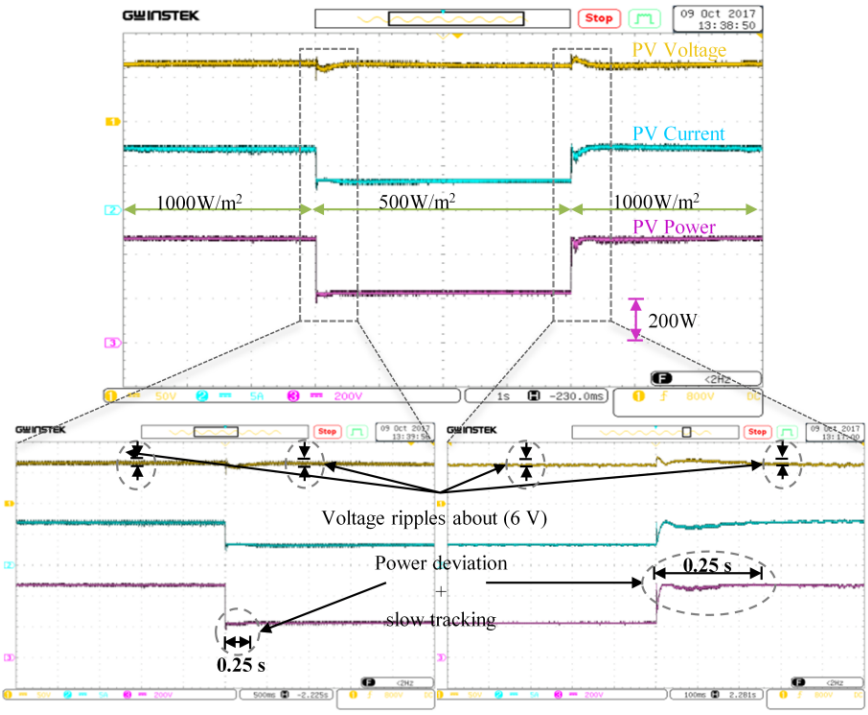

Figure 4.13: Experimental responses of the PV voltage, current and power for P&O/PI method

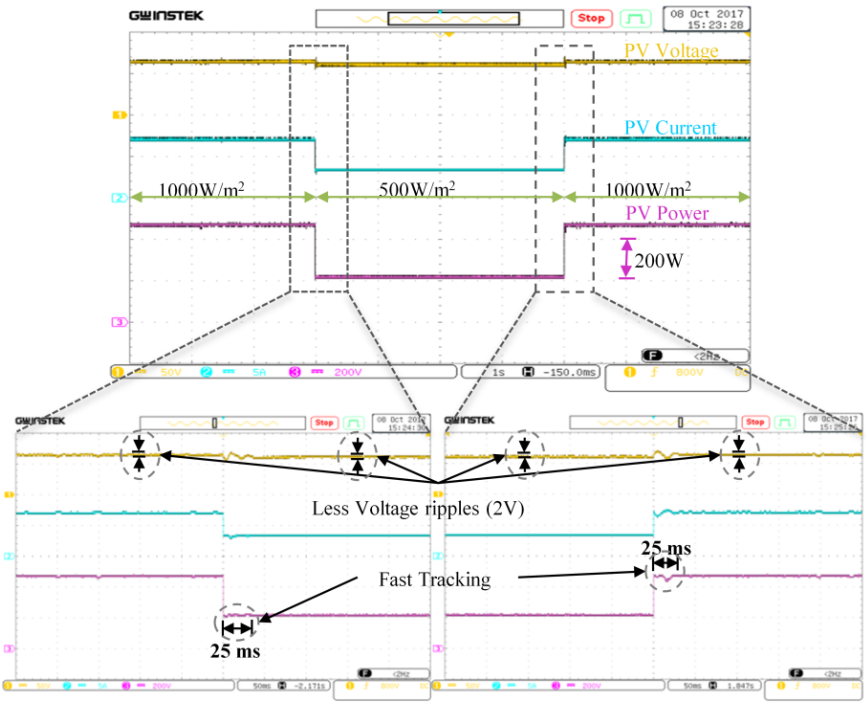

Figure 4.14: Experimental responses of the PV voltage, current and power for proposed control

In Figure 4.13, the P&O/PI method provides a better performance than the conventional P&O, particularly in steady state and at sudden decrease in solar irradiation. Where the voltage ripple in steady state is about 6 V. Moreover, it is shown that, the P&O/PI method needs 250 ms to reach the MPP with small overshoot compared to the P&O during sudden decrease in irradiation.

As shown in Figure 4.14, the proposed scheme tracks the MPP at any irradiation levels with high performance, where the power oscillation is minimized in steady state due to the low voltage ripples of about 2 V. Moreover, the MPP is accurately reached in case of fast irradiation changes. As it needs only 25 ms to reach the MPP during sudden change in irradiation levels from 1000 W/m^{2}to 500 W/m^{2}and from 500 W/m^{2}to 1000 W/m^2 without overshoots.

Finally, we observe that the results obtained experimentally are close to the simulation results, which validates the effectiveness and feasibility of the proposed MPPT.

4.7 CONCLUSION

A novel VO-MPPT method has been designed and detailed in this work. The reference voltage generated by P&O based V-MPPT algorithm is accurately tracked through the proposed voltage controller AIDSM. This latter is designed with a novel sliding surface to eliminate the overshoot during fast change in solar irradiation and minimize the steady state error. Then, the controller gains are identified using an adaptation mechanism. The performance of the proposed scheme has been tested through numerical simulations and validated experimentally. Moreover, it was compared with the conventional P&O and P&O/PI. The results obtained demonstrate that with the proposed scheme voltage fluctuation (ripples) is minimized. Furthermore, the overshoot also been eliminated, the tracking time is reduced and tracking efficiency is enhanced.

REFERENCES

[4.1] Femia, N., Petrone, G., Spagnuolo, G., Vitelli, M., 2012. Power Electronics and Control Techniques for Maximum Energy Harvesting in Photovoltaic Systems. CRC Press.

[4.2] Femia, N., Petrone, G., Spagnuolo, G., Vitelli, M., 2005. Optimization of perturb and observe maximum power point tracking method. IEEE Trans. Power Electron. 20 (4), 963–973.

[4.3] Ahmed, J. and Salam, Z., 2015. An improved perturb and observe (P&O) maximum power point tracking (MPPT) algorithm for higher efficiency. Applied Energy, 150, pp.97-108.

[4.4] de Brito, M.A.G., Galotto, L., Sampaio, L.P., e Melo, G.A., Canesin, C.A., 2013. Evaluation of the main MPPT techniques for photovoltaic applications. IEEE Trans. Ind. Electron. 60 (3), 1156–1167.

[4.5] Safari, A. and Mekhilef, S., 2011. Simulation and hardware implementation of incremental conductance MPPT with direct control method using cuk converter. IEEE transactions on industrial electronics, 58(4), 1154-1161.

[4.6] Loukriz, A., Haddadi, M. and Messalti, S., 2016. Simulation and experimental design of a new advanced variable step size Incremental Conductance MPPT algorithm for PV systems. ISA transactions, 62, 30-38.

[4.7] Belkaid, A., Colak, I. and Isik, O., 2016. Photovoltaic maximum power point tracking under fast varying of solar radiation. Applied energy, 179, 523-530.

[4.8] Rizzo, S.A. and Scelba, G., 2015. ANN based MPPT method for rapidly variable shading conditions. Applied Energy, 145, 124-132.

[4.9] Karatepe, E. and Hiyama, T., 2009. Artificial neural network-polar coordinated fuzzy controller based maximum power point tracking control under partially shaded conditions. IET Renewable Power Generation, 3(2), 239-253.

[4.10] Alajmi, B.N., Ahmed, K.H., Finney, S.J. and Williams, B.W., 2011. Fuzzy-logic-control approach of a modified hill-climbing method for maximum power point in microgrid standalone photovoltaic system. IEEE Transactions on power electronics, 26(4), 1022-1030.

[4.11] Al Nabulsi, A. and Dhaouadi, R., 2012. Efficiency optimization of a DSP-based standalone PV system using fuzzy logic and dual-MPPT control. IEEE Transactions on Industrial Informatics, 8(3), 573-584.

[4.12] Bendib, B., Belmili, H. and Krim, F., 2015. A survey of the most used MPPT methods: Conventional and advanced algorithms applied for photovoltaic systems. Renewable and Sustainable Energy Reviews, 45, 637-648.

[4.13] Shaiek, Y., Smida, M.B., Sakly, A. and Mimouni, M.F., 2013. Comparison between conventional methods and GA approach for maximum power point tracking of shaded solar PV generators. Solar energy, 90, 107-122.

[4.14] Ishaque, K., Salam, Z., Amjad, M. and Mekhilef, S., 2012. An improved particle swarm optimization (PSO)–based MPPT for PV with reduced steady-state oscillation. IEEE transactions on Power Electronics, 27(8), 3627-3638.

[4.15] Mohanty, S., Subudhi, B. and Ray, P.K., 2016. A new MPPT design using grey wolf optimization technique for photovoltaic system under partial shading conditions. IEEE Transactions on Sustainable Energy, 7(1), 181-188.

[4.16] Bianconi, E., Calvente, J., Giral, R., Mamarelis, E., Petrone, G., Ramos-Paja, C.A., Spagnuolo, G. and Vitelli, M., 2013. A fast current-based MPPT technique employing sliding mode control. IEEE Transactions on Industrial Electronics, 60(3), 1168-1178.

[4.17] Kakosimos, P.E., Kladas, A.G. and Manias, S.N., 2013. Fast photovoltaic-system voltage-or current-oriented MPPT employing a predictive digital current-controlled converter. IEEE transactions on Industrial Electronics, 60(12), 5673-5685.

[4.18] Talbi, B., Krim, F., Rekioua, T., Laib, A. and Feroura, H., 2017. Design and hardware validation of modified P&O algorithm by fuzzy logic approach based on model predictive control for MPPT of PV systems. Journal of Renewable and Sustainable Energy, 9(4), 043503.

[4.19] Elgendy, M.A., Zahawi, B. and Atkinson, D.J., 2012. Assessment of perturb and observe MPPT algorithm implementation techniques for PV pumping applications. IEEE transactions on sustainable energy, 3(1), 21-33.

[4.20] Farhat, M., Barambones, O. and Sbita, L., 2017. A new maximum power point method based on a sliding mode approach for solar energy harvesting. Applied energy, 185,

1185-1198.

[4.21] Kihel, A., Krim, F. and Laib, A., 2017, May. MPPT voltage oriented loop based on integral sliding mode control applied to the boost converter. In 2017 6th International Conference on Systems and Control (ICSC) (pp. 205-209). IEEE.

[4.22] Pradhan, R. and Subudhi, B., 2016. Double integral sliding mode MPPT control of a photovoltaic system. IEEE Transactions on Control Systems Technology, 24(1),285-292.

[4.23] Wai, R.J., 2007. Fuzzy sliding-mode control using adaptive tuning technique. IEEE Transactions on Industrial Electronics, 54(1), 586-594.

[4.24] Chiu, C.S. and Shen, C.T., 2012. Finite-time control of DC–DC buck converters via integral terminal sliding modes. International Journal of Electronics, 99(5), 643-655.

[4.25] Zainuri, M.A.A.M., Radzi, M. A. M., Soh, A.C., Abd Rahim, N. , 2014. Development of adaptive perturb and observe-fuzzy control maximum power point tracking for photovoltaic boost dc–dc converter. IET Renew. Power Gener. 8(2), 183–194.

[4.26] Harrag, A., Messalti, S., 2015. Variable step size modified P&O MPPT algorithm using GAbased hybrid offline/online PID controller. Renew. Sustain. Energy Rev. 49,1247–1260.

[4.27] Koofigar, H.R., 2016. Adaptive robust maximum power point tracking control for perturbed photovoltaic systems with output voltage estimation. ISA transactions, 60, 285-293.

[4.28] Fang, Y., Fei, J. and Ma, K., 2015. Model reference adaptive sliding mode control using RBF neural network for active power filter. International Journal of Electrical Power & Energy Systems, 73, 249-258.

[4.29] Azar, A.T. and Zhu, Q. eds., 2015. Advances and applications in sliding mode control systems. Cham: Springer International Publishing.

[4.30] Talbi, B., Krim, F., Rekioua, T., Mekhilef, S., Laib, A. and Belaout, A., 2018. A high-performance control scheme for photovoltaic pumping system under sudden irradiance and load changes. Solar Energy, 159, 353-368.

Chapter 5

A Robust Control of Two-Stage Grid-Tied PV Systems Employing Integral Sliding Mode Control

5.1 INTRODUCTION

To make PV power available for public use. The two-stage topology has been extensively employed since maximum power point tracking (MPPT) and control of generated power transfer into the grid are decoupled by different converters. This feature offers an easier and better control than the single stage topology control. To enhance the cost-effectiveness of this topology, maximum power point (MPP) should be tracked quickly and accurately under irradiation changes. Moreover, the DC-Link voltage and power injected into the grid must also be controlled accurately.

In this chapter, integral sliding mode control (ISMC) theory is used to develop effective and simple controllers for a two-stage grid-tied PV system. Moreover, the control law design has been modified, where an approximation of sign function is used as switching function resulting in a significant reduction of the chattering phenomenon. Firstly, a fixed switching frequency VO-MPPT based on ISMC theory is proposed to control the first stage (DC-DC converter) to achieve a fast and accurate MPP tracking under solar irradiation changes. Then, a new design of DC-Link voltage control based on ISMC theory is proposed to improve the regulation performance compared to other controller types, under linear solar irradiation changes. Furthermore, to control the injection of produced PV power into the grid with high grid current quality, a modified VOC based on ISMC theory is proposed. Numerical simulations through MATLAB/Simulink^{TM} and Simpower packages are carried out to confirm the improvement in control performance owing to the proposed scheme based on ISMC theory, under solar irradiation changes, in comparison with a conventional control scheme based on PI regulators.

5.2 SLIDING MODE CONTROL IN GRID-TIED PV SYSTEMS

Currently, sliding mode control (SMC) theory is widely introduced in power electronic converters control [5.1-7]. In grid-tied PV systems, SMC is employed for different purposes such as: to modify the voltage control loop of VO-MPPT [5.1-2], or internal current loop of VOC [5.6]. The application of SMC offers high control performance in addition to simple experimental implementation [5.3-8]. However, it suffers from an undesirable effect called chattering. This problem is inevitably caused by the conventional switching function (signum function) which leads to high switching frequency. To reduce this phenomenon, numerous research works use the saturation as switching function [5.1]. In [5.2, 6], the error between the selected variable and its reference has been used as input to switching surface. However, a steady-state error (SSE) remains. That is why an advanced theory in SMC was developed to enhance the SMC control performance and to reduce its disadvantage by adding an integral term to the sliding surface, which is called integral sliding mode control (ISMC).

5.3 OVERALL SYSTEM CONFIGURATION

The system under consideration, which is shown in Figure 5.1**,** represents two-stage topology of the grid-tied PV system. It is mainly composed of the following blocks: PV array which converts solar irradiation into electrical energy, DC-DC boost converter is used to track the MPP and to deliver it continuously to the DC-Link, two-level three-phase inverter whose role is to transfer the generated PV power from the boost converter to the mains grid through a passive filter "R_g, L_g" .

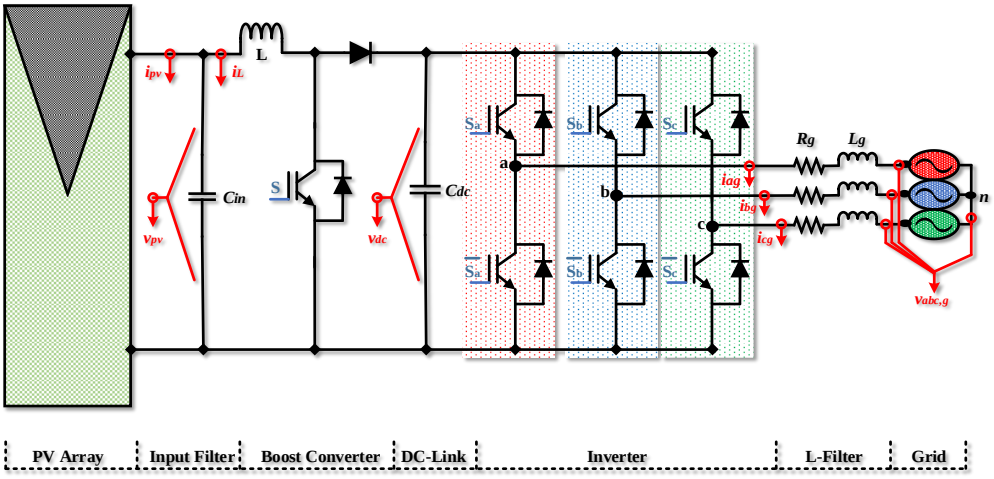

Figure 5.1: Two-stage grid-tied PV system topology.

5.4 PROPOSED CONTROL SCHEME

The proposed controllers for the two-stage grid-tied PV system are as follows:

- VO-MPPT based on ISMC, to enhance the PV energy conversion efficiency under any irradiation change.
- DC-Link voltage controller based on ISMC, to maintain the DC-Link voltage close to its reference under any irradiation change.
- VOC based on both the modified ISMC and SVM, to control the injection of the produced PV power into the grid.

5.4.1 Design of a Control Structure based on ISMC Theory

The concept of an integral sliding mode controller (ISMC) generally includes three steps. The first step concerns the design of a sliding surface on which the sliding motion will take place. The control law is designed in the second step. The control law concept depends on the selection of switching function to force the system state trajectories to track and to slide on the sliding surface. Whereas, the last step ensures the reachability condition, which pledges the existence of the sliding mode [5.8-9].

In the present contribution, a high-performance control scheme for grid-tied PV system using ISM controllers is proposed. In ISMC theory, an integral term is added to the sliding surface to obtain a high-performance control and to achieve a quick and accurate tracking. The sliding surface "s" in an ISM controller can be expressed as

$$s = e + k_i \int e\, dt \tag{5.1}$$

where, e is the error between the measured variable and its reference, k_i is the sliding surface coefficient.

Typically, the control law has a structure given as

$$u = u_{eq} + u_{dis} \tag{5.2}$$

where, u_{eq} is the equivalent part responsible for helping to keep sliding, and u_{dis} is the discontinuous part used to enforce the sliding mode to remain along the sliding surface traditionally written as follows

$$u_{dis} = -\mathcal{M}\ sign\ (s) \tag{5.3}$$

where, $\mathcal{M}$ is the proportional gain of discontinuous control and $sign\ (s)$ is sign function.

The discontinuity related with this part leads to chattering phenomenon. To eliminate this drawback, the sign function is replaced with its smoothing approximation, as shown in Figure 5.2. Hence u_{dis} can be expressed by the following equation

$$u_{dis} = -\mathcal{M}\frac{s}{\|s\| + \alpha} \tag{5.4}$$

where, α is a small positive value.

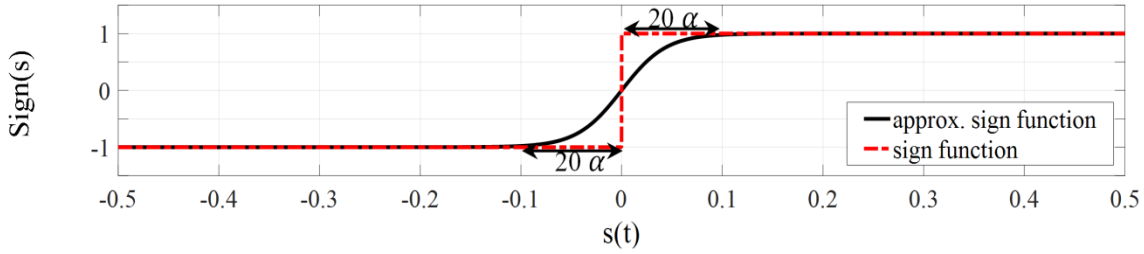

Figure 5.2: Approximation of sign function.

After the design of control law in the previous steps, the conditions required to ensure the control stability will be checked. Lyapunov function is used to examine the control stability. It is defined as follows

$$V = \frac{1}{2}s^2 \tag{5.5}$$

Therefore, to guarantee the convergence of V, it should be verified that the derivative of V is negative as follows

$$\dot{V} = s\dot{s} < 0 \tag{5.6}$$

Accordingly, one will define individually the reachability condition for each of the three proposed controllers, in the following sections.

5.4.2 MPPT Control

To obtain an optimal exploitation of the PV array during all solar irradiation changes, the proposed control scheme is divided in two steps as shown in Figure 5.3. Firstly, a P&O-based voltage MPPT (V-MPPT) generates the reference voltage V_{ref}. Then, an improved ISMC-based cascade voltage regulator is proposed to enforce the PV voltage v_{pv} to track V_{ref} generated previously by providing the suitable duty cycle D to PWM modulation stage to

control the boost converter. Therefore, the dynamic model of the boost converter is mentioned in chapter 2 subsection 2.4.1 and can be expressed as [5.10]:

$$\begin{cases} \dfrac{dv_{pv}}{dt} = \dfrac{i_{pv} - i_L}{C_{in}} \\ \dfrac{di_L}{dt} = \dfrac{v_{pv} - v_{dc} + Dv_{dc}}{L} \end{cases} \tag{5.7}$$

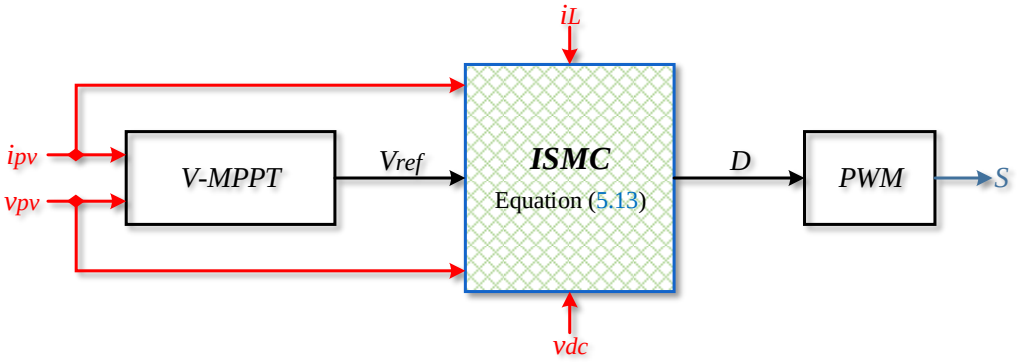

Figure 5.3: Block diagram of proposed VO-MPPT.

5.4.2.1 V-MPPT

The objective of the V-MPPT is to generate V_{ref} corresponding to the MPP. For this purpose, P&O-based V-MPPT technique is employed due to its featuring effectiveness and simplicity as shown in Figure 5.4.

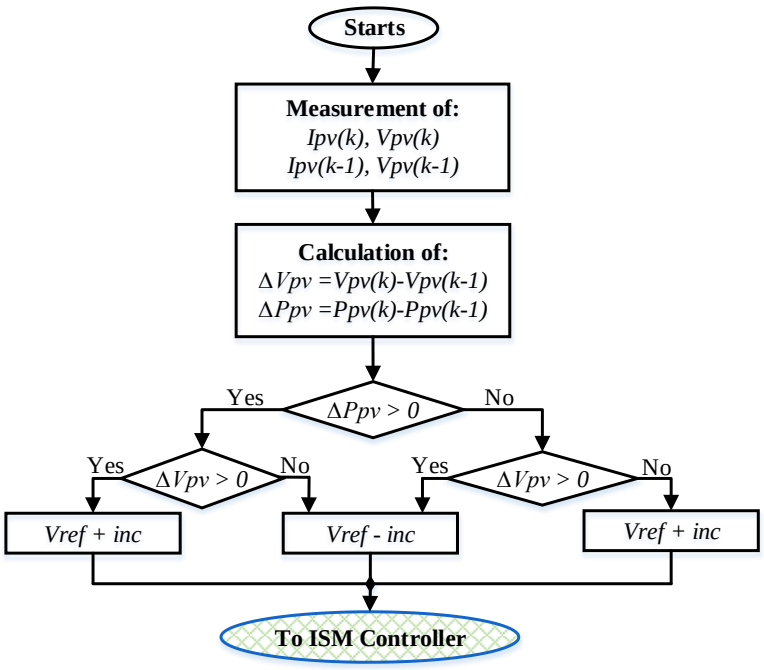

Figure 5.4: V-MPPT flowchart.

5.4.2.2 Design of ISMC

In this section, an enhanced cascade voltage regulator based on ISMC theory is proposed to provide the suitable duty ratio D to drive the boost converter towards V_{ref} to improve the power extraction from the PV array. Hence, in the controller strategy the sliding surface has the same form as that given in equation (5.1) and expressed as

$$s_{pv} = e_{pv} + k_{i,PV} \int e_{pv}\ dt \tag{5.8}$$

where, $e_{pv}(t)$ is the voltage error between "V_{ref}" and "v_{pv}" and $k_{i,PV}$ is the sliding surface coefficient.

It is considered that δ is the sliding surface derivative, which is also called the sliding manifold, given as

$$\delta = \dot{s}_{pv} = \dot{e}_{pv} + k_{i,PV} e_{pv} \tag{5.9}$$

To obtain the equivalent control signal, equation (5.9) must be derived and equated to zero as follows

$$\begin{gathered} \dot{\delta} = \ddot{e}_{pv} + k_{i,PV}\dot{e}_{pv} = 0 \\ \text{Or} \\ -\ddot{v}_{pv} - k_{i,PV}\dot{v}_{pv} = 0 \end{gathered} \tag{5.10}$$

By using equation (2.7), equation (5.10) can be written as

$$-\frac{\left(\dot{i}_{pv} - \frac{1}{L}\left[v_{pv} - v_{dc} + v_{dc}\cdot D\right]\right)}{C_{in}} - \frac{k_{i,PV}[i_{pv} - i_L]}{C_{in}} = 0 \tag{5.11}$$

Thus, the equivalent control can be expressed as

$$D_{eq} = \frac{\left(v_{dc} - v_{pv} + L\cdot k_{i,PV}\left[i_{pv} - i_L\right] + L\cdot \dot{i}_{pv}\right)}{v_{dc}} \tag{5.12}$$

Hence, one part of the control input can be obtained; the second part called D_{dis} is given by equation (5.4).

Therefore, the overall sliding mode controller is expressed as

$$D = \frac{\left(v_{dc} - v_{pv} + L\cdot k_{i,PV}\left[i_{pv} - i_L\right] + L\cdot \dot{i}_{pv}\right)}{v_{dc}} - \mathcal{M}_{PV}\ \frac{s_{pv}}{\|s_{pv}\| + \alpha} \tag{5.13}$$

where, $\mathcal{M}_{PV}$ is the proportional gain of discontinuous control part.

The controller described by equation (5.13) must satisfy the reachability condition. From equation (2.7), we obtain

$$\begin{cases} \dot{v}_{pv} = \dfrac{[i_{pv} - i_L]}{C_{in}} \\ \ddot{v}_{pv} = \dfrac{\left[\dot{i}_{pv} - \dfrac{1}{L}[v_{pv} - v_{dc} + Dv_{dc}]\right]}{C_{in}} \end{cases} \tag{5.14}$$

By substituting $\dot{v}_{pv}$ and $\ddot{v}_{pv}$ in equation (5.10), we get

$$\dot{\delta} = -\frac{\left[\dot{i}_{pv} - \dfrac{1}{L}[v_{pv} - v_{dc} + D \cdot v_{dc}]\right]}{C_{in}} - k_{i,PV}\frac{[i_{pv} - i_L]}{C_{in}} \tag{5.15}$$

By substituting the overall control law D given by equation (5.13) in equation (5.15) and after some simplifications, we get

$$\dot{\delta} = -\mathcal{M}_{PV}\left(\frac{v_{dc}}{L \cdot C_{in}}\frac{s_{pv}}{\|s_{pv}\| + \alpha}\right) \tag{5.16}$$

Finally, the reachability condition must be verified, which means $\delta.\dot{\delta} < 0$. Thus

$$\delta \cdot \dot{\delta} = \|\delta\|\left\{-\mathcal{M}_{PV}\left(\frac{v_{dc}}{L \cdot C_{in}}\frac{s_{pv}}{\|s_{pv}\| + \alpha}\right)\right\} < 0 \tag{5.17}$$

Since $\frac{s_{pv}}{\|s_{pv}\|+\alpha}$ and $\frac{v_{dc}}{L \cdot C_{in}}$ are always positive, it is obvious that the reachability condition is verified if only$\mathcal{M}_{PV}$ is chosen positive.

5.4.3 Design of DC-Link Voltage Controller

As mentioned above, the objective of DC-Link regulation is to maintain the DC-Link voltage close to its reference value and to estimate the reference *d*-axis grid current "i_{dg}^{*}" whatever the produced PV power. For this purpose, a novel design based on ISMC theory for the DC-Link voltage control is discussed in this section. The block diagram of the proposed DC-Link controller is shown in Figure 5.5.

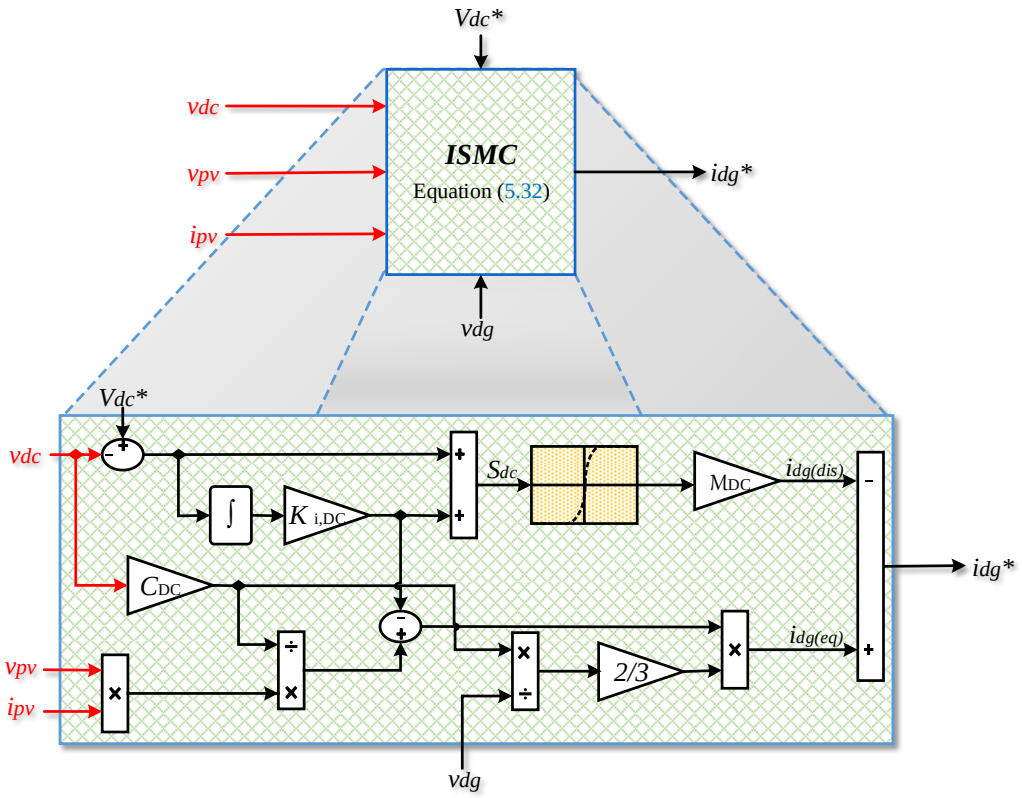

Figure 5.5: Block diagram of the proposed DC-Link voltage controller based on ISMC theory.

The proposed sliding surface of the DC-Link voltage control is given below

$$s_{dc} = e_{dc} + k_{i,DC} \int e_{dc}\ dt \tag{5.18}$$

where, e_{dc} is the voltage error between the DC-Link voltage v_{dc} and its reference value V_{dc}^{*} and $k_{i,DC}$ is the sliding surface coefficient.

The time derivative of the previous equation is given by

$$\dot{s}_{dc} = -\dot{v}_{dc} + k_{i,DC} e_{dc} \tag{5.19}$$

By considering energy conservation, it yields

$$p_{pv} = p_{dc} = p_g \tag{5.20}$$

Where, p_{pv} , p_{dc} and p_g are the produced PV power, DC-Link power and power injected into the grid, respectively.

The injected power into the three-phase grid system (in synchronous d-q frame) is expressed as

$$p_g = \frac{3}{2}\left(v_{dg}\, i_{dg} + v_{qg}\, i_{qg}\right) \tag{5.21}$$

The aim of the proposed controller is to inject only the produced PV power. According to this condition, the q-axis grid current i_{qg} becomes null and equation (5.21) can be rewritten as

$$p_g = \frac{3}{2}\left(v_{dg}\, i_{dg}\right) \tag{5.22}$$

The inverter input power is given as

$$p_{dc} = v_{dc}\, i_{inv} \tag{5.23}$$

By applying Kirchhoff current law at the DC-Link between the inverter and boost converter it yields

$$\begin{gathered} i_{dc} = C_{dc}\frac{dv_{dc}}{dt} = (i_{out} - i_{inv}) \\ \text{Or} \\ \dot{v}_{dc} = \frac{(i_{out} - i_{inv})}{C_{dc}} \end{gathered} \tag{5.24}$$

where, i_{out} is the boost output current, i_{inv} inverter input current and C_{dc} is the DC-Link capacitor.

By substituting equations (5.22) and (5.23) in equation (5.20), it yields

$$\begin{gathered} v_{dc}\, i_{inv} = \frac{3}{2}\,(v_{dg}\, i_{dg}) \\ \text{Or} \\ i_{inv} = \frac{3v_{dg}}{2v_{dc}}\, i_{dg} \end{gathered} \tag{5.25}$$

By assuming that the DC-Link voltage v_{dc} is properly regulated, the derivative of the DC-Link voltage $\dot{v}_{dc}$ (or capacitor current i_{dc}) becomes close to zero. Then (5.24) can be written as

$$i_{inv} = i_{out} \tag{5.26}$$

Then,

$$p_{dc} = v_{dc} \cdot i_{out} = p_{pv} \tag{5.27}$$

The current i_{out} can be determined as

$$i_{out} = \frac{p_{pv}}{v_{dc}} \tag{5.28}$$

By replacing equations (5.25) and (5.28) in equation (5.24), we get

$$\dot{v}_{dc} = \frac{1}{C_{dc}}\left(\frac{p_{pv}}{v_{dc}} - \frac{3v_{dg}}{2v_{dc}}\, i_{dg}\right) \tag{5.29}$$

To determine the equivalent control, equation (5.19) must be set to zero as follows

$$\begin{gathered} \dot{s}_{dc} = -\dot{v}_{dc}(t) + k_{i,DC}\, e_{dc}(t) = 0 \\ \Rightarrow -\frac{1}{C_{dc}}\left(\frac{p_{pv}}{v_{dc}} - \frac{3v_{dg}}{2v_{dc}}\, i_{dg}\right) + k_{i,DC}\, e_{dc}(t) = 0 \end{gathered} \tag{5.30}$$

From equation (5.30) the equivalent control law is expressed as

$$i^*_{dg(eq)} = \frac{2C_{dc}v_{dc}}{3v_{dg}}\left(\frac{p_{pv}}{C_{dc}v_{dc}} - k_{i,DC}\, e_{dc}(t)\right) \tag{5.31}$$

Therefore, the global control law can be written as

$$i^*_{dg} = \frac{2C_{dc}v_{dc}}{3v_{dg}}\left(\frac{p_{pv}}{C_{dc}v_{dc}} - k_{i,DC}\, e_{dc}(t)\right) - \mathcal{M}_{DC}\, \frac{s_{dc}}{\|s_{dc}\| + \alpha} \tag{5.32}$$

where, $\mathcal{M}_{DC}$ is the proportional gain of discontinuous control part.

To confirm that the controller described by equation (5.32) satisfies the reachability condition, $\dot{s}_{dc}$ needs to be evaluated.

By substituting equation (5.29) in equation (5.19), we get

$$\dot{s}_{dc} = -\frac{1}{C_{dc}}\left(\frac{p_{pv}}{v_{dc}} - \frac{3v_{dg}}{2v_{dc}} i_{dg}\right) + k_{i,DC}\, e_{dc} \tag{5.33}$$

By substituting the overall control law i^*_{dg} given by equation (5.32) in equation (5.33), we get

$$\dot{s}_{dc} = -\mathcal{M}_{DC}\, \frac{3v_{dg}}{2C_{dc}v_{dc}}\left(\frac{s_{dc}}{\|s_{dc}\| + \alpha}\right) \tag{5.34}$$

As previously, the condition $s_{dc} \cdot \dot{s}_{dc} < 0$ must be verified. Thus

$$s_{dc} \cdot \dot{s}_{dc} = -\mathcal{M}_{DC}\left\{\frac{3v_{dg}}{2C_{dc}v_{dc}}\, \frac{{s_{dc}}^2}{\|s_{dc}\| + \alpha}\right\} < 0 \tag{5.35}$$

Since $\left(\frac{{s_{dc}}^2}{\|s_{dc}\|+\alpha}\right)$ and $\left(\frac{3v_{dg}}{2C_{dc}v_{dc}}\right)$ are positive, so it is clear that the reachability condition is verified if only$\mathcal{M}_{DC}$ is chosen positive.

5.4.4 VOC Based ISMC

In this section, a modified VOC based on ISM control theory (VOC-ISMC) is presented and detailed. The main objective of the proposed control scheme is to inject the generated PV power into the grid with high grid current quality. VOC-ISMC is based on the calculation of the reference voltage vector which is applied through SVM in order to minimize the error between the rotating frame currents i_{dg}, i_{qg} and their references i_{dg}^*, i_{qg}^*. Figure 5.6 summarizes the functionality of VOC-ISMC. Firstly, i_{dg}^* is estimated by the DC-Link voltage regulator presented in the above section, while i_{qg}^* is set to zero to eliminate the injection of reactive power into the grid. Then, the obtained reference voltage vector $(v_d^*,\ v_q^*)$ is transformed to α-β frame $(v_\alpha^*,\ v_\beta^*)$ and applied through SVM to control grid-tied inverter. The phase-locked loop (PLL) allows controlling an estimated angle θ_g with respect to the grid phase angle and it is also needed for the Park's transformation.

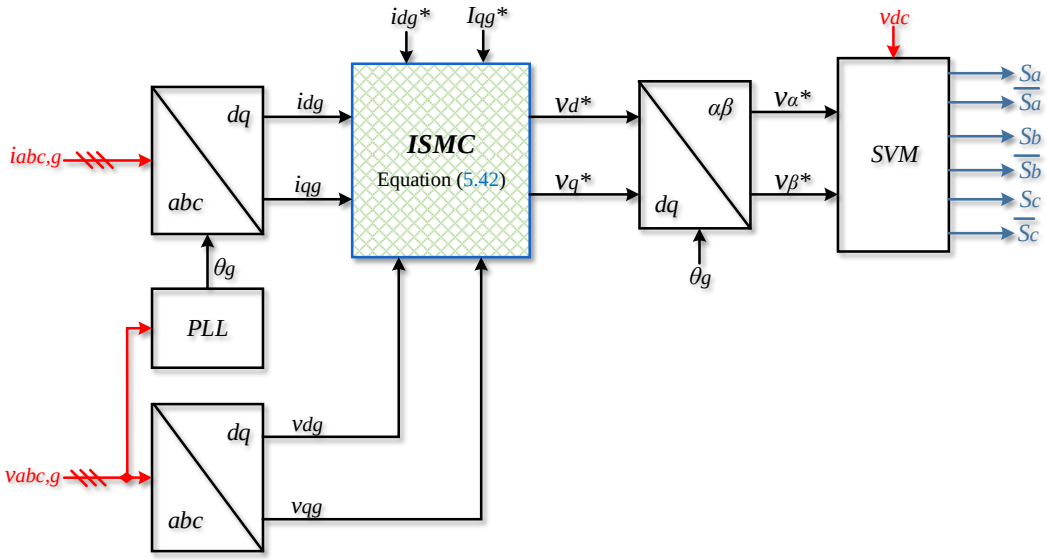

Figure 5.6: The proposed VOC based on ISMC.

The development of the proposed control scheme needs the mathematical model of the grid-tied inverter in d-q rotating frame which can be described in terms of inverter voltages, grid voltages, and filter inductance [5.11] as,

$$\begin{cases} \dfrac{di_{dg}}{dt} = \dot{i}_{dg} = \dfrac{\left(-R_g i_{dg} - v_{dg} + V_d\right)}{L_g} + \omega i_{qg} \\ \dfrac{di_{qg}}{dt} = \dot{i}_{qg} = \dfrac{\left(-R_g i_{qg} - v_{qg} + V_q\right)}{L_g} - \omega i_{dg} \end{cases} \tag{5.36}$$

where $(v_{dg},\ v_{qg})$, $(i_{dg},\ i_{qg})$ and $(V_d,\ V_q)$ are the (d-q) components of grid voltages, grid currents and inverter output voltages respectively; ω is the grid angular frequency; R_g and L_g are the resistance and inductance of the filter, respectively.

The proposed sliding mode surfaces are defined as follows;

$$\begin{cases} s_d = e_d + k_{i,d} \int e_d \, dt \\ s_q = e_q + k_{i,q} \int e_q \, dt \end{cases} \tag{5.37}$$

where, e_d is the error between i_{dg}^* and i_{dg} currents, while e_q is the error between i_{qg}^* and i_{qg} currents $k_{i,d}$, $k_{i,q}$ are constant gains.

The time derivative of the above equation yields

$$\begin{cases} \dot{s}_d = -\dot{i}_{dg} + k_{i,d} e_d \\ \dot{s}_q = -\dot{i}_{qg} + k_{i,q} e_q \end{cases} \tag{5.38}$$

The equivalent control terms are obtained by setting $\dot{s}_d$ and $\dot{s}_q$ to zero. Thus

$$\begin{cases} \dot{s}_d = -\dot{i}_{dg} + k_{i,d} e_d = 0 \\ \dot{s}_q = -\dot{i}_{qg} + k_{i,q} e_q = 0 \end{cases} \tag{5.39}$$

By substituting equation (5.36) in equation (5.39), we get

$$\begin{cases} -\left[\dfrac{\left(-R_g i_{dg} - v_{dg} + v_{d(eq)}^*\right)}{L_g} + \omega i_{qg}\right] + k_{i,d} e_d = 0 \\ -\left[\dfrac{\left(-R_g i_{qg} - v_{qg} + v_{q(eq)}^*\right)}{L_g} - \omega i_{dg}\right] + k_{i,q} e_q = 0 \end{cases} \tag{5.40}$$

The equivalent control terms are given by

$$\begin{cases} v_{d(eq)}^* = R_g i_{dg} - \omega L_g i_{qg} + v_{dg} + L_g k_{i,d} e_d \\ v_{d(eq)}^* = R_g i_{qg} + \omega L_g i_{dg} + v_{qg} + L_g k_{i,q} e_q \end{cases} \tag{5.41}$$

The global control law is summarized as follows

$$\begin{cases} v_d^* = R_g i_{dg} - \omega L_g i_{qg} + v_{dg} + L_g k_{i,d} e_d - \mathcal{M}_d \dfrac{s_d}{\|s_d\| + \alpha} \\ v_q^* = R_g i_{qg} + \omega L_g i_{dg} + v_{qg} + L_g k_{i,q} e_q - \mathcal{M}_q \dfrac{s_q}{\|s_q\| + \alpha} \end{cases} \tag{5.42}$$

where, $\mathcal{M}_d$ and $\mathcal{M}_q$ are proportional gains of the discontinuous control parts.

To confirm that the controller described in equation (5.42) satisfies the reachability condition, the expressions of $\dot{s}_d$ and $\dot{s}_q$ are needed.

So, by substituting equation (5.36) in equation (5.38), we get

$$\begin{cases} \dot{s}_d = -\left[\dfrac{\left(-R_g i_{dg} - v_{dg} + V_d\right)}{L_g} + \omega i_{qg}\right] + k_{i,d} e_d \\ \dot{s}_q = -\left[\dfrac{\left(-R_g i_{qg} - v_{qg} + V_q\right)}{L_g} - \omega i_{dg}\right] + k_{i,q} e_q \end{cases} \tag{5.43}$$

Then, by replacing the global control law (v_d^* and v_q^*) given by equation (5.42) in equation (5.43), we obtain

$$\begin{cases} \dot{s}_d = \dfrac{\mathcal{M}_d}{L_g} \dfrac{s_d}{\|s_d\| + \alpha} \\ \dot{s}_q = \dfrac{\mathcal{M}_q}{L_g} \dfrac{s_q}{\|s_q\| + \alpha} \end{cases} \tag{5.44}$$

The reachability condition can be expressed as

$$\begin{cases} s_d \cdot \dot{s}_d < 0 \\ s_q \cdot \dot{s}_q < 0 \end{cases} \tag{5.45}$$

By substituting equation (5.44) in equation (5.45), we obtain

$$\begin{cases} s_d \cdot \dot{s}_d = \mathcal{M}_d \left\{\dfrac{1}{L_g} \dfrac{s_d^2}{\|s_d\| + \alpha}\right\} < 0 \\ s_q \cdot \dot{s}_q = \mathcal{M}_q \left\{\dfrac{1}{L_g} \dfrac{s_q^2}{\|s_q\| + \alpha}\right\} < 0 \end{cases} \tag{5.46}$$

As known that the terms $\frac{s_d^2}{\|s_d\|+\alpha}$, $\frac{s_q^2}{\|s_q\|+\alpha}$ and $\frac{1}{L_g}$ are positive, the gains $\mathcal{M}_d$ and $\mathcal{M}_q$ must be chosen negative in order to satisfy the reachability condition of the controller described in equation (5.46).

5.5 SIMULATION RESULTS

Numerical simulations using MATLAB/Simulink™ environment are carried out to confirm the performance of the proposed scheme compared to the conventional scheme. The specifications are listed in Table 5.1. The DC-Link reference voltage is fixed at 220 V. The reference current i_{qg}^{*} is set to zero (injecting only the active power). As discussed in Chapter 2, the temperature has a little effect on the MPP position of the PV array; in contrast, the irradiation level affects significantly the PV array performance. That is why the proposed control scheme is verified under suddenly and linearly varying irradiation as shown in Figure 5.7 by considering a fixed temperature value of 25 °C. The proposed control scheme is compared with the conventional scheme (PI-based controller), with the same specifications in Table 5.1 to provide a fair comparison.

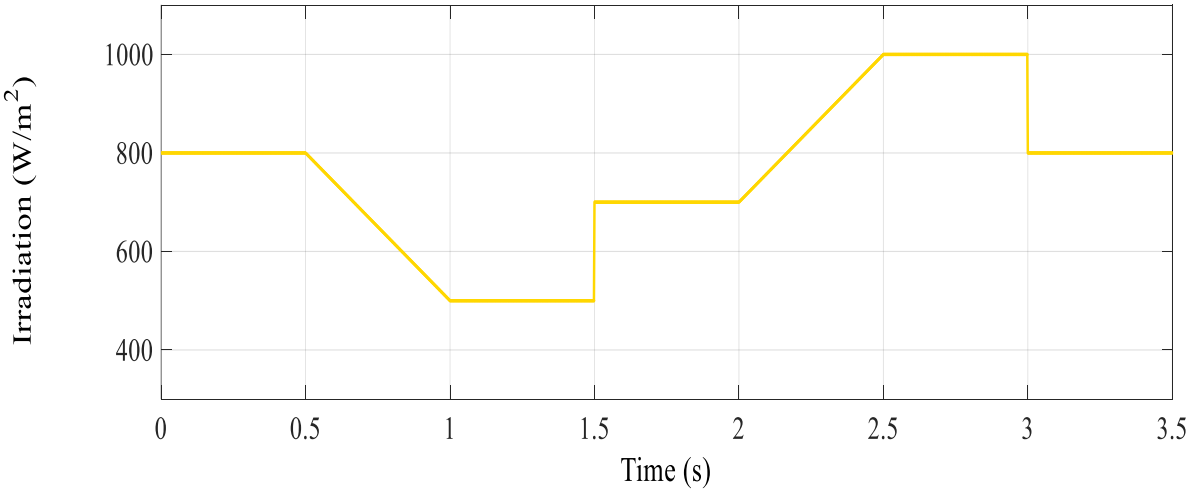

Figure 5.7: Solar irradiation profile.

TABLE 5.1: Global system specifications.

GPV	**Nominal values**
Open circuit voltage ($\boldsymbol{V_{OC}}$)	42.1 [V]
Optimum operating voltage($\boldsymbol{V_{mpp}}$)	33.7 [V]
Short circuit current ($\boldsymbol{I_{SC}}$)	3.87 [A]
Optimum operating current ($\boldsymbol{I_{mpp}}$)	3.56 [A]
Maximum power ($\boldsymbol{P_{mpp}}$)	120 [W]
Number of cells connected in series ($\boldsymbol{N_s}$)	72
Number of cells connected in parallel ($\boldsymbol{N_p}$)	1
Number of panels connected in series ($\boldsymbol{N_{ss}}$)	2
Number of panels connected in parallel ($\boldsymbol{N_{pp}}$)	2
Boost converter	**value**
Inductance ($\boldsymbol{L}$)	1 [mH]
Input capacitor ($\boldsymbol{C_{in}}$)	470 [µF]
output capacitor ($\boldsymbol{C_{dc}}$)	100 [µF]
Electrical parameters of grid connected	**value**
Output filter inductance ($\boldsymbol{L_g}$)	10 [mH]
Line resistance ($\boldsymbol{R_g}$)	0.1 [Ω]
Nominal grid frequency ($\boldsymbol{f_g}$)	50 [Hz]
Nominal line voltage of the 3-phase grid ($\boldsymbol{v_g}$)	100 [V]
Simulation parameters	**value**
V-MPPT sampling frequency ($\boldsymbol{T_s}$)	1 [kHz]
PWM switching frequency ($\boldsymbol{f_{s,PWM}}$)	5 [kHz]
SVM switching frequency ($\boldsymbol{f_{s,SVM}}$)	25 [kHz]

Figures 5.8 and 5.9 represent the results obtained with the conventional and proposed control schemes, respectively. From top to bottom, the waveforms given in Figures 5.8 and

5.9 are: (a) PV voltage, (b) PV current, (c) PV power, (d) DC-Link voltage with its desired reference, (e) i_{dg} current with its reference, (f) i_{qg} current with its reference.

At the outset, the results confirm the low tracking speed of the conventional control scheme (PI-based controller) under irradiation changes with significant PV voltage fluctuation in steady-state. In contrast, a high tracking performance was exhibited by using the proposed control scheme. Also, an instantaneous effect on the PV voltage is displayed under irradiation changes without overshoots and with less fluctuation, as shown in Figure 5.10. Due to the relationship between the PV power and PV voltage, the performance of MPP tracking is affected by the PV voltage behavior, when the PV voltage fluctuation and tracking time are small, the extracted PV power loss is minimized. Moreover, Figure 5.11 illustrates the improvement in the extracted PV power using the proposed control scheme compared to the conventional VO-MPPT. For more details, the main simulation results obtained from both MPPT methods are summarized in Table 5.2.

TABLE 5.2: Comparison results for MPPT methods.

MPPT Technique	**Step change in irradiance 500→700 W/m²**		**Step change in irradiance 1000→800 W/m²**		**Linear change in irradiance 800→500 W/m² and 700→1000 W/m²**
	Power oscillation (W)	Tracking speed time (s)	Power oscillation (W)	Tracking speed time (s)	Tracking Accuracy
Conventional VO-MPPT	0.17	0.022	0.23	0.02	Low
Proposed VO-MPPT	Less than 0.03	0.0085	0.051	0.0061	Very good

Furthermore, we examine the DC-Link voltage regulation using the conventional PI controller and the proposed ISMC scheme. The obtained results shown in Figure 5.12 confirm the tracking superiority of the proposed control scheme compared to the conventional one under solar irradiation changes. It can be observed, that by using the conventional PI controller, the DC-Link voltage deviates from its reference in case of linear changes in solar irradiation. Moreover, in case of step irradiation changes, the overshoot and response time are significantly large. In contrast, the desired reference is accurately tracked by employing the proposed ISMC in addition to, insignificant overshoot and short response time under step

irradiation changes. To show the performance improvement by using the proposed control scheme compared to the conventional scheme, key results are presented in Table 5.3.

TABLE 5.3: Comparison results for DC-Link regulation.

Control Scheme	**Linear Change in Irradiance 800→500 W/m²**	**Step Change in Irradiance 500→700 W/m²**		**Linear Change in Irradiance 700→1000 W/m²**	**Step Change in Irradiance 1000→800 W/m²**	
	Static Error Average (%)	Overshoot (%)	Settling Time (s)	Static error Average (%)	Overshoot (%)	Settling Time (s)
Conventional PI	1.512	6.95	0.175	1.478	7.47	0.179
Proposed scheme	0.051	2.2	0.035	0.057	2.98	0.08

We also observe that the proposed VOC-ISMC scheme allows injecting the extracted PV power into the grid with high quality and efficiency, contrary to the conventional control scheme (VOC-PI controller). It can be observed that by applying the proposed control scheme, i_{dg} and i_{qg} currents are completely regulated to their references. It is found that i_{dg} current exhibits fast response with less fluctuation compared to the conventional control, as shown in Figure 5.9(e), which leads to increase the quality of grid currents and their amplitudes follow almost instantaneously the irradiation changes, as shown in Figure 5.13(b). In contrast, the grid current waveforms obtained by using the conventional control scheme are relatively of poor quality due to the large fluctuation and response time of i_{dg} current, as shown in Figure 5.13(a). A comparison summary in terms of key indexes such as grid current THD% and i_{dg} current ripples for various irradiation levels is depicted in Figure 5.14.

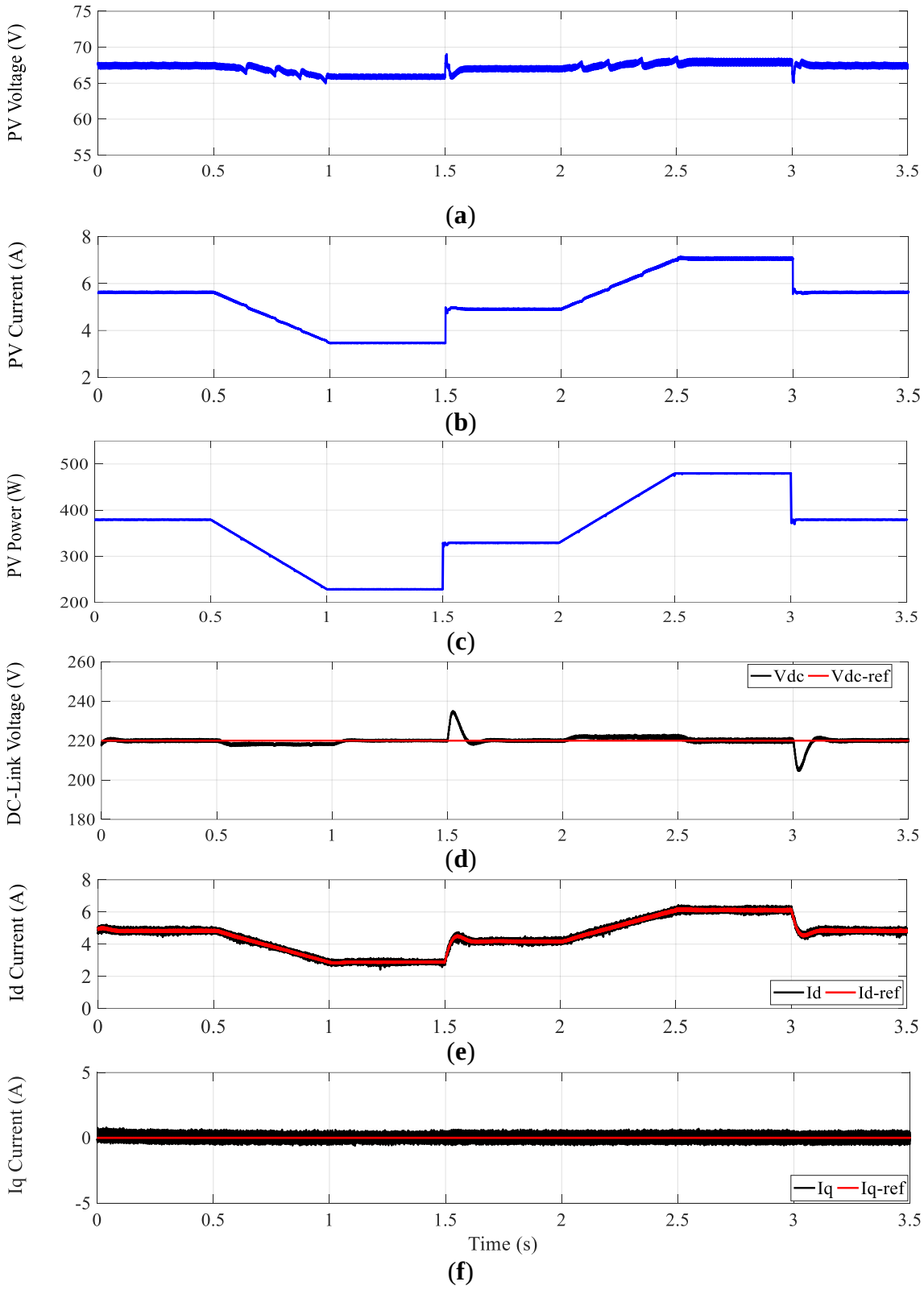

Figure 5.8: Simulation results of grid-tied PV system with the conventional control scheme; under irradiation changes. (**a**) PV Voltage; (**b**) PV Current; (**c**) PV Power; (**d**) DC−Link Voltage; (**e**) Id Current and (**f**) Iq Current.

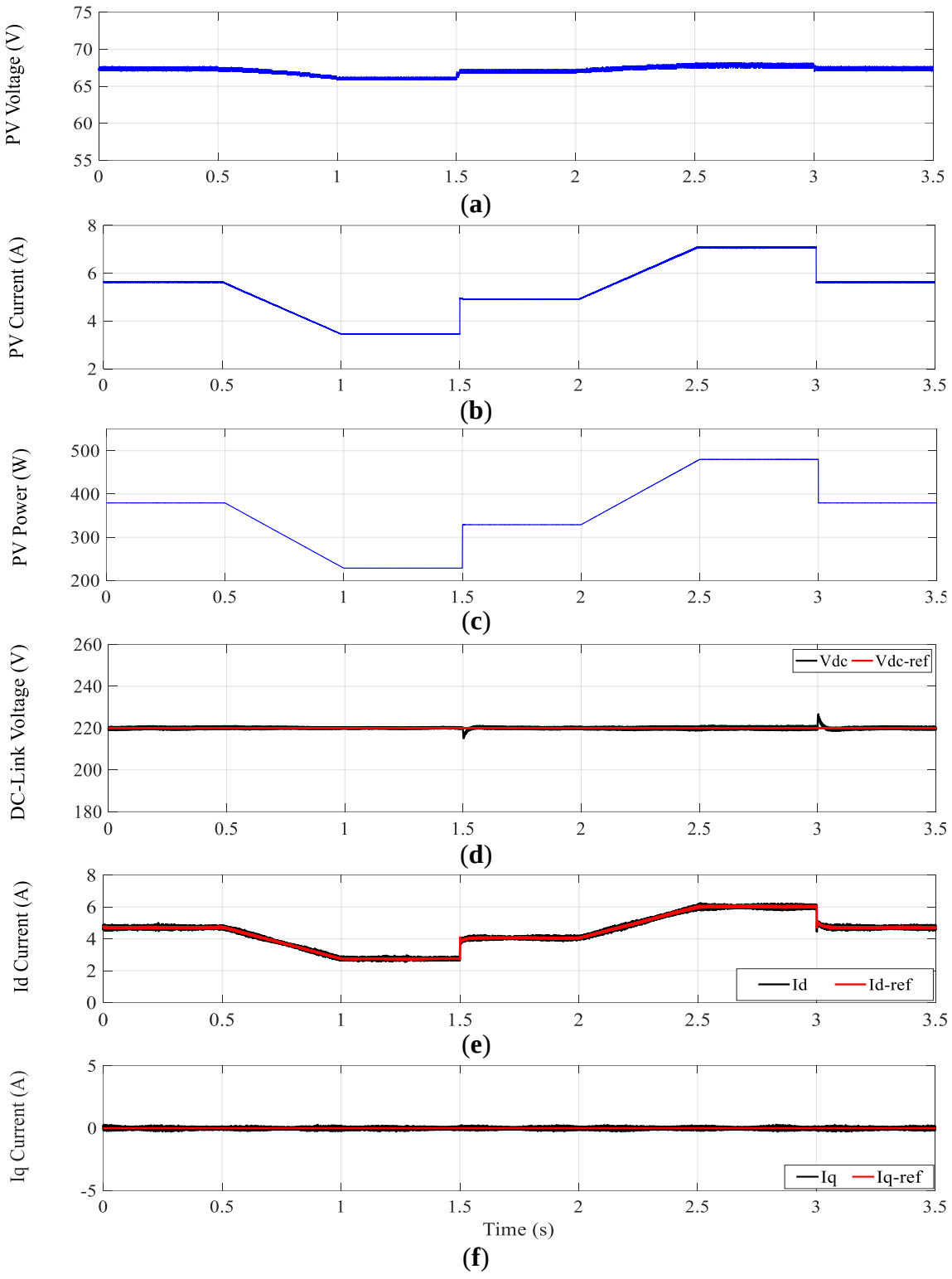

Figure 5.9: Simulation results of grid-tied PV system with the proposed control scheme; under irradiation changes. (**a**) PV Voltage; (**b**) PV Current; (**c**) PV Power; (**d**) DC−Link Voltage; (**e**) Id Current and (**f**) Iq Current.

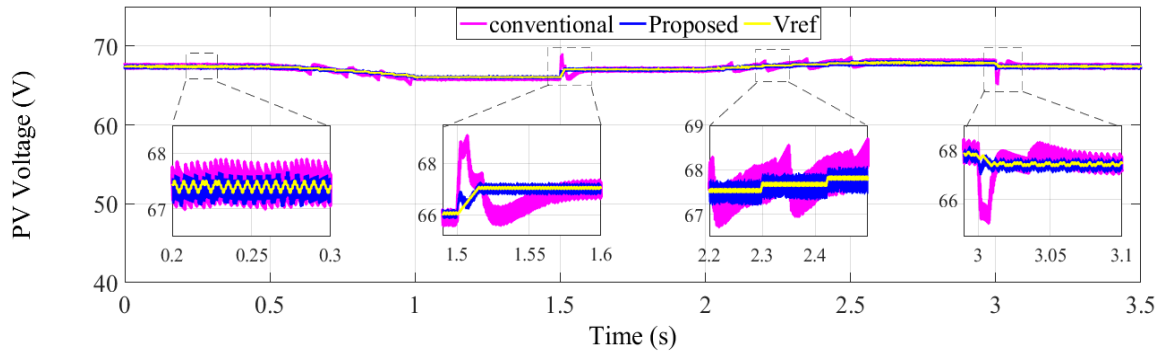

Figure 5.10: PV voltages with conventional and proposed VO-MPPT methods.

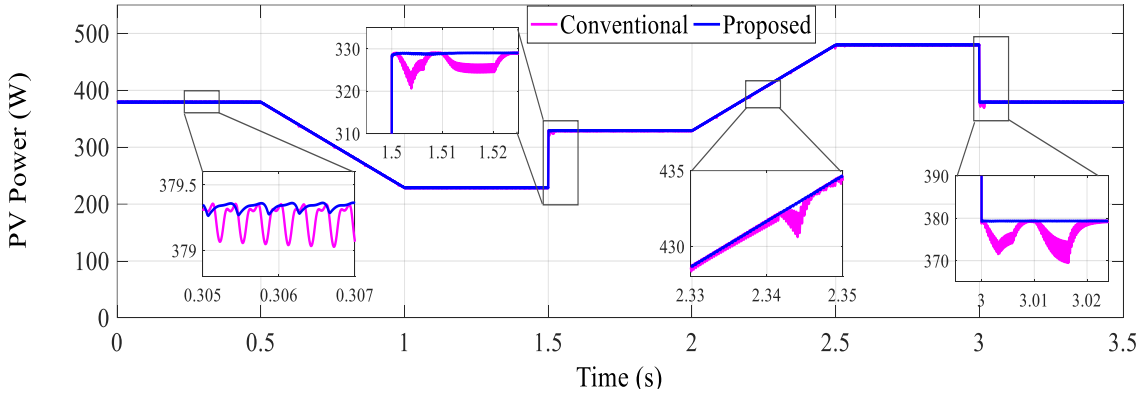

Figure 5.11: Extracted PV power with conventional and proposed VO-MPPT methods.

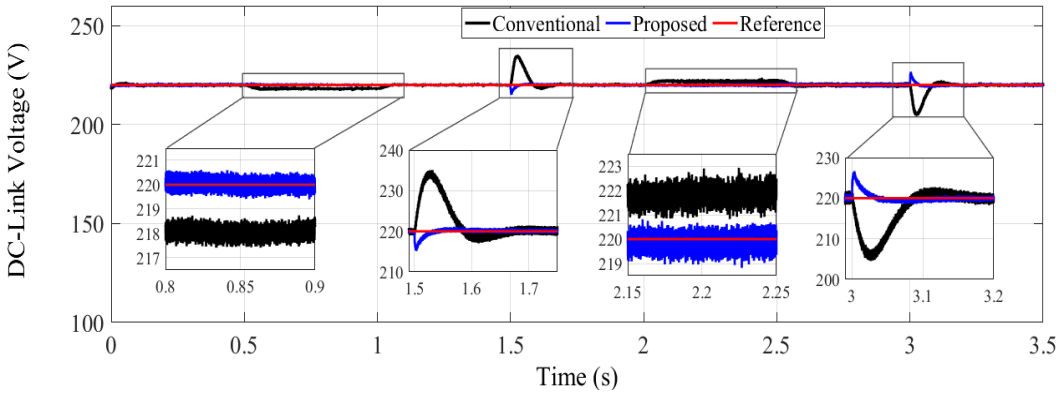

Figure 5.12: DC-Link voltage responses with conventional and proposed methods.

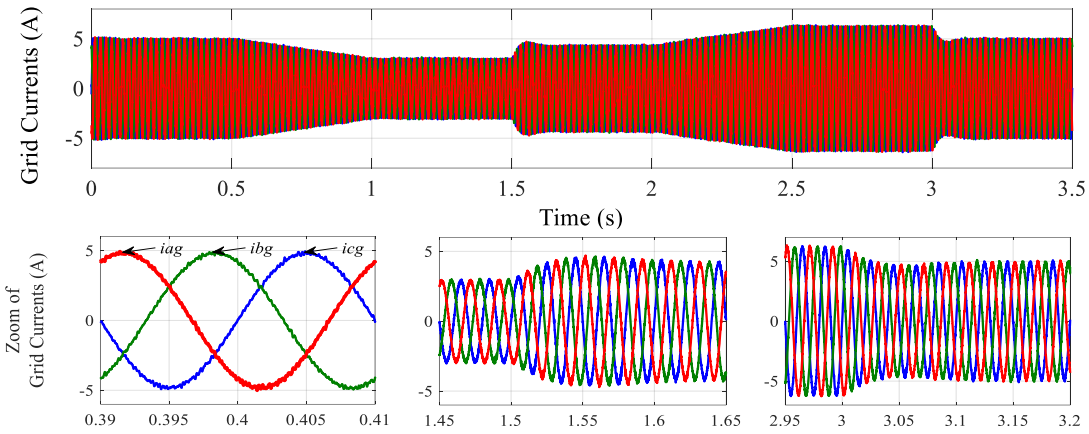

(a)

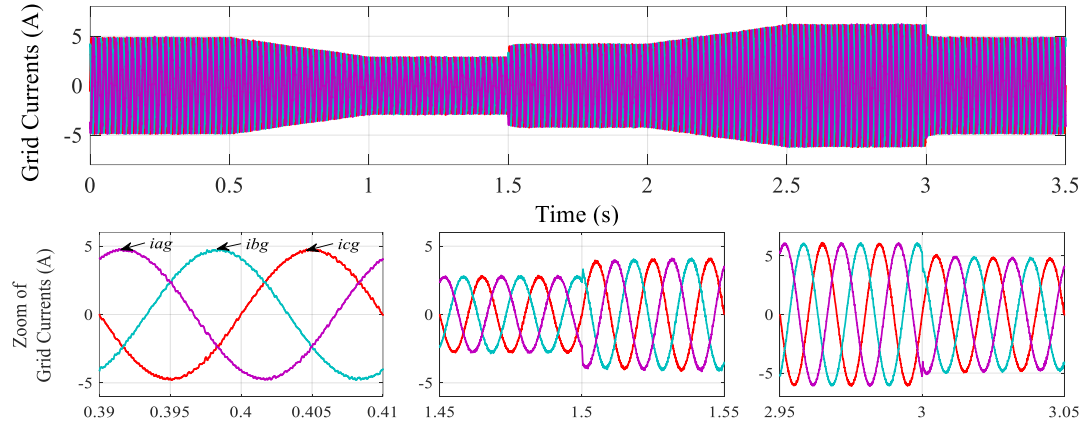

(b)

Figure 5.13: Grid currents and their zoom waveforms: (**a**) conventional control scheme; (**b**) proposed control schemes; under irradiation changes.

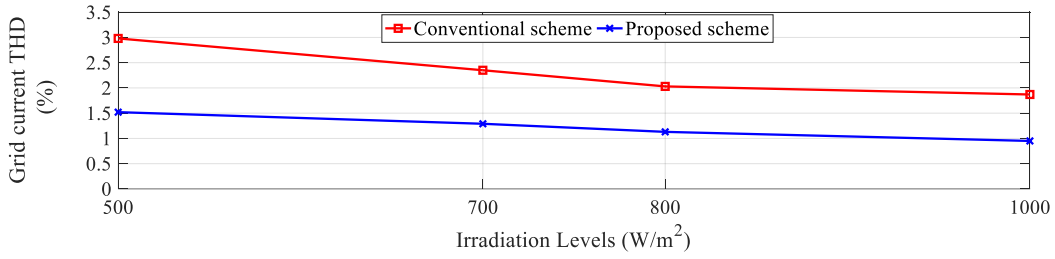

(a)

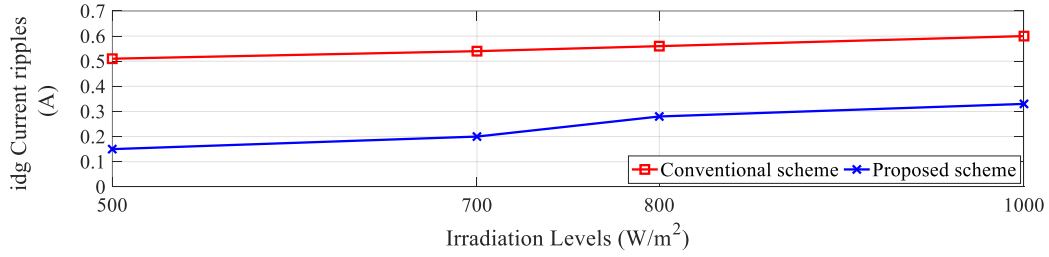

(b)

Figure 5.14: Comparison of: (**a**) grid current THD%; (**b**) grid current ripples; under irradiation changes.

5.6 EXPERIMENTAL RESULTS

In this section, the proposed control scheme for two stage-grid-tied PV system has been verified through real-time hardware in the loop (HIL) implementation, with the same parameters used in numerical simulation. The present HIL system is based on a dSPACE platform dedicated to the implementation of controller model, while, a real-time central processing unit (CPU) includes code for the physical system that is generated from the plant model. The results obtained are plotted and recorded via an oscilloscope. The controllers have been implemented with a sampling time of 50 µs.

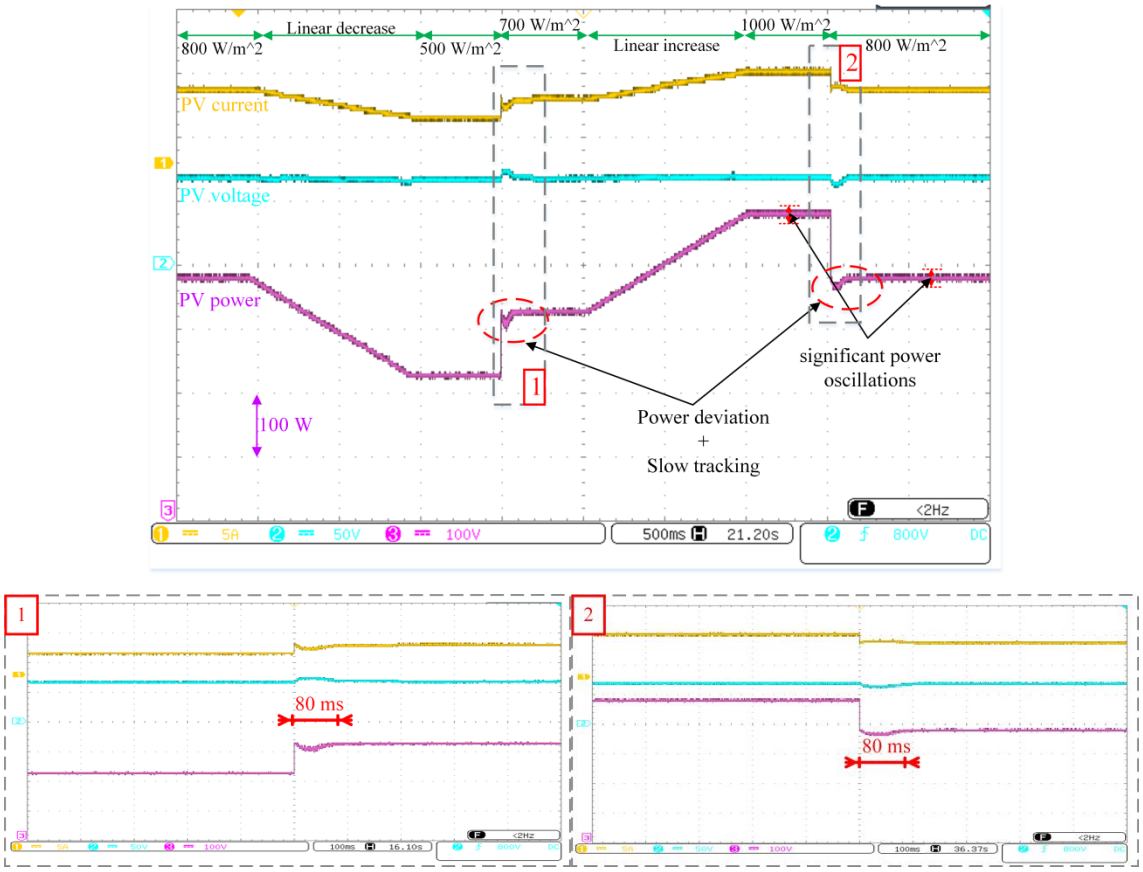

Figure 5.15: Performance of conventional MPPT (based on PI controller) under irradiation changes.

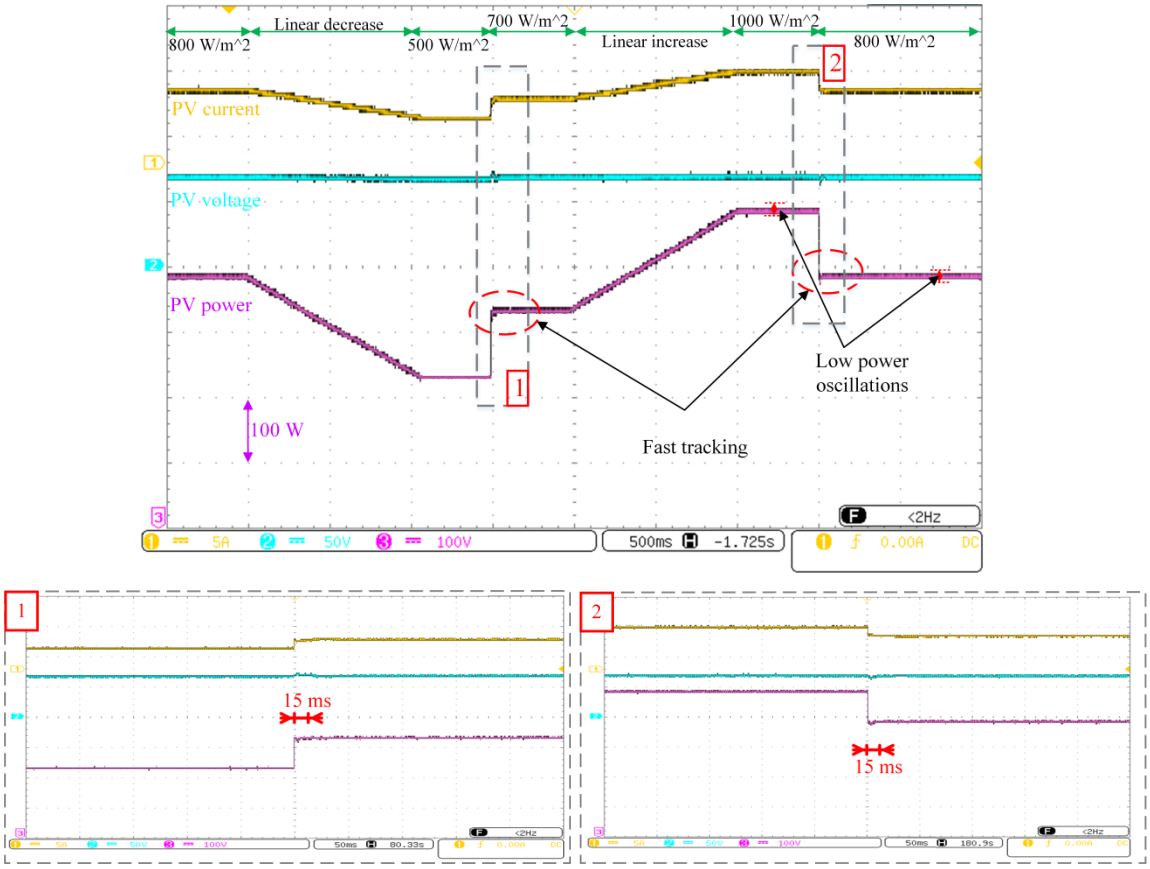

Figure 5.16: Performance of proposed MPPT under irradiation changes.

Figures 5.15 and 5.16 represent respectively the HIL results of the conventional and proposed MPPT methods. As expected, the proposed MPPT is capable to reach MPP more rapidly and provides good dynamic performance under sudden changes in irradiation with lower oscillations in steady-state operation compared to the conventional method. Where, the conventional scheme takes about 80 ms to achieve the MPP in case of sudden changes in solar irradiation with a presence of power deviations and steady-state oscillations about 5 W. Alternatively, the proposed scheme takes only 15 ms to reach the MPP with insignificant power divinations and less steady-state oscillations about 2 W. As observed, the HIL results validate the simulation results.

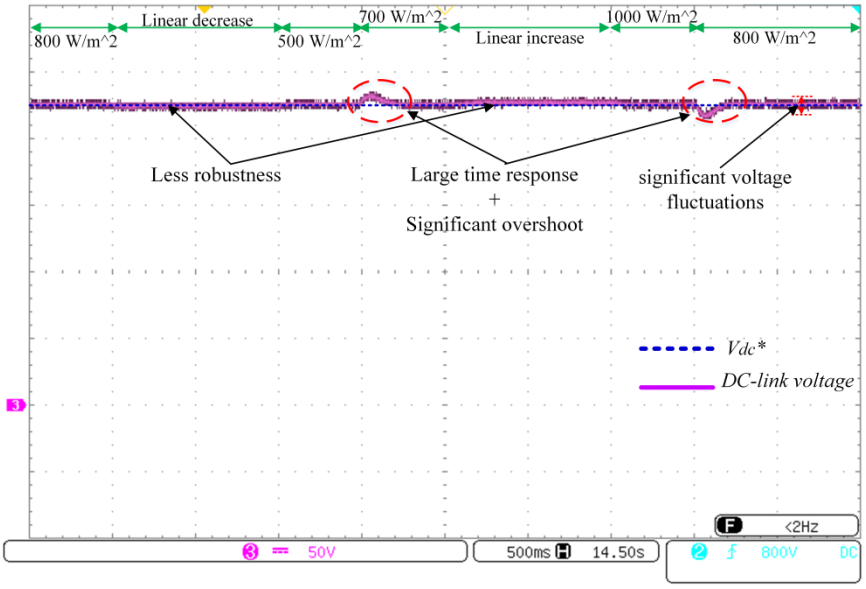

Figure 5.17: Performance of the DC-link voltage for conventional controller under irradiation changes.

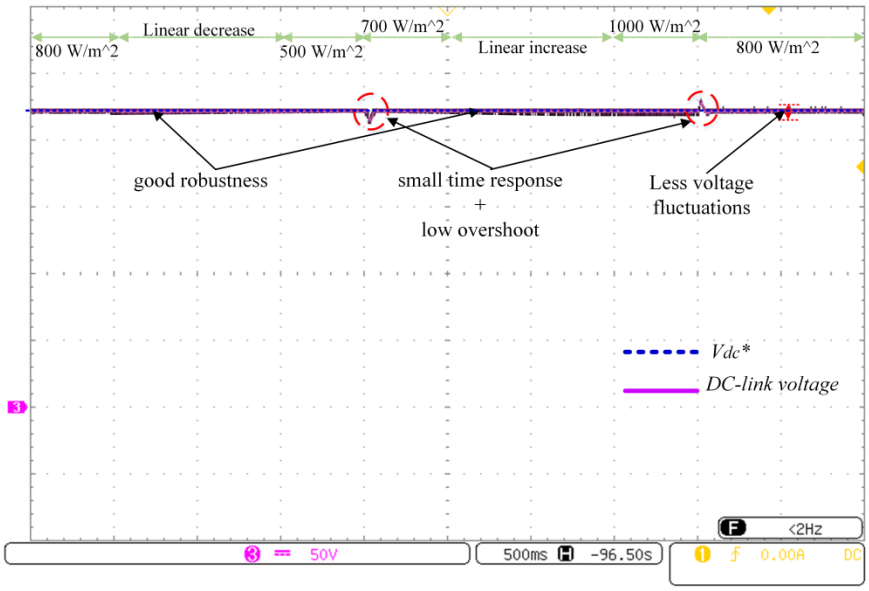

Figure 5.18: Performance of the DC-link voltage for proposed controller under irradiation changes.

The HIL responses of DC-Link voltage by using the conventional and proposed schemes are shown in Figures 5.17 and 5.18 respectively. These figures show that the DC link voltage obtained with the proposed controller offers more dynamic performance and robust tracking over conventional controllers during any change in irradiation level. When a sudden change in solar irradiation occurs, the proposed scheme tracks the desired

voltage in smooth, accurate and fast manner with unimportant overshoot and low fluctuations in steady-state operation, while the conventional scheme suffers from an inaccurate tracking in case of linear changing in solar irradiation, also exhibits a significant overshoot during sudden change in solar irradiation with significant steady-state fluctuation.

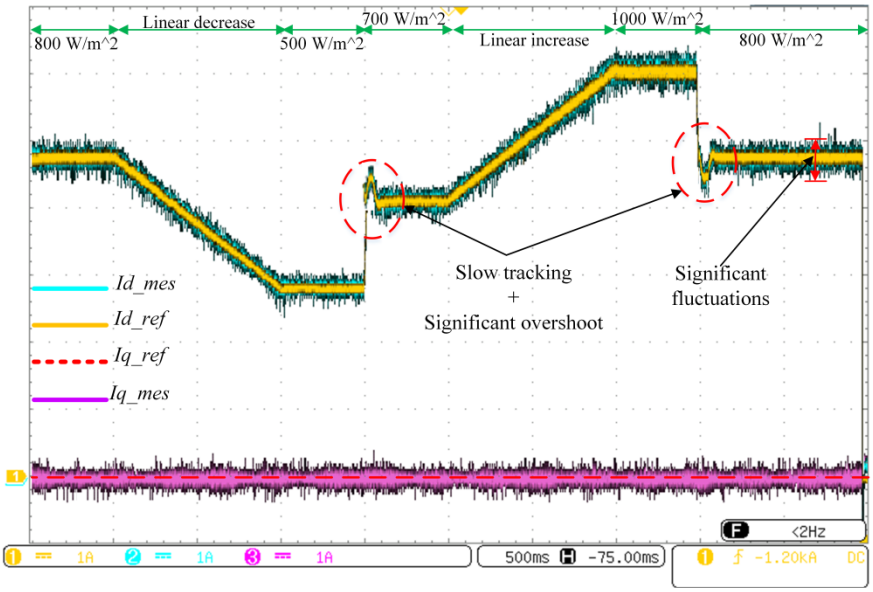

Figure 5.19: Performance of the peak of the injected currents (i_{dg} , i_{qg}) with their references for conventional scheme under irradiation changes.

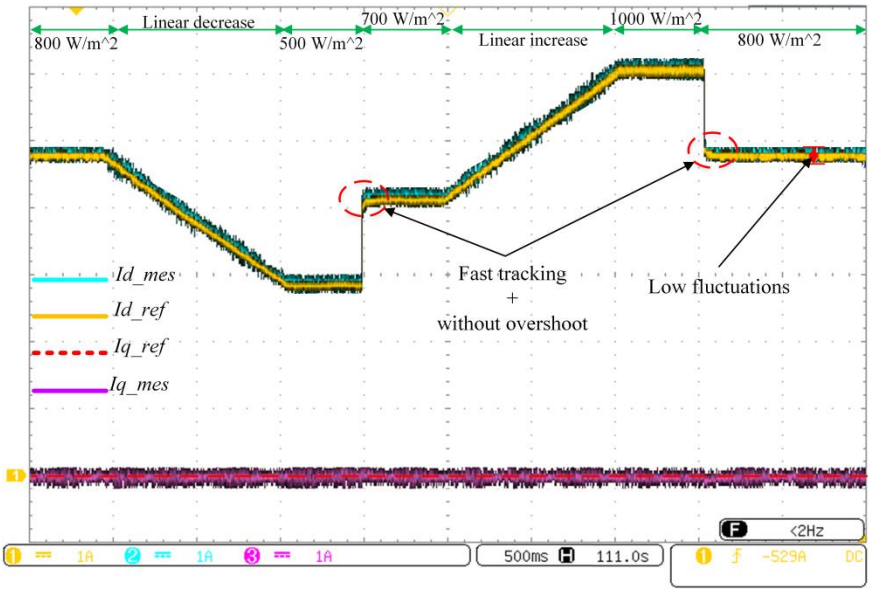

Figure 5.20: Performance of the peak of the injected currents (i_{dg} , i_{qg}) with their references for proposed scheme under irradiation changes.

Figures 5.19 and 5.20 display the HIL responses of the peak of the injected grid currents (i_{dg-ref} , i_{qg-ref}) and the measured currents (i_{dg} , i_{qg}) for the conventional and proposed schemes. It can be observed that the proposed scheme exhibits fast response with less fluctuation compared to the conventional control scheme. On the other hand, the HIL results of the injected grid currents for the conventional and proposed schemes are represented in Figures 5.21 and 5.22 respectively. From these Figures, it can be observed that the injected grid currents exhibit a good quality (low THD) with fast response when sudden irradiation changes occur by using the proposed scheme.

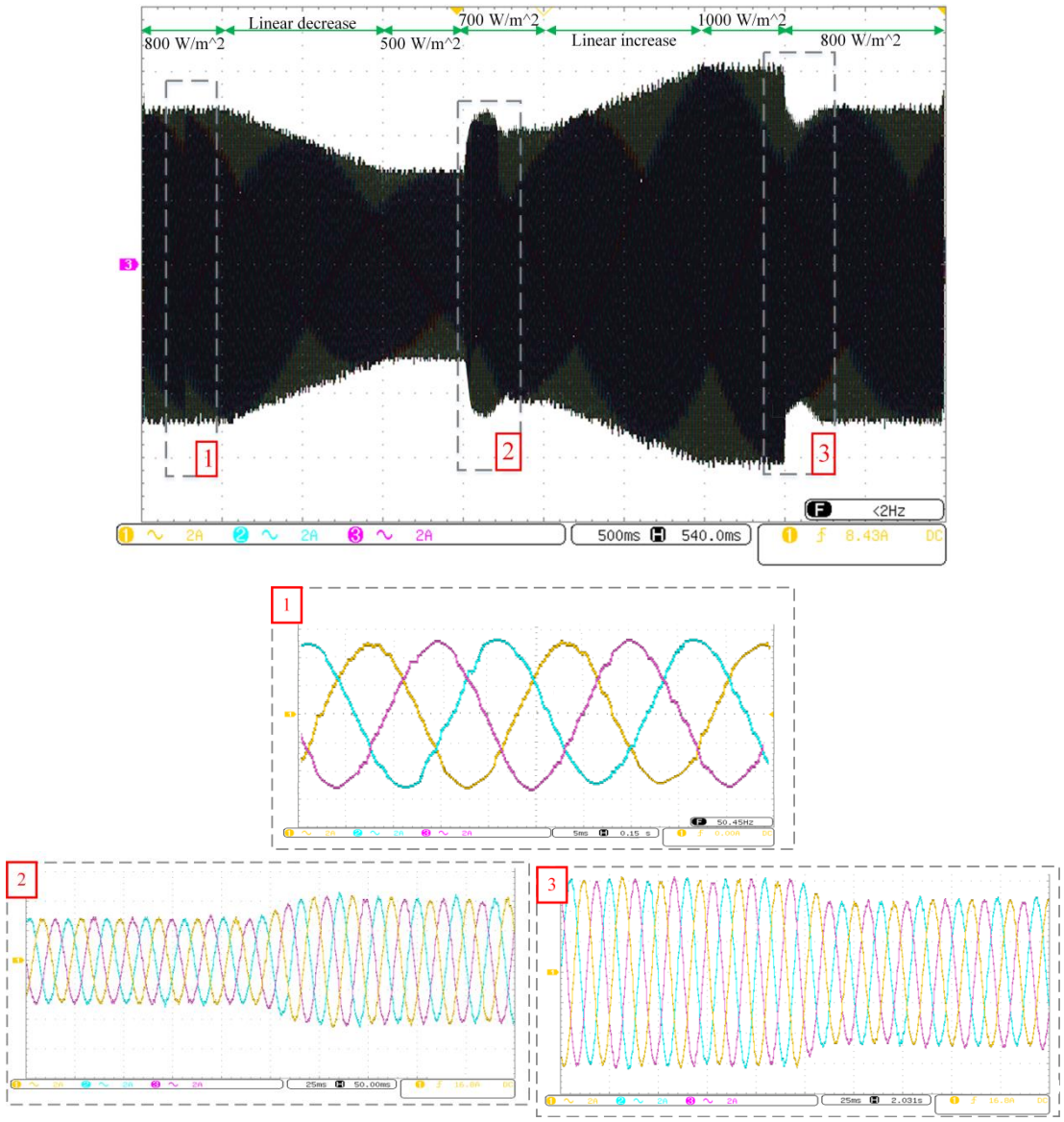

Figure 5.21: Performance of the injected grid currents for conventional scheme under irradiation changes.

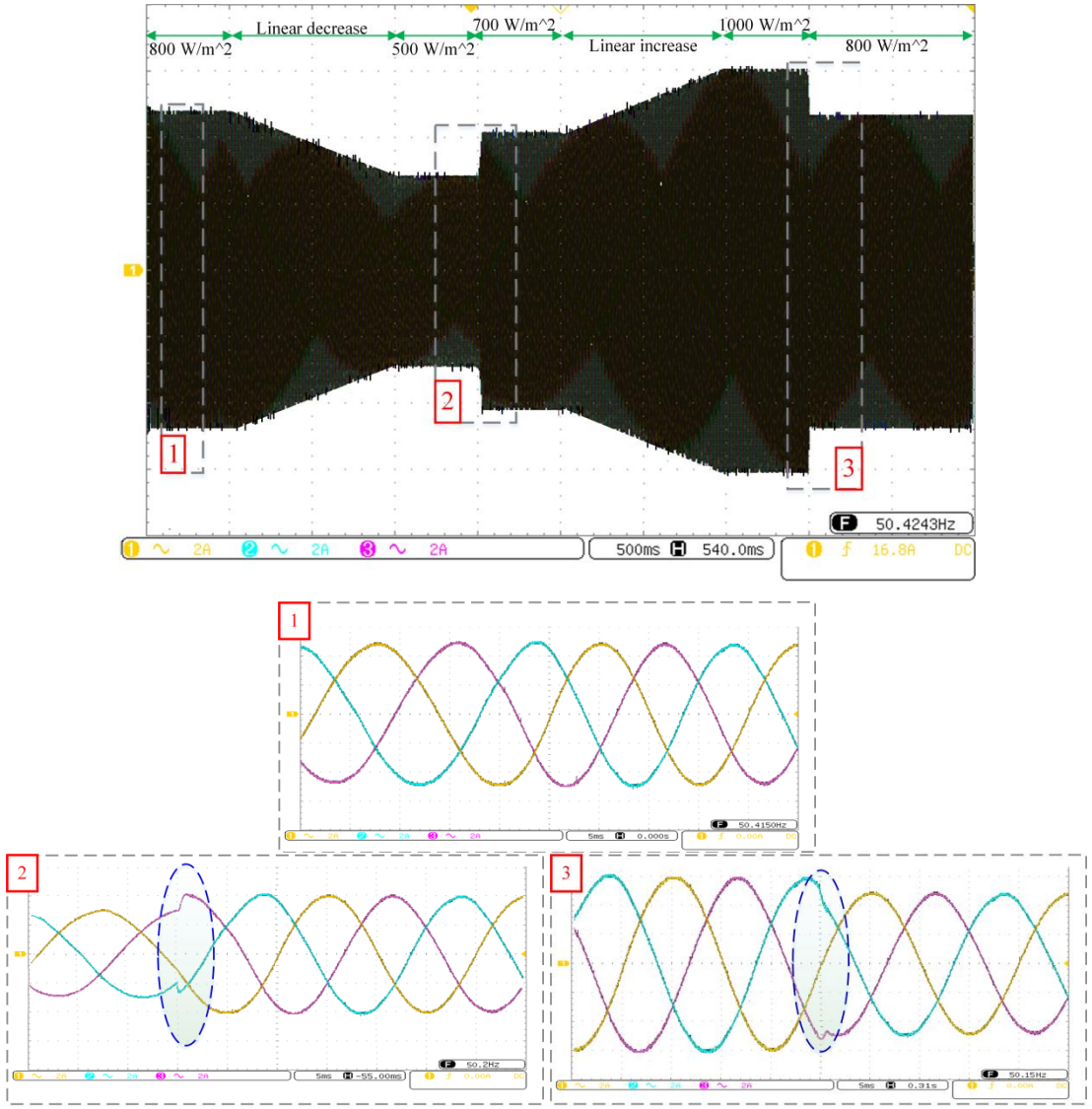

Figure 5.22: Performance of the injected grid currents for proposed scheme under irradiation changes.

5.7 CONCLUSION

This chapter has introduced the proposed high-performance control scheme for a two-stage grid-tied PV system. The control structure of the proposed scheme is based on ISMC theory and consists of MPPT control, DC-Link voltage regulation loop, and VOC based on inner current control loops to improve system performance during all climatic conditions. As a two-stage system, the PV power is provided to the grid through a DC-DC boost converter and three-phase voltage source inverter. An ISM controller for the boost converter has been proposed for MPP tracking. Moreover, for proper inverter operation as well sinusoidal currents injection into the mains grid with low THD% (<5%), a novel design for DC-Link

voltage regulation is suggested to maintain the DC-Link voltage fixed at the desired value and to estimate the reference currents for the VOC scheme, which is based on ISM controllers and space vector modulators. The simulation and experimental results obtained confirm the feasibility, effectiveness, and performance improvement of the proposed control scheme.

REFERENCES

[5.1] Pradhan, R. and Subudhi, B., 2016. Double integral sliding mode MPPT control of a photovoltaic system. IEEE Transactions on Control Systems Technology, 24(1), 285-292.

[5.2] Farhat, M., Barambones, O. and Sbita, L., 2017. A new maximum power point method based on a sliding mode approach for solar energy harvesting. Applied energy, 185, 1185-1198.

[5.3] Utkin, V.I., 1993. Sliding mode control design principles and applications to electric drives. IEEE transactions on industrial electronics, 40(1), 23-36.

[5.4] Edwards, C. and Spurgeon, S., 1998. Sliding mode control: theory and applications. Crc Press.

[5.5] Tan, S.C., Lai, Y.M. and Tse, C.K., 2011. Sliding mode control of switching power converters: techniques and implementation. CRC press.

[5.6] Sebaaly, F., Vahedi, H., Kanaan, H.Y., Moubayed, N. and Al-Haddad, K., 2016. Sliding mode fixed frequency current controller design for grid-connected NPC inverter. IEEE Journal of Emerging and Selected Topics in Power Electronics, 4(4), 1397-1405.

[5.7] Van Dijk, E., Spruijt, J.N., O'sullivan, D.M. and Klaassens, J.B., 1995. PWM-switch modeling of DC-DC converters. IEEE transactions on power electronics, 10(6), 659-665.

[5.8] Utkin, V.I. and Chang, H.C., 2002. Sliding mode control on electro-mechanical systems. Mathematical problems in Engineering, 8(4-5), 451-473.

[5.9] Hamayun, M.T., Edwards, C. and Alwi, H., 2016. Fault tolerant control schemes using integral sliding modes. Springer International Publishing.

[5.10] Rodriguez, J., Pontt, J., Silva, C.A.C.A., Correa, P., Lezana, P., Cortes, P., Ammann, U.,2007. Predictive current control of a voltage source inverter. IEEE Trans. Ind. Electron. 54 (1), 495–503.

[5.11] Yaramasu, V., Wu, B. and Chen, J., 2013. Model-predictive control of grid-tied four-level diode-clamped inverters for high-power wind energy conversion systems. IEEE transactions on power electronics, 29(6), 2861-2873.

Chapter 6

Conclusions

6.1 GENERAL CONCLUSION

According to the benefits of photovoltaic (PV) energy such as renewability, cleanness, and non-noisiness PV energy represents a promising and encouraging renewable energy technology for future electricity production and recently gained worldwide attention. Furthermore, the demand of this type of energy has increased in many field applications among these fields, a grid connected PV system is considered the most requested on the PV market because it allows a better use of PV energy. Also, it does not need to energy storage devices, which reduces costs with less maintenance. On the other hand, the efficiency resulting from these systems is depended not only on the working conditions, but also on the complete conversion chain. This can be achieved by a judicious choice of configurations or topologies, good sizing of components and effective control techniques. The contribution of this thesis was to choose simple and reliable topologies and to propose a powerful control scheme to optimize the efficiency of two-stage grid-connected PV system.

In this thesis, for maximum power point (MPP) tracking, an adaptive voltage-oriented VO-MPPT control is proposed of PV systems under abrupt and ramp irradiance changes. The P&O voltage-based (V-MPPT) algorithm is intended to generate the PV output voltage reference. Then, an adaptive integral derivative sliding mode controller (A-IDSMC) is proposed to regulate the PV current according to the reference current. Moreover, the proposed controller is designed with a novel sliding surface to eliminate the overshoot during abrupt change in solar irradiation and minimize the steady state error. Then, the controller gains are identified using an adaptation mechanism. The performance of the proposed scheme has been tested through numerical simulations and validated experimentally. Moreover, it was compared with the conventional P&O and P&O/PI, the obtained results demonstrate that with the proposed scheme, voltage fluctuation (ripples) is minimized. Furthermore, the overshoot has also been eliminated, the tracking time is reduced and tracking efficiency is enhanced.

In addition, a high-performance control scheme for a two-stage grid-connected PV system is proposed. The control structure of the proposed scheme is based on integral sliding

mode control (ISMC) and consists of MPPT control, DC-Link voltage regulation loop, and VOC based on inner current control loops to improve system performance during all climatic conditions. As it is a two-stage system, the PV power is provided to the grid through a DC-DC boost converter and three-phase voltage source inverter (VSI). For MPP tracking, the proposed voltage controller (ISMC) is proposed to regulate the PV output voltage allowing to its reference value generated by V-MPPT unit. Moreover, for proper inverter operation as well as sinusoidal currents injection into the mains grid with low THD% (<5%), for DC-Link voltage regulation a novel design based on ISM was developed to maintain the DC-Link voltage at the desired value and to estimate the reference currents. Moreover, voltage oriented control (VOC) based on ISM controllers and space vector modulation were used to control the injected grid current. To demonstrate the performance enhancement of the proposed control scheme for grid-connected PV system, a comprehensive simulation model was established using MATLAB/Simulink^{TM} environment and validated by using real-time hardware in the loop (HIL) system. The obtained results confirm the feasibility, effectiveness, and performance improvement of the proposed control scheme.

6.2 PRINCIPAL CONTRIBUTIONS OF THE RESEARCH

The principal contributions of the research presented in this thesis can be summarized as follows:

- ✓ An adaptive controller based on sliding mode theory with modified control law for MPPT of PV systems is proposed in this thesis to solve abrupt changing irradiation problem.
- ✓ An efficient and robust control scheme based on a modified control law of integral sliding mode control for two-stage grid-connected photovoltaic system is proposed in this thesis.
- ✓ A new design of DC-Link voltage regulation based on integral sliding mode control is proposed to maintain the DC-Link voltage at the desired value especially under linear changing in irradiation and to estimate the reference currents.
- ✓ To increase the quality and to exhibit fast response of the injected grid currents, a voltage oriented control based on the modified control law of integral sliding mode control and space vector modulation (VOC-ISMC-SVM) is also presented to control the inverter.

6.3 FUTURE WORKS

Besides on the research presented in this thesis, some of the suggested studies in the future are summarized as follows:

- ✓ Perform experimental tests with real solar panels and not with a programmable source.
- ✓ Test of the proposed MPPT control to extract the global maximum power point for inhomogeneous insulation taking into account the shading phenomenon.
- ✓ The insertion of sliding observers (SMO) in the proposed control scheme to estimate accurately the required variables and reduce the number of sensors, thereby reducing the total cost of the system.
- ✓ The application of other inverter types such as Z-source inverter (ZSI) and split-source inverter (SSI) for grid-connected PV system decreases the number of switching devices which allows reducing the cost-effectiveness.
- ✓ Development of an effective control system for PV systems connected to the grid, taking into account faults occurring in the electrical grid.
- ✓ Fabrication of the control circuit board.

List of Publications

The following list includes all the papers published by the author during his graduate studies. Papers designated by "*" are directly related with research results presented in this dissertation.

Journal Papers

*[1] **Kihal. A,** Krim. F, Talbi. B, Laib. A, Sahli. A. (2018, October). A Robust Control of Two-Stage Grid-Tied PV Systems Employing Integral Sliding Mode Theory. Energies, 11(10), 2791. https://doi.org/10.3390/en11102791. (Impact Factor: 2.676).

*[2] **Kihal. A**, Krim. F, Laib. A, Talbi. B, Afghoul. H. (2018 Nov 26) An improved MPPT scheme employing adaptive integral derivative sliding mode control for photovoltaic systems under fast irradiation changes. ISA transactions. https://doi.org/10.1016/j.isatra.2018.11.020. (Impact Factor: 3.370).

[3] Afghoul. H, Krim. F, Babes. B**,** Beddar. A**, Kihel. A**. (2018, July). Design and real time implementation of sliding mode supervised fractional controller for wind energy conversion system under sever working condition. Energy Conversion and Management, 167:91-101. https://doi.org/10.1016/j.enconman.2018.04.097. (Impact Factor: 6.377).

[4] Laib. A, Krim. F, Talbi.B, **Kihal. A**, Feroura. H. (2018). Improved Control for Three Phase dual-Stage Grid-Connected PV Systems Based on Predictive Control Strategy. Journal of Control Engineering and Applied Informatics, 20(3), 12-23.
(Impact Factor: 1.036).

[4] Laib. A, Krim. F, Talbi.B, Feroura. H, **Kihal. A**. (2018). Decoupled active and reactive ôwer control strategy of grid-connected six-level diode-clambed inverters based on finit set model predictive for photovoltaic application. Journal of Control Engineering and Applied Informatics, 20(3), 12-23.
(Impact Factor: 1.036).

Conference Papers

*[5] **Kihal. A**, Krim. F, Laib. A. (2017). MPPT voltage oriented loop based on integral sliding mode control applied to the boost converter. IEEE 6th International Conference on Systems and Control (ICSC), 7-9 May, Batna, Algeria, pp. 205-209.

[6] Laib. A, Krim. F, Talbi.B, **Kihal. A**, Sahli. A. (2017, November). Predictive control strategy for double-stage grid connected PV systems. The Third International Conference on Electrical Engineering and Control Applications (ICEECA'2017), 21-22 Nov, Constantine, Algeria.

Advanced approach for the optimization of a grid-tied photovoltaic system

Abstract:

This Ph. D thesis is one of the core research activities of the exploitation of photovoltaic (PV) energy. The use of PV energy has drawn global attention for future electricity production to meet the increased energy demand. Amongst the application fields of this energy type, the grid-tied PV system is considered as the most requested on the PV market because it allows a better use of PV energy and does not need energy storage devices, which reduces cost with less maintenance. The grid-tied PV systems are broadly classified into two categories, single and two conversion stages. The efficiency resulting from these systems depends not only on the working conditions, but also on the complete conversion chain. This can be achieved by a judicious choice of configurations or topologies, good sizing of components and effective control techniques. The research work presented in this thesis is to contribute to the efficiency optimization of grid-tied PV systems. This contribution concerns the modeling, sizing and control of a two-stage grid connected PV system. Nevertheless, the main part of our research is to propose powerful control scheme capable to attain the aforementioned objective. Firstly, the development of a Maximum power point tracking (MPPT) methods based on a non-linear approach called sliding mode control (SMC) to achieve an optimal exploitation of PV generator under solar irradiation changes. Also, the development of new design based on SMC theory for DC-Link voltage controller to maintain the DC-link voltage constant at the desired value during any case of solar irradiation changes. Afterwards, the development of a voltage oriented control (VOC) based on ISMC and space vector modulation for proper inverter operation as well sinusoidal currents injection into the mains grid with low total harmonic distortion (THD < 5%).In addition, these schemes have been performed through numerical simulation with MATLAB/Simulink® environment, and validated practically through real-time hardware in the loop system using a dSPACE DS 1104 system.

Keywords: Photovoltaic energy; Grid-tied photovoltaic system; MPPT; Sliding mode control; Total harmonic distortion.

Approche avancée pour l'optimisation d'une installation photovoltaïque interconnectée au réseau

Résumé :

Cette thèse de doctorat est l'une des activités de recherche fondamentales de l'exploitation de l'énergie photovoltaïque (PV). L'utilisation de l'énergie PV a attiré l'attention mondiale sur la production future d'électricité afin de répondre à la demande accrue en énergie. Parmi les domaines d'application de ce type d'énergie, un système PV connecté au réseau est considéré comme le plus demandé sur le marché PV, car il permet une meilleure utilisation de l'énergie photovoltaïque et ne nécessite pas de dispositifs de stockage d'énergie, ce qui réduit les coûts tout en nécessitant moins de maintenance. Les systèmes PV connectés au réseau sont généralement classés en deux catégories, à un et deux étages de conversion. L'efficacité résultant de ces systèmes dépend non seulement des conditions de travail, mais également de la chaîne de conversion complète. Cela peut être réalisé par un choix judicieux de configurations ou de topologies, un bon dimensionnement des composants et des techniques de contrôle efficaces. Le travail de recherche présenté dans cette thèse a pour objectif de contribuer à l'optimisation de l'efficacité des systèmes PV connectés au réseau. Cette contribution concerne la modélisation, le dimensionnement et le contrôle d'un système PV à deux étages, connecté au réseau. Néanmoins, l'essentiel de nos travaux de recherche visent à proposer un système de contrôle puissant capable d'atteindre l'objectif susmentionné. Premièrement, le développement de méthodes de suivi du point de puissance maximale (MPPT) basées sur une approche non linéaire appelée contrôle de mode glissant (SMC) pour obtenir une exploitation optimale du générateur PV sous une variation du rayonnement solaire. En outre, le développement d'une nouvelle technique basée sur la théorie SMC pour le contrôleur de la tension intermédiaire permettant de maintenir la tension de liaison continue fixée à la valeur souhaitée, quelle que soit l'irradiation solaire. Par la suite, une commande axée sur la tension (VOC) basée sur la modulation SMC et la modulation vectorielle pour un bon fonctionnement de l'onduleur ainsi que l'injection de courants sinusoïdaux dans le réseau avec un faible taux global d'harmoniques (THD <5%). Toutes ces techniques ont été simulées numériquement sous l'environnement MATLAB / Simulink® et validée pratiquement par un système en temps réel, à l'aide de la carte dSPACE DS 1104.

Mots clés : Energie photovoltaïque; Système photovoltaïque connecté au réseau; MPPT; mode glissant; Distorsion harmonique globale.

نهج متقدم لتحسين الشبكة الكهروضوئية المتصلة بالشبكة

ملخص:

هذه الرسالة هي واحدة من الأنشطة البحثية الأساسية لاستغلال الطاقة الكهروضوئية. وقد جذب استخدام الطاقة الكهروضوئية الانتباه العالمي لإنتاج الكهرباء في المستقبل لتلبية الطلب المتزايد على الطاقة. من بين مجالات التطبيق لهذا النوع من الطاقة ، يعتبر النظام الكهروضوئي المتصل بالشبكة الأكثر طلبًا في سوق الكهروضوئية لأنه يسمح باستخدام أفضل للطاقة الكهروضوئية ولا يحتاج إلى أجهزة تخزين الطاقة ، مما يقلل من التكاليف و بأقل الصيانة. تصنف الأنظمة الكهروضوئية المتصلة بالشبكة على نطاق واسع إلى فئتين ، احادي مرحلة التحويل وثنائي مرحلة التحويل. الكفاءة الناتجة عن هذه الأنظمة لا تعتمد فقط على ظروف العمل، ولكن أيضًا على سلسلة التحويل الكاملة. ويمكن تحقيق ذلك من خلال اختيار حكيم للتكوينات أو الطوبولوجيا ، والتحجيم الجيد للمكونات وتقنيات التحكم الفعالة. البحث المقدم في هذه الرسالة هو للمساهمة في تحسين كفاءة النظام الكهروضوئي المرتبط بالشبكة. وتتعلق هذه المساهمة بالنمذجة والتحجيم والتحكم في النظام الكهروضوئي المتصل بالشبكة على مرحلتين. ومع ذلك ، فإن الجزء الرئيسي من بحثنا هو اقتراح خطة تحكم قوية قادرة على تحقيق الهدف المذكور أعلاه. أولاً ، تطوير طرق التتبع القصوى لنقاط القدرة (MPPT) مؤسس على نهج غير خطي يسمى التحكم بالطريقة الانزلاقية (ت.ط.إ) لتحقيق الاستغلال الأمثل لمولد PV في ظل تغيرات التشعيع الشمسي. أيضا ، تطوير تصميم جديد يستند إلى نظرية (ت.ط.إ) لوحدة تحكم في الجهد المستمر بين المحولين للحفاظ على ثابت الجهد مرتبطا بالقيمة المرغوبة خلال أي حالة من تغيرات التشعيع الشمسي. بعد ذلك، تطوير التحكم بالجهد الموجه استنادًا إلى (ت.ط.إ) وتشكيل تعديل ناقل من أجل تشغيل العاكس بشكل صحيح بالإضافة إلى حقن التيارات الجيبية في الشبكة الرئيسية مع انخفاض التشوه التوافقي الكلي (THD <5٪). تم تنفيذ مخططات التحكم هذه من خلال المحاكاة الرقمية باستخدام برنامج ماتلاب ، وتم التحقق من ذلك عمليًا بإستخدام نظام hardware in the loop ومن خلال البطاقة الرقمية dSPACE DS 1104

الكلمات المفتاحية: الطاقة الكهروضوئية; نظام كهروضوئي متصل بالشبكة; MPPT; التحكم بالطريقة الانزلاقية; التشوه التوافقي الكل